# RESOURCE ALLOCATION FOR VEHICULAR COMMUNICATIONS

A Dissertation
Presented to
The Academic Faculty

By

Le Liang

In Partial Fulfillment
of the Requirements for the Degree
Doctor of Philosophy in the
School of Electrical and Computer Engineering

Georgia Institute of Technology

December 2018

# RESOURCE ALLOCATION FOR VEHICULAR COMMUNICATIONS

Approved by:

Dr. Geoffrey Ye Li, Advisor
School of Electrical and Computer
Engineering
*Georgia Institute of Technology*

Dr. Gordon L. Stüber
School of Electrical and Computer
Engineering
*Georgia Institute of Technology*

Dr. Xiaoli Ma
School of Electrical and Computer
Engineering
*Georgia Institute of Technology*

Dr. Mary Ann Weitnauer
School of Electrical and Computer
Engineering
*Georgia Institute of Technology*

Dr. Xingxing Yu
School of Mathematics
*Georgia Institute of Technology*

*To my family*

# ACKNOWLEDGEMENTS

I wish to thank a number of people for making my experience as a Ph.D. student at Georgia Tech as exciting and rewarding as it is. Foremost, I would like to thank my advisor Professor Geoffrey Ye Li for his continual guidance and support throughout my research and study in the past three years. My sincere thanks also go to Professor Gordon L. Stüber, Professor Xiaoli Ma, Professor Mary Ann Weitnauer and Professor Xingxing Yu for serving on my dissertation committee. My understanding of many issues central to vehicular communications has been substantially deepened thanks to Professor Gordon L. Stüber's course on mobile communications and Professor Justin Romberg's course on advanced digital signal processing. Thanks are also due to them.

I am deeply indebted to my friends and roommates, Xiaoyu Sun, Wenbo Ding, and Hao Ye for many stimulating discussions and much fun during the time we spent together. I also wish to express my heartfelt gratitude to all members of our research group, from whom I have learned a lot. In particular, I would like to thank Cen Lin, Yinsheng Liu, Qingqing Wu, Yinjun Liu, Yunlong Cai, Deli Qiao, Rui Yin, Yongtao Ma, Chongtao Guo, Peihao Dong, Ziyi Chen, and Ziyan He for many inspiring discussions. I am grateful to the collaboration on graph theory with Shijie Xie and Professor Xingxing Yu from the School of Mathematics. It is such an intriguing experience to have academic discussions with "sciency" and respectable people like them.

Finally, I express my heartfelt gratitude to all my friends, both inside and outside of Georgia Tech, whose friendship makes my three years in Atlanta unforgettable. This dissertation is dedicated to my family whose support and love have always been a source of courage and confidence for me.

# TABLE OF CONTENTS

# LIST OF FIGURES

# SUMMARY

The emerging vehicular communications are expected to enable a whole new set of services and hold significant potential in making our daily experience on wheels safer and more convenient. Judicious resource allocation design is central to mitigating interference, optimizing resource utilization, and unleashing the full potentials of vehicular communications. This thesis aims to develop efficient and effective resource allocation schemes to meet the diverse quality-of-service requirements of vehicular communications while taking into account the strong dynamics in vehicular environments.

Specifically, we study the spectrum and power allocation problem in device-to-device (D2D)-enabled vehicular networks. We design low-complexity algorithms to maximize the capacity of vehicle-to-infrastructure (V2I) links while guaranteeing the reliability of each vehicle-to-vehicle (V2V) link, evaluated in terms of outage probabilities, using only slowly varying large-scale fading information or delayed rapidly varying small-scale fading information from periodic feedback. To further improve spectrum utilization, we investigate the case where each V2I link shares spectrum with multiple V2V links and exploit graph theoretic tools to develop high performance approximation algorithms to support flexible spectrum sharing in vehicular communications. For ease of (semi-)distributed resource management, we exploit recent results in multi-agent reinforcement learning to develop a learning-based resource allocation algorithm for vehicular agents. Resource sharing decisions are made based on a mix of slowly-varying global large-scale channel information and fast-varying local observations. The four proposed schemes, including both centralized and semi-distributed designs with varying complexity-performance tradeoffs, constitute a comprehensive study of the resource allocation problem in vehicular communications.

# CHAPTER 1

# INTRODUCTION

Wireless networks that support high mobility broadband access have received more and more attention from both industry and academia in recent years [1, 2, 3, 4, 5, 6]. In particular, the concept of connected vehicles or vehicular communications, commonly abbreviated as V2X, has gained substantial momentum to bring a new level of connectivity to vehicles and, along with novel onboard computing and sensing technologies, serve as a key enabler of intelligent transportation systems (ITS) and smart cities [7]. This new generation of networks will ultimately have a profound impact on the society, making everyday traveling safer, greener, and more efficient and comfortable.

To coordinate efforts of different stakeholders in vehicular communications, several sets of standards have been developed across the globe over the past decade, e.g., dedicated short-range communications (DSRC) standards in the US [8] and ITS-G5 standards developed by the European Telecommunications Standards Institute (ETSI) [9]. Both standards are based on the IEEE 802.11p technology, establishing the foundation for communications in vehicular ad hoc networks. More recently, the 3rd Generation Partnership Project (3GPP) has been looking to support V2X services in long-term evolution (LTE) [10] and future 5G cellular networks [11]. Cross-industry consortium, such as the 5G automotive association (5GAA), has been founded by leaders from both telecommunication and automotive industries to push development, testing, and deployment of cellular V2X technologies.

An illustrative structure of vehicular networks is depicted in Fig. 1.1. Onboard information and entertainment (infotainment) applications and traffic efficiency services generally require frequent access to the Internet or remote servers for media streaming, content sharing, etc., involving considerable amount of data exchange. Hence, they are ideally supported by the high-capacity vehicle-to-infrastructure (V2I) links. Meanwhile, safety-
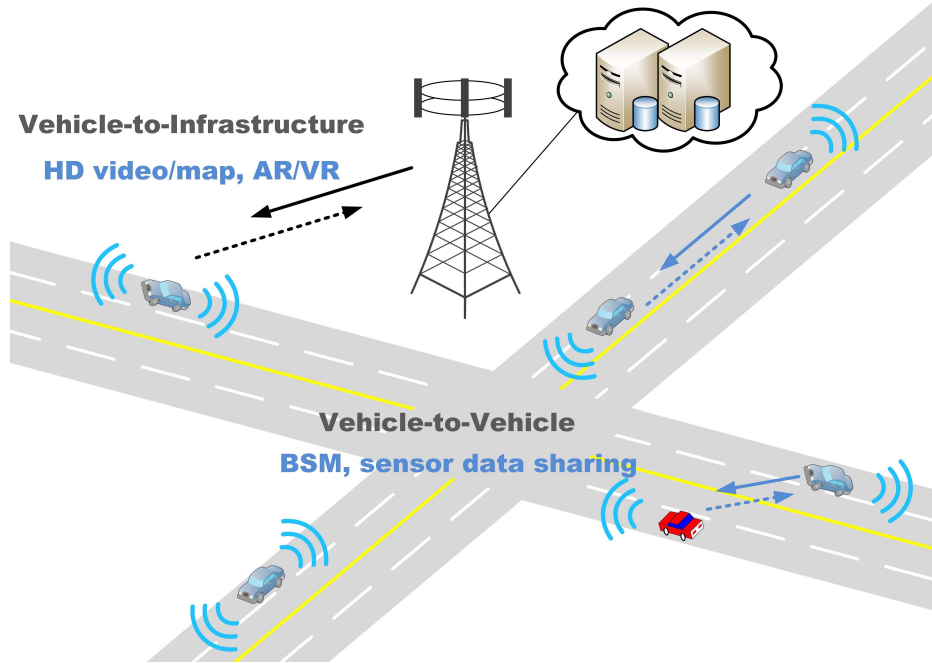
Figure 1.1: An illustrative structure of vehicular networks. HD: high-definition; AR: augmented reality; VR: virtual reality; BSM: basic safety message.

critical information, such as cooperative awareness messages (CAMs) and decentralized environmental notification messages (DENM) [3], usually entails spreading safety related messages among neighboring vehicles either in a periodic or event triggered way. As such, it is naturally supported by the vehicle-to-vehicle (V2V) links, which impose strict reliability and timeliness requirements. For example, the European union Mobile and Wireless Communications Enablers for Twenty-twenty (2020) Information Society (METIS) project requires less than 5 ms of end-to-end latency and transmission reliability of $99.999\%$ for message sizes of about 1600 bytes in such links [12].

Among an array of issues in designing and optimizing vehicular networks, resource allocation is particularly challenging due to strong underlying dynamics and the strict and diverse quality-of-service (QoS) requirements. This thesis aims at designing efficient resource allocation schemes that help bring the full benefits of vehicular communication to fruition while not causing significant network overhead. The resource allocation problem is approached from different perspectives, with both centralized and semi-distributed design-

s and varying performance-complexity tradeoffs. The remainder of this chapter provides necessary background introduction and outlines the contribution of this thesis.

## 1.1 Literature Review and Motivation

In this section, we introduce the background information and review the state-of-the-art research on resource allocation for vehicular communications. We begin with a discussion of pros and cons of the two major and most relevant technology candidates, i.e., cellular-based V2X (C-V2X) and IEEE 802.11p based technologies, for vehicular communications, and then review some traditional resource allocation designs for device-to-device (D2D) communications since this thesis mainly deals with D2D-based vehicular communications. We then review studies of resource allocation with special treatment of unique characteristics in vehicular communications. Afterwards, an overview of applying graph theoretic tools in resource allocation for wireless networks is presented as such tools are extensively leveraged in the thesis. Finally, we discuss the major motivation behind this thesis.

### 1.1.1 Cellular and IEEE 802.11p Based Technologies for V2X

The IEEE 802.11p is an amendment to the IEEE 802.11 standard adapted for the ITS applications and is commonly considered as the *de facto* standard for vehicular networking. It includes sets of physical (PHY) and medium access control (MAC) layer specifications and supports communications among high mobility vehicles and between vehicles and the roadside infrastructure, in the ITS band of 5.9 GHz [13]. However, recent studies [3, 5, 14] show that vehicular communications based on IEEE 802.11p face several challenges, such as short-lived V2I connections, potentially unbounded channel access delay, and lack of QoS guarantee, due to its PHY and MAC layer designs inherited from IEEE 802.11 standards that have been originally optimized for wireless local area networks with low mobility.

Recently, 3GPP has also started looking into supporting V2X services in cellular net-

works [5, 6, 10]. Widely deployed cellular networks, assisted with direct D2D underlay communications [3, 15], potentially provide a promising solution to enable efficient and reliable V2V and V2I communications, to meet demanding V2X requirements and provide immunity to high mobility due to several intrinsic advantages. First, cellular networks exercise flexible centralized control over network resources, such as fast link adaptation and dynamic user scheduling, which guarantee optimal network performance [16]. Second, the large capacity and proven maturity of cellular networks can provide reliable support for a wide variety of bandwidth-thirsty applications and also ease V2X implementation . Finally, the side D2D links, complementing the centralized cellular architecture, will provide direct local message dissemination with substantially reduced latency, thus suitable for delay-sensitive V2V communications [3]. Meanwhile, existence of the always-on base station can be beneficial to communications among vehicles through providing side information to the V2V links.

## 1.1.2    Resource Management for Traditional D2D Communications

The D2D communications have been the subject of much recent research endeavor [15, 17]. Both spectral and energy efficiencies of the wireless networks can be substantially improved in D2D-assisted cellular systems by properly harvesting the proximity gain, reuse gain, and hop gain [15]. D2D users can work in two different modes: the reuse mode and the dedicated mode, where D2D users share the same resources as the cellular users and occupy dedicated resources, respectively. The dedicated mode is easier to implement since it causes no interference to the existing cellular users while the reuse mode can further improve the spectral efficiency. Effective radio resource management strategies need to be in place to properly coordinate mutual interference between cellular and D2D users in the reuse mode. In [18], the transmit power of D2D users has been restricted such that interference inflicting cellular receivers is controlled when the D2D transmitter reuses cellular resources. An interference limited area control scheme has been proposed in [19] to pro-

tect D2D receivers from cellular interference, where D2D users are not allowed to share spectrum with a cellular user located in the interference limited area where the interference-to-noise ratio at the D2D receiver is above a predetermined threshold. In [20], interference nulling has been introduced to control interference from the cellular link to D2D communications when multiple antennas are installed at the base station. The sum rate of both cellular and D2D users has been maximized with a minimum rate guarantee for the cellular user in [21] for a network comprising only a single D2D pair and a single cellular user. For more practical scenarios with multiple cellular and D2D users, spectrum and power allocation design has been considered in [22, 23]. In [22], the D2D transmit power has been regulated by the base station such that the signal-to-interference-plus-noise ratio (SINR) of D2D links is maximized while the interference experienced by the cellular link is kept at an acceptable level. Moreover, a three-step approach has been proposed in [23] to design power control and spectrum allocation to maximize system throughput with minimum SINR guarantee for both cellular and D2D links.

### 1.1.3 Resource Allocation for D2D-Based Vehicular Communications

Vehicular channels experience fast temporal variation due to vehicle mobility [24]. Therefore, traditional resource allocation designs for D2D communications dominated with full channel state information (CSI) assumptions are no longer applicable due to the formidable signaling overhead to track channel variation on such a short time scale. Applying D2D techniques to support vehicular communications thus mandates further study on radio resource management accounting for fast vehicular channel variation.

A feasibility study of D2D for vehicular communications has been performed in [7] to evaluate the applicability of D2D underlay in supporting joint V2V and V2I connections in cellular networks. It has been shown in [7] that D2D-aided vehicular communications can outperform the traditional V2V-only mode, the V2I-only mode, or the V2V overlay mode in terms of achievable transmission rates. In [25], a heuristic location dependent uplink

resource allocation scheme has been proposed for D2D terminals in vehicular networks, which features spatial resource reuse with no explicit requirement on full CSI and, as a result, significantly reduces signaling overhead. A framework comprising vehicle grouping, reuse channel selection, and power control has been developed in [26] to maximize the sum rate or minimally achievable rate of V2V links while restraining the aggregate interference to the uplink cellular transmission. A series of simplifications have been applied to the power control problem to reduce the requirement of full CSI and the dependence on centralized control as well as the computational complexity. In [27], latency and reliability requirements of V2V communications have been transformed into optimization constraints computable using large-scale fading information only. A heuristic algorithm has been developed to address the proposed radio resource management optimization problem, which adapts to the large-scale fading of vehicular channels, i.e., pathloss and shadowing that vary on a slow time scale. Similar system setups have been further considered in [28], where multiple resource blocks are allowed to be shared not only between cellular and D2D users but also among different D2D-capable vehicles. In [29], power control based on channel inversion using pathloss information and D2D mode selection based on biased channel quality have been proposed to enable vehicular D2D communications in cellular networks. Two representative performance metrics, SINR outage probability and network throughput, have been analyzed in the established theoretical framework.

### 1.1.4   Graph-Based Resource Allocation

As an effective tool to address problems of discrete nature, graph theory has long been exploited for resource allocation design in wireless networks. Interference management using graph coloring algorithms has been explored in [30] for multi-cell orthogonal frequency division multiplexing access (OFDMA) networks with dynamic fractional frequency reuse. More sophisticated two-phase intercell interference management has been further studied in [31] through transforming the original problem into a MAX $k$-CUT problem in graph

theory. To optimize the sum or average utility [32, 23], the Hungarian algorithm can help find a maximum matching for D2D and cognitive radio networks, respectively. For fairness consideration, the preference of diverse user groups can be accounted for according to the concept of stable matching [33]. Efficient algorithms, such as the Gale-Shapley (GS) algorithm [34], have been used to find a stable channel access solution with polynomial complexity for cognitive radio systems [35]. Two truncated stable matching algorithms have been further proposed in [36] to improve resource allocation robustness to CSI variation. In addition, the joint problem of path selection and power allocation for decode-and-forward relay systems has been studied in [37], where the minimum source-relay-destination link rate has been maximized.

A local search method for 3-dimensional matching has been proposed in [38] to maximize the throughput of non-safety vehicle users while satisfying the QoS requirements of cellular users and safety vehicle users. For hypergraph matching and weighted hypergraph matching problems, it has been shown in [39] that the integrality gap of the standard linear programming relaxation of the problems is exactly $k - 1 + \frac{1}{k}$ for $k$-uniform hypergraphs, and is exactly $k - 1$ for $k$-partite hypergraphs. Moreover, for the weighted $k$-uniform hypergraphs matching problem and any fixed $\epsilon > 0$, a $(k - 1 + \epsilon)$-approximation algorithm has been presented in [40], a $(\frac{2(k+1)}{3} + \epsilon)$-approximation algorithm has been proposed in [41], and a $(\frac{k+1}{2} + \epsilon)$-approximation algorithm has been presented in [42]. These approximation algorithms perform local search and obtain solutions in polynomial time. Local search is a heuristic method for solving computationally hard optimization problems that always moves from one state to another by applying local changes until convergence to a local optimum or when a time bound is reached.

### 1.1.5 Motivation

Resource allocation is key to the success of vehicular networks, especially in view of their diverse QoS requirements and the strong underlying dynamics in vehicular environments.

Traditional contention-based spectrum access designs of IEEE 802.11p cannot be directly applied to cellular-based vehicular communication systems. While the D2D technology promises to improve the suitability of cellular networks for vehicular communications through enabling direct data exchange between vehicles, a wide array of issues still remain. In terms of resource allocation, the vast majority of D2D-based communications has been dominated with full CSI assumption, which is hard, if not impossible, to meet in high mobility vehicular environments. Moreover, cellular communications with D2D underlay normally treat the direct communications between devices as secondary whereas cellular links are assigned highest priority. This causes problems in vehicular networks as the V2V links, deemed a good fit for D2D communications, are mainly responsible for disseminating safety-critical information. They typically require higher reliability and are strictly less delay tolerant. At the very least, V2V links should be treated with equal (normally higher) priority when performing system level resource allocation.

In the very few exceptions that propose specialized treatment for vehicular communications under the D2D-based architecture, inadequate care has been taken with respect to the unique vehicular channel fading as well as the special QoS requirements. For example, in [25, 27, 28], the channel small-scale fading effects are totally ignored in the capacity evaluation and hence it will not reflect the real capacity performance of the networks. As a result, the developed resource allocation schemes are generally suboptimal. In response to these issues, we are motivated to conduct a comprehensive and systematic investigation into the resource allocation problem of vehicular communications that factor in the unique characteristics of the system, reveal fundamental performance limits, and develop efficient solutions with varying performance-complexity tradeoffs.

## 1.2  Overview of Thesis

This thesis studies resource allocation for vehicular communications and in particular, we focus on the D2D-based network architecture, where V2I and V2V transmissions are

supported by cellular and D2D links, respectively. Three centralized resource allocation schemes are developed in Chapters 2-4 and one semi-distributed design is proposed in Chapter 5 to meet the diverse QoS requirements of vehicular communications while considering the underlying vehicular dynamics.

In Chapter 2, we perform spectrum sharing and power allocation based only on slowly varying large-scale fading information of wireless channels. Pursuant to differing requirements for different types of links, i.e., high capacity for V2I links and ultra reliability for V2V links, we maximize the ergodic capacity of V2I connections while ensuring reliability guarantee for each V2V link. Sum ergodic capacity of all V2I links is first taken as the optimization objective to maximize the overall V2I link throughput. Minimum ergodic capacity maximization is then considered to provide a more uniform capacity performance across all V2I links. Novel algorithms that yield optimal resource allocation and are robust to channel variations are proposed.

In Chapter 3, we begin with the observation that CSI at the base station is critical to resource allocation design for wireless networks, but it is hard to obtain accurate CSI in a high mobility vehicular environment. We study the spectrum and power allocation problem in D2D-enabled vehicular networks, where CSI of vehicular links is reported to the BS periodically with inevitable delay. We maximize the sum throughput of all V2I links while guaranteeing the reliability of each V2V link with the delayed CSI feedback. We propose a low-complexity algorithm to find the optimal spectrum sharing strategy among V2I and V2V links and properly adjust their transmit powers.

In Chapter 4, we consider the generic case when each V2I link shares spectrum with multiple V2V links and the spectrum is not assumed to be preassigned to V2I links. Leveraging the slow fading statistical CSI of mobile links, we maximize the sum V2I capacity while guaranteeing the reliability of all V2V links. We use graph partitioning tools to divide highly interfering V2V links into different clusters before formulating the spectrum sharing problem as a weighted 3-dimensional matching problem. We propose a suite of

9

algorithms, including a baseline graph-based resource allocation algorithm, a greedy resource allocation algorithm, and a randomized resource allocation algorithm, to address the performance-complexity tradeoffs. We further investigate resource allocation adaption in response to slow fading CSI of all vehicular links and develop a low-complexity randomized algorithm.

Chapter 5 continues the study of spectrum sharing in vehicular networks, yet from a semi-distributed perspective. We model the resource sharing design as a multi-agent reinforcement learning (RL) problem, which is then solved using a fingerprint-based deep Q-network method. The V2V links, each acting as an agent, collectively interact with the vehicular environment, receive distinctive observations yet a common reward, and then improve policy design through updating their Q-networks with gained experiences. Preliminary experiments demonstrate desirable performance of the proposed resource allocation scheme based on multi-agent RL in terms of both V2I capacity and V2V payload transmission success probability.

Finally in Chapter 6, we summarize key points in the thesis and make concluding remarks.

# CHAPTER 2

## RESOURCE ALLOCATION WITH LARGE-SCALE FADING CSI

In this chapter, we propose to support vehicular communications under the device-to-device (D2D)-enabled cellular architecture where the vehicle-to-infrastructure (V2I) connectivity is enabled by macro cellular link and the vehicle-to-vehicle (V2V) connectivity is supported through localized D2D links. We base resource management on slow fading parameters and statistical information of the channel instead of instantaneous channel state information (CSI) to address the challenges caused by the inability to track fast changing wireless channels. Moreover, we identify and incorporate into problem formulation differentiated quality-of-service (QoS) requirements for V2I and V2V links in correspondence with their supported applications. That is, high link capacity is desired for V2I connections while safety-critical information of V2V connections places greater emphasis on link reliability. Sum and minimum ergodic capacities (long-term average over fast fading) of V2I links are maximized with a minimum QoS guarantee for V2I and V2V links, where the V2V link reliability is ensured by maintaining the outage probability of received SINR below a small threshold.

The rest of the chapter is organized as follows. The system model is introduced in Section 2.1. Section 2.2 considers the sum V2I capacity maximization design with minimum QoS guarantee for V2I and V2V connections, whereas Section 2.3 addresses the resource allocation problem to maximize the minimum V2I capacity. Computer simulation results are presented in Section 2.4 and concluding remarks are finally made in Section 2.5.

## 2.1    System Model

Consider a D2D-enabled vehicular communications network shown in Fig. 2.1, where there exist $M$ vehicles requiring high-capacity V2I communications, denoted as CUEs (cellular
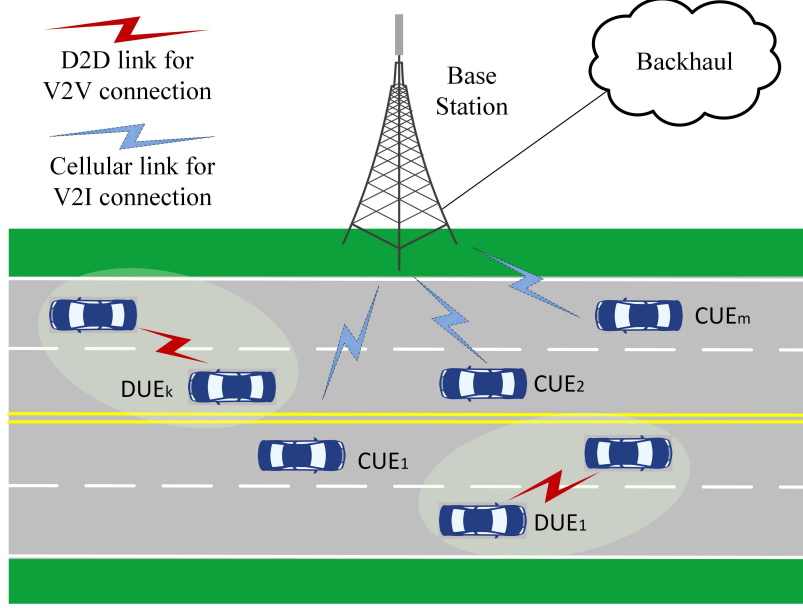
Figure 2.1: D2D-enabled vehicular communications for both V2I and V2V links.

users), and $K$ pairs of vehicles doing local V2V data exchange in the form of D2D communications, denoted as DUEs (D2D users). We note that all vehicles are capable of doing both V2I and V2V connections simultaneously, implying that CUEs and DUEs might refer to the same vehicle equipped with multiple radios in this chapter. We assume that all communicating parties in this chapter are equipped with a single antenna. Denote the CUE set as $\mathcal{M} = \{1, \cdots, M\}$ and the DUE set as $\mathcal{K} = \{1, \cdots, K\}$. To improve spectrum utilization efficiency, orthogonally allocated uplink spectrum of CUEs is reused by the DUEs since uplink resources are less intensively used and interference at the BS is more manageable.

The channel power gain, $h_{m,B}$, between CUE $m$ and the BS is assumed to follow

$$h_{m,B} = g_{m,B}\beta_{m,B}AL_{m,B}^{-\gamma} \triangleq g_{m,B}\alpha_{m,B},\qquad(2.1)$$

where $g_{m,B}$ is the small-scale fast fading power component and assumed to be exponentially distributed with unit mean, $A$ is the pathloss constant, $L_{m,B}$ is the distance between the $m$th CUE and the BS, $\gamma$ is the decay exponent, and $\beta_{m,B}$ is a log-normal shadow fading

random variable with a standard deviation $\xi$. Channel $h_k$ between the $k$th D2D pair, interfering channel $h_{k,B}$ from the $k$th DUE to the BS, and interfering channel $h_{m,k}$ from the $m$th CUE to the $k$th DUE are similarly defined.

We assume that the large-scale fading components of the channel, i.e., the path loss and shadowing of all links, are known at the BS since they are usually dependent on locations of users and vary on a slow scale [27]. Such information can be estimated at the BS for links between CUEs/DUEs and BS, i.e., $\alpha_{m,B}$ and $\alpha_{k,B}$, while for links between vehicles, i.e., $\alpha_k$ and $\alpha_{m,k}$, the parameters will be measured at the DUE receiver and reported to the BS periodically. Meanwhile, each realization of the fast fading is unavailable at the BS since it varies rapidly in a vehicular environment with high mobility, whereas its statistical characterization is assumed to be known.

To this point, the received signal-to-interference-plus-noise ratios (SINRs) at the BS for the $m$th CUE and at the $k$th DUE can be expressed as

$$\gamma_m^c = \frac{P_m^c h_{m,B}}{\sigma^2 + \sum\limits_{k \in \mathcal{K}} \rho_{m,k} P_k^d h_{k,B}}, \tag{2.2}$$

and

$$\gamma_k^d = \frac{P_k^d h_k}{\sigma^2 + \sum\limits_{m \in \mathcal{M}} \rho_{m,k} P_m^c h_{m,k}}, \tag{2.3}$$

respectively, where $P_m^c$ and $P_k^d$ denote transmit powers of the $m$th CUE and the $k$th DUE, respectively, $\sigma^2$ is the noise power, and $\rho_{m,k}$ is the spectrum allocation indicator with $\rho_{m,k} = 1$ indicating the $k$th DUE reuses the spectrum of the $m$th CUE and $\rho_{m,k} = 0$ otherwise. The ergodic capacity of the $m$th CUE with the assumption of Gaussian inputs is then given by

$$C_m = \mathbb{E}\left[\log_2\left(1 + \gamma_m^c\right)\right], \tag{2.4}$$

13

where the expectation $\mathbb{E}[\cdot]$ is taken over the fast fading distribution.

## 2.2   Sum CUE Capacity Maximization Design

In this section, we develop a robust spectrum and power allocation scheme to improve the vehicular communications performance while taking into account the unique characteristics of D2D-enabled vehicular networks. The proposed scheme depends solely on the slowly varying large-scale channel parameters and only needs to be updated every few hundred milliseconds, thus significantly reducing the signaling overheads than if directly applying traditional resource allocation schemes in vehicular networks.

Recognizing QoS differentiation for different types of links, i.e., large capacity for V2I connections and high reliability for V2V connections, we maximize the sum ergodic capacity of $M$ CUEs while guaranteeing the minimum reliability for each DUE. In addition, we set a minimum capacity requirement for each CUE as well to provide a minimum guaranteed QoS for them. The reliability of DUEs is guaranteed through controlling the probability of outage events, where its received SINR $\gamma_k^d$ is below a predetermined threshold $\gamma_0^d$. The ergodic capacity of CUEs is computed through the long-term average over the fast fading, which implies the codeword length spans several coherence periods over the time scale of slow fading [43]. It should be noted that how close the system performance can approach the ergodic capacity ultimately depends on the temporal variation of the vehicular channels as well as the tolerable delay. Faster variation induces more channel states within a given period, which makes the system performance approach the computed ergodic capacity quicker as the codeword needs to traverse most, if not all, channel states to average out the fading effects. To this end, the radio resource allocation problem in vehicular networks is formulated as

$$\max_{\substack{\{\rho_{m,k}\} \\ \{P_m^c\},\{P_k^d\}}} \sum_{m \in \mathcal{M}} \mathbb{E}\left[\log_2\left(1 + \gamma_m^c\right)\right] \tag{2.5}$$

$$\text{s. t.} \quad \mathbb{E}\left[\log_2(1 + \gamma_m^c)\right] \geq r_0^c, \forall m \in \mathcal{M} \tag{2.5a}$$

$$\Pr\{\gamma_k^d \leq \gamma_0^d\} \leq p_0, \forall k \in \mathcal{K} \tag{2.5b}$$

$$0 \leq P_m^c \leq P_{\max}^c, \forall m \in \mathcal{M} \tag{2.5c}$$

$$0 \leq P_k^d \leq P_{\max}^d, \forall k \in \mathcal{K} \tag{2.5d}$$

$$\sum_{m \in \mathcal{M}} \rho_{m,k} \leq 1, \rho_{m,k} \in \{0,1\}, \forall k \in \mathcal{K} \tag{2.5e}$$

$$\sum_{k \in \mathcal{K}} \rho_{m,k} \leq 1, \rho_{m,k} \in \{0,1\}, \forall m \in \mathcal{M}, \tag{2.5f}$$

where $r_0^c$ is the minimum capacity requirement of the data rate intensive CUEs and $\gamma_0^d$ is the minimum SINR needed by the DUEs to establish a reliable link. $\Pr\{\cdot\}$ evaluates the probability of the input and $p_0$ is the tolerable outage probability at the physical layer of the V2V links. $P_{\max}^c$ and $P_{\max}^d$ are the maximum transmit powers of the CUE and DUE, respectively. Constraints (2.5a) and (2.5b) represent the minimum capacity and reliability requirements for each CUE and DUE, respectively. (2.5c) and (2.5d) ensure that the transmit powers of CUEs and DUEs cannot go beyond their maximum limit. (2.5e) and (2.5f) mathematically model our assumption that the spectrum of one CUE can only be shared with a single DUE and one DUE is only allowed to access the spectrum of a single CUE. This assumption reduces the complexity brought by the complicated interference scenarios in D2D-enabled vehicular networks and serves as a good starting point to study the challenging resource allocation problem in vehicular networks.

The proposed optimization problem represents a novel formulation that factors in the unique features of time varying channels of vehicular communications as well as differentiated QoS requirements for V2I and V2V links. However, this is a highly nonconvex

optimization problem due to its combinatorial nature and the complicated objective function. We attempt to approach the optimization problem in (2.5) in two steps inspired by [23]. First, we exploit the separability of power allocation and spectrum reuse pattern design by noting that interference exists only within each CUE-DUE reuse pair as dictated by the constraints (2.5e) and (2.5f). Focusing on each pair of CUE-DUE, we study its optimal power allocation to maximize the ergodic capacity of the CUE with reliability guaranteed for the DUE. Second, we check the feasibility of each CUE-DUE pair against the minimum capacity requirement for the CUE, rule out infeasible pairs, and construct a bipartite graph to find the optimal spectrum sharing pattern between the sets of CUEs and DUEs using the Hungarian method [33]. We note that the proposed approach will lead to the globally optimal solution to the resource allocation problem in (2.5) since it can jointly find the optimal spectrum sharing pattern between CUEs and DUEs among all possible options and yield the best power control strategy for each reuse pair in an efficient way.

### 2.2.1 Power Allocation for Single CUE-DUE Pairs

In this part, we study the optimal power allocation for each possible DUE and CUE reuse pair. Given an arbitrary spectrum reuse pattern, e.g., the $k$th DUE sharing the band of the $m$th CUE, the power allocation problem for the single CUE-DUE pair is simplified into

$$\max_{P_m^c, P_k^d} \mathbb{E}\left[\log_2\left(1 + \gamma_m^c\right)\right] \tag{2.6}$$

$$\text{s.t. } \Pr\{\gamma_k^d \leq \gamma_0^d\} \leq p_0 \tag{2.6a}$$

$$0 \leq P_m^c \leq P_{\max}^c \tag{2.6b}$$

$$0 \leq P_k^d \leq P_{\max}^d, \tag{2.6c}$$

where the minimum capacity constraint for the CUE is temporarily left out and would be accounted for in the next step.

We evaluate the reliability constraint for the $k$th DUE in the following lemma, and then

visually depict the feasible regions of the simplified single pair power optimization problem described above.

**Lemma 1.** *The reliability constraint for the $k$th DUE, i.e. (2.6a) in the proposed single pair power allocation problem in (2.6), can be expressed as*

$$P_m^c \leq \frac{\alpha_k P_k^d}{\gamma_0^d \alpha_{m,k}} \left( \frac{e^{-\frac{\gamma_0^d \sigma^2}{P_k^d \alpha_k}}}{1 - p_0} - 1 \right) \triangleq f\left(P_k^d\right). \tag{2.7}$$

*Proof.* Given an arbitrary reuse pattern, e.g., $\rho_{m,k} = 1$, and substituting the channel model (2.1) in (2.6a), we derive the reliability constraint as

$$\Pr\{\gamma_k^d \leq \gamma_0^d\}$$

$$= \Pr\left\{ \frac{P_k^d \alpha_k g_k}{\sigma^2 + P_m^c \alpha_{m,k} g_{m,k}} \leq \gamma_0^d \right\}$$

$$= \int_0^\infty dg_{m,k} \int_0^{\frac{\gamma_0^d(\sigma^2 + P_m^c \alpha_{m,k} g_{m,k})}{P_k^d \alpha_k}} e^{-(g_k + g_{m,k})} dg_k$$

$$= 1 - \frac{P_k^d \alpha_k e^{-\frac{\gamma_0^d \sigma^2}{P_k^d \alpha_k}}}{P_k^d \alpha_k + \gamma_0^d P_m^c \alpha_{m,k}} \leq p_0, \tag{2.8}$$
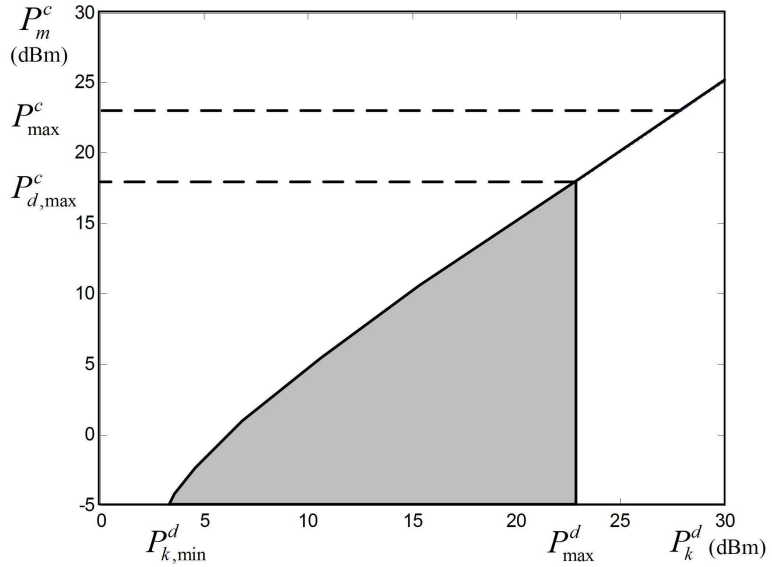
where we have assumed that $g_k$ and $g_{m,k}$ are independent and identically distributed (i.i.d.) exponential random variables with unit mean. Rearranging the terms from the last inequality completes the proof. $\qquad\square$

Considering $P_m^c \geq 0$ and from (2.7), we obtain the zero-crossing point by setting $f\left(P_k^d\right) = 0$ as[1]
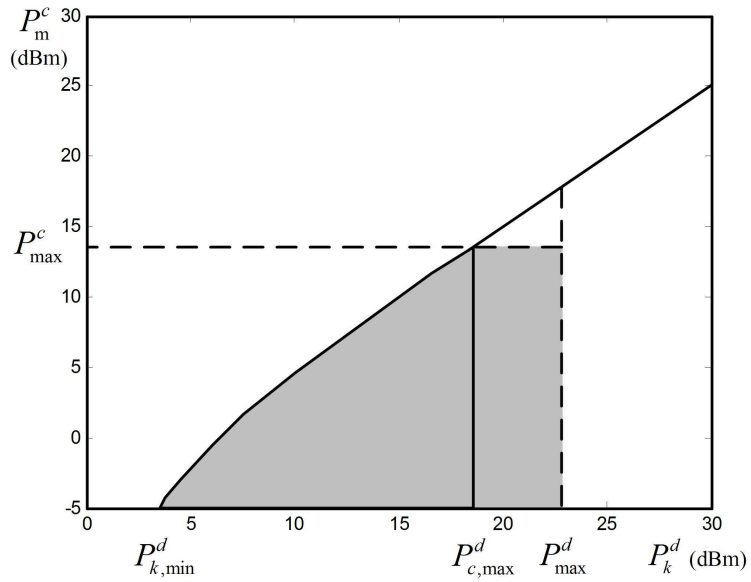
$$P_k^d = \frac{-\gamma_0^d \sigma^2}{\alpha_k \ln(1 - p_0)} \triangleq P_{k,\text{min}}^d. \tag{2.9}$$

It can be observed from (2.7) that $f\left(P_k^d\right)$ is monotonically increasing with respect to the

---

[1]The other zero-crossing point $P_k^d = 0$ is irrelevant here.

(a) The feasible region, Case I.



(b) The feasible region, Case II.

Figure 2.2: Two cases of feasible regions for (2.6) depending on the magnitudes of $P_{\max}^c$ and $P_{\max}^d$.

DUE power, $P_k^d$, in the range of $\left(P_{k,\min}^d, +\infty\right)$. This observation makes intuitive sense as an increase of the DUE power would lead to a higher interference margin, implying the DUE is more tolerable to interference from the CUE.

With the closed-form expression for reliability constraint (2.6a) given in Lemma 1, the

feasible regions of (2.6) are plotted in Fig. 2.2, where $P^c_{d,\max} = f\left(P^d_{\max}\right)$ and $P^d_{c,\max} = f^{-1}\left(P^c_{\max}\right)$. Note that $P^d_{c,\max}$ can be obtained through bisection search over the function $f(\cdot)$, which is a monotonically increasing function in the range of interest. As shown in the figure, the feasible regions are classified into two cases depending on the magnitudes of $P^c_{\max}$ and $P^d_{\max}$. We now derive the optimal solution to (2.6) in the following theorem.

**Theorem 1.** *The optimal power allocation solution to optimization problem* (2.6) *is given by*

$$P^{c^*}_m = \min(P^c_{max}, P^c_{d,max}),$$

*and*

$$P^{d^*}_k = \min(P^d_{max}, P^d_{c,max}). \tag{2.10}$$

*Proof.* Assuming that $g_{m,B}$ and $g_{k,B}$ are i.i.d. exponential random variables with unit mean, the ergodic capacity, $C_{m,k}(P^c_m, P^d_k)$, of the $m$th CUE in (2.6) when sharing the spectrum with the $k$th DUE can be written as

$$
\begin{aligned}
C_{m,k}(P^c_m, P^d_k) =& \mathbb{E}\left[\log_2(1+\gamma^c_m)\right] \\
=& \int_0^\infty \int_0^\infty \log_2\left(1 + \frac{P^c_m \alpha_{m,B} g_{m,B}}{\sigma^2 + P^d_k \alpha_{k,B} g_{k,B}}\right) \\
& \times e^{-(g_{m,B}+g_{k,B})} \mathrm{d}g_{m,B}\mathrm{d}g_{k,B}
\end{aligned} \tag{2.11}
$$

from which we can easily make the following observations

- With fixed $P^d_k$, the ergodic capacity $C_{m,k}(P^c_m, P^d_k)$ increases monotonically with $P^c_m$;

- With fixed $P^c_m$, the ergodic capacity $C_{m,k}(P^c_m, P^d_k)$ decreases monotonically with $P^d_k$.

These observations lead to the conclusion that the optimal solution of (2.6) can only reside at the upper boundary line of the feasible region defined by $P^c_m = f\left(P^d_k\right)$ from $(P^d_{k,\min}, 0)$

19

up to the point $(P_{\max}^d, P_{d,\max}^c)$ for Case I or $(P_{c,\max}^d, P_{\max}^c)$ for Case II in Fig. 2.2, by acknowledging the fact that $P_m^c = f\left(P_k^d\right)$ is a monotonically increasing function in the range of $(P_{k,\min}^d, +\infty)$.

What remains is to study the ergodic capacity $C_{m,k}(P_m^c, P_k^d)$ along the upper boundary line which could be done by substituting $P_m^c = f\left(P_k^d\right)$ in (2.11). The SINR term $\gamma_m^c$ is then given by

$$
\frac{P_m^c \alpha_{m,B} g_{m,B}}{\sigma^2 + P_k^d \alpha_{k,B} g_{k,B}}
$$

$$
= \frac{\alpha_k \alpha_{m,B} g_{m,B}}{\gamma_0^d \alpha_{m,k} \left(\frac{\sigma^2}{P_k^d} + \alpha_{k,B} g_{k,B}\right)} \left(\frac{e^{-\frac{\gamma_0^d \sigma^2}{P_k^d \alpha_k}}}{1 - p_0} - 1\right), \tag{2.12}
$$

which can be shown to monotonically increase with $P_k^d$ in the range $(P_{k,\min}^d, +\infty)$. Hence, the optimal power of the problem (2.6) is the intersection point $(P_{\max}^d, P_{d,\max}^c)$ for Case I or $(P_{c,\max}^d, P_{\max}^c)$ for Case II, which can be written in a compact form as in (2.10).

$\square$

Theorem 1 yields the optimal power allocation for a single CUE-DUE pair that maximizes ergodic capacity of the investigated CUE and ensures reliability for its reusing DUE. As mentioned earlier, interference exists only within each reuse pair and the original resource allocation problem in (2.5) to maximize the sum ergodic capacity of all CUEs has been decoupled into two major parts. The first part deals with the optimal power allocation for each single pair, which has been given by Theorem 1. The rest is to perform optimal spectrum reuse pair matching to maximize the sum ergodic capacity of CUEs while respecting all QoS constraints.

## 2.2.2  Pair Matching for All Vehicles

To this end, we have obtained the optimal power allocation for each CUE-DUE pair. In the next step, we need to eliminate those CUE-DUE combinations that do not satisfy

the minimum QoS requirement for the CUE, i.e., (2.5a), even when the optimal allocation scheme obtained from (2.10) is applied. The closed-form expression for the ergodic capacity of the $m$th CUE when sharing spectrum with the $k$th DUE, defined as $C_{m,k}\left(P_m^c, P_k^d\right) \triangleq \mathbb{E}\left[\log_2(1 + \gamma_m^c)\right]$, is derived in the following lemma.

**Lemma 2.** *The ergodic capacity, $C_{m,k}\left(P_m^c, P_k^d\right)$, of the $m$th CUE when sharing spectrum with the $k$th DUE is given by*

$$
\begin{aligned}
& C_{m,k}\left(P_m^c, P_k^d\right) \\
& = \frac{a}{(a-b)\ln 2}\left[e^{\frac{1}{a}}E_1\left(\frac{1}{a}\right) - e^{\frac{1}{b}}E_1\left(\frac{1}{b}\right)\right],
\end{aligned}
\tag{2.13}
$$

*where $a = \frac{P_m^c \alpha_{m,B}}{\sigma^2}$, $b = \frac{P_k^d \alpha_{k,B}}{\sigma^2}$, and $E_1(x) = \int_x^\infty \frac{e^{-t}}{t}dt$ is the exponential integral function of the first order [44].*

*Proof.* The ergodic capacity $C_{m,k}(P_m^c, P_k^d)$ can be written as

$$
\begin{aligned}
C_{m,k}(P_m^c, P_k^d) &= \mathbb{E}\left[\log_2\left(1 + \frac{P_m^c \alpha_{m,B} g_{m,B}}{\sigma^2 + P_k^d \alpha_{k,B} g_{k,B}}\right)\right] \\
&\triangleq \mathbb{E}\left[\log_2\left(1 + \frac{aX}{1 + bY}\right)\right],
\end{aligned}
\tag{2.14}
$$

where we denote $g_{m,B}$ and $g_{k,B}$ by $X$ and $Y$, respectively, and define $a = \frac{P_m^c \alpha_{m,B}}{\sigma^2}$ and $b = \frac{P_k^d \alpha_{k,B}}{\sigma^2}$. Defining $Z = \frac{aX}{1+bY}$ and assuming $g_{m,B}$ and $g_{k,B}$ are i.i.d. exponential random variables with unit mean, we have its CDF as

$$
\begin{aligned}
F_Z(z) &= \Pr\left\{\frac{aX}{1+bY} \leq z\right\} \\
&= \int_0^\infty \mathrm{d}y \int_0^{\frac{z(1+by)}{a}} e^{-(x+y)}\mathrm{d}x \\
&= 1 - e^{-\frac{z}{a}}\frac{a}{a+bz}.
\end{aligned}
\tag{2.15}
$$

21

Then, we obtain the ergodic capacity of the $m$th CUE as

$$
\begin{aligned}
& C_{m,k}(P_m^c, P_k^d) \\
& = \frac{1}{\ln 2} \int_0^\infty \ln(1+z) f_Z(z) \mathrm{d}z \\
& = \frac{1}{\ln 2} \int_0^\infty \frac{1 - F_Z(z)}{1+z} \mathrm{d}z \\
& = \frac{a}{(a-b)\ln 2} \left[ \int_0^\infty \frac{e^{-\frac{z}{a}}}{z+1} \mathrm{d}z - \int_0^\infty \frac{e^{-\frac{z}{a}}}{z+\frac{a}{b}} \mathrm{d}z \right] \\
& = \frac{a}{(a-b)\ln 2} \left[ e^{\frac{1}{a}} E_1\left(\frac{1}{a}\right) - e^{\frac{1}{b}} E_1\left(\frac{1}{b}\right) \right],
\end{aligned}
$$

(2.16)

(2.17)

where we obtain (2.16) by using integration by parts and (2.17) follows from [44, E-q. (3.352.4)].

□

Substituting the optimal power allocation (2.10) in (2.13) yields the maximum ergodic capacity achieved when the $m$th CUE shares its spectrum with the $k$th DUE, denoted as $C_{m,k}^*$. If it is less than $r_0^c$, then this combination cannot meet the minimum capacity requirement for the CUE. Therefore, such a CUE-DUE pair is not feasible and we set $C_{m,k}^* = -\infty$, i.e.,

$$
C_{m,k}^* = \begin{cases} C_{m,k}\left(P_m^{c*}, P_k^{d*}\right), & \text{if } C_{m,k}\left(P_m^{c*}, P_k^{d*}\right) \geq r_0^c, \\ -\infty, & \text{otherwise.} \end{cases}
$$

(2.18)

After evaluating all possible combinations of the CUE-DUE pairs, the resource alloca-

tion problem (2.5) reduces to

$$\max_{\{\rho_{m,k}\}} \sum_{m\in\mathcal{M}} \sum_{k\in\mathcal{K}} \rho_{m,k} C^*_{m,k} \tag{2.19}$$

$$\text{s.t.} \sum_{m\in\mathcal{M}} \rho_{m,k} \leq 1, \rho_{m,k} \in \{0,1\}, \forall k \in \mathcal{K} \tag{2.19a}$$

$$\sum_{k\in\mathcal{K}} \rho_{m,k} \leq 1, \rho_{m,k} \in \{0,1\}, \forall m \in \mathcal{M}, \tag{2.19b}$$

which turns out to be a maximum weight bipartite matching problem and can be efficiently solved by the Hungarian method in polynomial time [33].

From the above discussion, our algorithm to find the optimal solution to the resource allocation problem in (2.5) for D2D-enabled vehicular communications can be summarized in Table 2.1[2]. Supposing an accuracy of $\epsilon$ is required, the bisection search for the optimal power allocation of a single CUE-DUE pair as given in (2.10) requires $\log(1/\epsilon)$ iterations. This leads to the total complexity of $\mathcal{O}(KM \log(1/\epsilon))$ to compute the optimal power allocation for all CUE-DUE pairs. The Hungarian method will solve the pair matching problem in $\mathcal{O}(M^3)$ time assuming $M \geq K$. Therefore, the total complexity of the proposed algorithm is $\mathcal{O}(KM \log(1/\epsilon) + M^3)$.

## 2.3 Minimum CUE Capacity Maximization Design

The sum capacity maximization design considered in Section 2.2 can ensure a high overall throughput from the network operator's perspective. However, it tends to be unfair from each CUE's point of view, especially for those vehicles experiencing bad channel conditions. In such a case, the CUEs with bad channel conditions will be sacrificed in exchange for the overall performance improvement. In this section, we will address this issue by maximizing the minimum capacity among all CUEs so as to provide a more uniform per-

---

[2]There exist possible scenarios rendering the considered optimization problems infeasible. In such cases, the BS will report the infeasibility information and then initiate another round of user scheduling. The newly admitted users will then be serviced under the proposed RRM scheme.

Table 2.1: Optimal Resource Allocation Algorithm for (2.5) in D2D-Enabled Vehicular Communications

---

**Algorithm 1** Optimal Resource Allocation Algorithm for (2.5)

---

1: **for** $m = 1 : M$ **do**
2:   **for** $k = 1 : K$ **do**
3:     Obtain the optimal power allocation $(P_m^{c^*}, P_k^{d^*})$ from (2.10) for the single CUE-DUE pair.
4:     Substitute $(P_m^{c^*}, P_k^{d^*})$ into (2.13) to obtain $C_{m,k}^*$.
5:     **if** $C_{m,k}^* < r_0^c$ **then**
6:       $C_{m,k}^* = -\infty$.
7:     **end if**
8:   **end for**
9: **end for**
10: Use the Hungarian method [33] to find the optimal reuse pattern $\{\rho_{m,k}^*\}$ based on $\{C_{m,k}^*\}$.
11: Return the optimal spectrum reuse pattern $\{\rho_{m,k}^*\}$ and the corresponding power allocation $\{(P_m^{c^*}, P_k^{d^*})\}$.

---

formance across all CUEs.

The proposed optimization problem is stated as

$$\max_{\substack{\{\rho_{m,k}\} \\ \{P_m^c\},\{P_k^d\}}} \min_{m \in \mathcal{M}} \mathbb{E}\left[\log_2\left(1 + \gamma_m^c\right)\right] \tag{2.20}$$

$$\text{s.t.} \quad (2.5a) - (2.5f).$$

From [45] and [46], this max-min optimization problem is guaranteed to reach the Pareto boundary where none of the CUEs' ergodic capacity can be improved without degrading other CUEs' ergodic capacity. This is a key concept in multi-objective optimization (MOO) and the max-min formulation in (2.20) is in fact a special case of the weighted Chebyshev objective function with all weights set to one, which is the safest choice in converting MOO to single objective optimization (SOO) while ensuring Pareto optimality [45]. As such, the solution to the proposed problem can be guaranteed to be Pareto optimal.

### 2.3.1 Resource Allocation Design

To solve the proposed resource allocation problem in (2.20), we make use of the optimal power control results given in (2.10) for each CUE-DUE pair and the closed-form ergodic capacity for each CUE derived in (2.13), by acknowledging that interference only occurs within each CUE-DUE pair. Then the original problem in (2.20) is simplified into the following form

$$\max_{\{\rho_{m,k}\}} \min_{m \in \mathcal{M}} \sum_{k \in \mathcal{K}} \rho_{m,k} C^*_{m,k} \tag{2.21}$$

$$\text{s. t.} \quad \sum_{m \in \mathcal{M}} \rho_{m,k} \le 1, \rho_{m,k} \in \{0,1\}, \forall k \in \mathcal{K} \tag{2.21a}$$

$$\sum_{k \in \mathcal{K}} \rho_{m,k} \le 1, \rho_{m,k} \in \{0,1\}, \forall m \in \mathcal{M}. \tag{2.21b}$$

We further attempt to develop a low-complexity algorithm to solve the optimization problem in (2.21) through exploiting the Hungarian method, which has polynomial time computational complexity. The proposed optimal resource allocation algorithm is listed in Table 2.2 and comprises two essential parts.

The first part checks in polynomial time whether an arbitrarily given number $\tau$ is above the desired optimal minimum ergodic capacity or not. It operates as follows.

- Initialize an all-zero matrix $\mathbf{F}$ of size $M \times K$.

- Scan each element of the capacity matrix, $\{C^*_{m,k}\}$, obtained from Algorithm 1 and if it is less than $\tau$, set the corresponding entry of $\mathbf{F}$ to 1 and leave it as 0 otherwise, i.e., $\forall m, k$,

$$\mathbf{F}_{m,k} = \begin{cases} 1, & \text{if } \mathbf{C}^*_{m,k} < \tau, \\ 0, & \text{otherwise.} \end{cases} \tag{2.22}$$

- Apply the Hungarian method to $\mathbf{F}$ and return the lowest total cost, denoted as $c$,

i.e., the sum of all the assigned elements. If $c$ equals zero, all elements of such an assignment are no smaller than $\tau$, or equivalently, $\tau$ is less than or equal to the desired optimal minimum ergodic capacity. Correspondingly, if $c$ is greater than $0$, then there exists no assignment that guarantees that all the assigned elements are no smaller than $\tau$, i.e., $\tau$ is greater than the desired optimal minimum ergodic capacity.

The second part starts with ordering all $KM$ elements of the original capacity matrix, $\{C^*_{m,k}\}$, and then searches for the position of the optimal minimum ergodic capacity using bisection search based on the checking method derived in the first part. Finally, the spectrum sharing assignment is what the Hungarian method yields when the bisection search ends.

The major computational burden of the proposed algorithm lies in the generation of the capacity matrix, $\{C^*_{m,k}\}$, whose complexity is $\mathcal{O}\left(KM\log(1/\epsilon)\right)$, the ordering of all elements in $\{C^*_{m,k}\}$ whose complexity is $\mathcal{O}\left(KM\log(KM)\right)$, and the bisection search for the optimal value based on the Hungarian method with complexity $\mathcal{O}\left(M^3\log M\right)$ if $M \geq K$. Then the complexity of Algorithm 2 is $\mathcal{O}\left(KM\log(1/\epsilon) + KM\log(KM) + M^3\log M\right)$.

## 2.4  Simulation Results

In this section, simulation results are presented to validate the proposed spectrum and power allocation algorithms for D2D-enabled vehicular networks. We follow the simulation setup for the freeway case detailed in 3GPP TR 36.885 [10] and model a multi-lane freeway that passes through a single cell where the BS is located at its center as illustrated in Fig. 2.1. The vehicles are dropped on the roads according to spatial Poisson process and the vehicle density is determined by the vehicle speed. The $M$ CUEs and $K$ DUEs are randomly chosen among generated vehicles, where DUE pairs are always formed between neighboring vehicles and the CUEs are assumed to have equal shares of the total bandwidth. The major simulation parameters are listed in Table 2.3 and the channel models for V2I and V2V links are described in Table 2.4. Note that all parameters are set to the values spec-

Table 2.2: Optimal Resource Allocation Algorithm for (2.20) in D2D-Enabled Vehicular Communications

---

**Algorithm 2** Optimal Resource Allocation Algorithm for (2.20)

---

1: Initialize $\{C_{m,k}^*\}$ and $\{(P_m^{c^*}, P_k^{d^*})\}$ from Algorithm 1.
2: Initialize $i = 1$ and $j = KM$.
3: Sort all elements of $\{C_{m,k}^*\}$ in ascending order and store them in a vector $\mathbf{v}$.
4: **while** $(j - i) > 1$ **do**
5:     $l = (i + j)/2$;
6:     $\mathbf{F} = \mathbf{0}_{M \times K}$;
7:     **for** $m = 1 : M$ **do**
8:       **for** $k = 1 : K$ **do**
9:         **if** $C_{m,k}^* < \mathbf{v}_l$ **then**
10:          $\mathbf{F}_{m,k} = 1$;
11:        **else**
12:          $\mathbf{F}_{m,k} = 0$;
13:        **end if**
14:       **end for**
15:     **end for**
16:     Apply the Hungarian method [33] to find the assignment, denoted as $\mathbf{A}$, and the lowest total cost, denoted as $c$, based on the matrix $\mathbf{F}$.
17:     **if** $c > 0$ **then**
18:       $j = l$;
19:     **else**
20:       $i = l$;
21:       $\{\rho_{m,k}^*\} = \mathbf{A}$;
22:     **end if**
23: **end while**
24: Return the optimal spectrum reuse pattern $\{\rho_{m,k}^*\}$ and the corresponding power allocation $\{(P_m^{c^*}, P_k^{d^*})\}$.

---

ified in Tables 2.3 and 2.4 by default, whereas the settings in each figure take precedence wherever applicable. The results in each figure are obtained from averaging a minimum of $10,000$ channel realizations and in particular, Fig. 2.4 is plotted with $1,000,000$ channel realizations.

Fig. 2.3 demonstrates the sum and minimum ergodic capacities of CUEs achieved by our proposed algorithms with respect to a genie-aided benchmark based on a modified

Table 2.3: Simulation Parameters [10, 47]
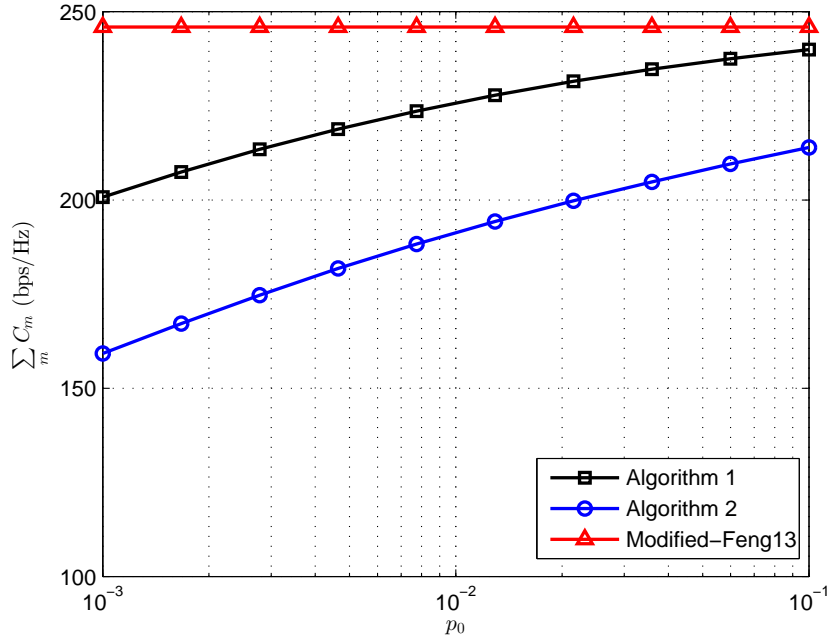
| Parameter | Value |
|---|---|
| Carrier frequency | 2 GHz |
| Bandwidth | 10 MHz |
| Cell radius | 500 m |
| BS antenna height | 25 m |
| BS antenna gain | 8 dBi |
| BS receiver noise figure | 5 dB |
| Distance between BS and highway | 35 m |
| Vehicle antenna height | 1.5 m |
| Vehicle antenna gain | 3 dBi |
| Vehicle receiver noise figure | 9 dB |
| Absolute vehicle speed $v$ | 70 km/h |
| Vehicle drop model | spatial Poisson process |
| Number of lanes | 3 in each direction (6 in total) |
| Lane width | 4 m |
| Vehicle density | Average inter-vehicle distance is 2.5 sec $\times$ absolute vehicle speed. |
| Minimum capacity of DUE $r_0^c$ | 0.5 bps/Hz |
| SINR threshold for DUE $\gamma_0^d$ | 5 dB |
| Reliability for DUE $p_0$ | 0.001 |
| Number of DUEs $K$ | 20 |
| Number of CUEs $M$ | 20 |
| Maximum CUE transmit power $P_{\max}^c$ | 17, 23 dBm |
| Maximum DUE transmit power $P_{\max}^d$ | 17, 23 dBm |
| Noise power $\sigma^2$ | -114 dBm |
| Bisection search accuracy $\epsilon$ | $10^{-5}$ |

Table 2.4: Channel Models for V2I and V2V Links [10]
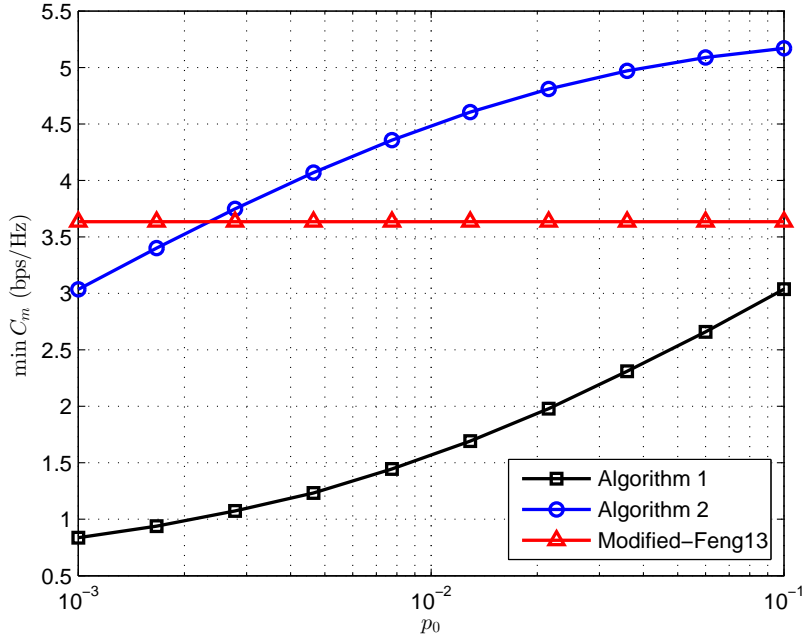
| Parameter | V2I Link | V2V Link |
|---|---|---|
| Pathloss model | $128.1 + 37.6\log_{10} d$, $d$ in km | LOS in WINNER + B1 [48] |
| Shadowing distribution | Log-normal | Log-normal |
| Shadowing standard deviation $\xi$ | 8 dB | 3 dB |
| Fast fading | Rayleigh fading | Rayleigh fading |

traditional D2D resource allocation scheme developed in [23][3], where accurate knowledge

---

[3]The modification lies in replacing the original objective function to maximize the sum throughput of both CUEs and DUEs with the one to maximize the sum throughput of CUEs only, and the capacity and reliability

(a) Sum ergodic capacity of CUEs.
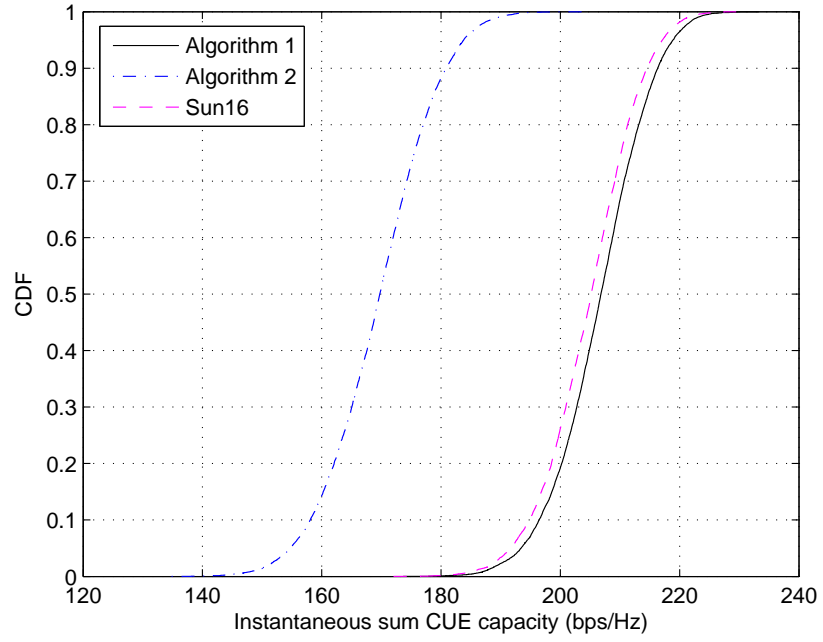


(b) Minimum ergodic capacity of CUEs.

Figure 2.3: Capacity performance of CUEs with varying DUE outage probability $p_0$, assuming $P_{\max}^d = P_{\max}^c = 23$ dBm.

---
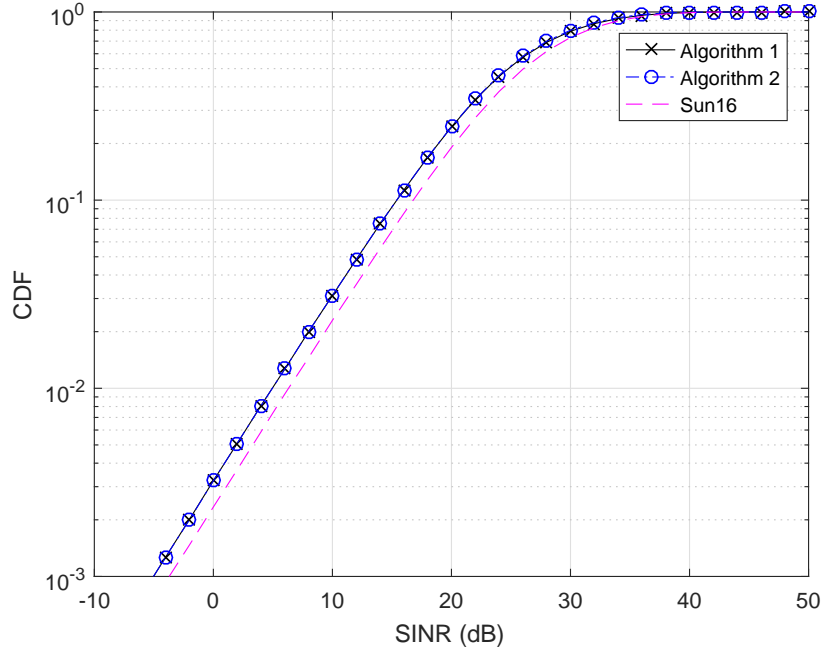
constraints are equivalently transformed into SINR requirements. The same three-step method is then applied to solve the RRM problem.

of instantaneous CSI for all links is assumed to be perfectly known at the BS. We note that in high speed vehicular environments, such full CSI assumption is by no means realistic, but it serves as an ideal reference to benchmark our proposed algorithms. It is observed that both sum and minimum ergodic capacities of CUEs achieved by both Algorithms 1 and 2 get larger if higher outage probability of DUEs is allowed. This is due to the fact that higher acceptable outage of DUEs renders them more tolerable to interference from CUEs, thus encouraging CUEs to increase their transmit powers. As a result, the CUE capacity grows larger. From Fig. 2.3(a), the performance of Algorithm 1 is well close to the ideal benchmark scheme in terms of sum capacity at fairly low outage probability, e.g., $p_0 = 0.1$. As for the minimum CUE capacity shown in Fig. 2.3(b), Algorithm 2 shows superior performance even over the ideal benchmark when the acceptable outage is a bit larger than $0.001$. These are encouraging findings as the proposed resource allocation schemes make use of slowly varying large-scale fading parameters only and update every few hundred milliseconds. Nonetheless, they can achieve performance measurably close to the genie-aided benchmark scheme (or even surpass it if minimum capacity maximization is pursued), which requires accurate real-time CSI of all links and is inapplicable in a vehicular environment featuring high mobility.

To demonstrate the superiority of our proposed scheme when only large-scale fading information is available at the BS, we compare in Fig. 2.4(a) the cumulative distribution functions (CDF) of the instantaneous sum CUE capacity achieved by Algorithms 1 and 2 against the SOLEN scheme developed in [27]. To achieve fair comparison, we exploit the method given in Lemma 1 of [27] to generate an equivalent SINR threshold expressed in terms of large-scale fading parameters only. In addition, the minimum capacity requirement in the original problem formulation is not considered as there is no convenient way to convert such a constraint into an equivalent form to be used for the SOLEN scheme. We observe that the proposed Algorithm 1 achieves strictly better performance than the SOLEN scheme of [27] while Algorithm 2 has the worst performance when the maximum sum CUE

(a) Sum ergodic capacity of CUEs.
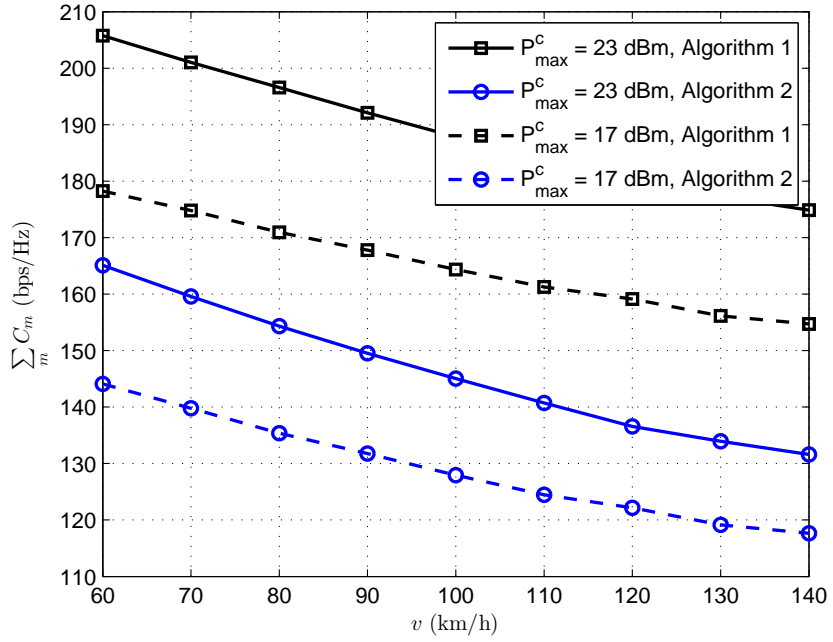


(b) SINR of an arbitrary DUE.
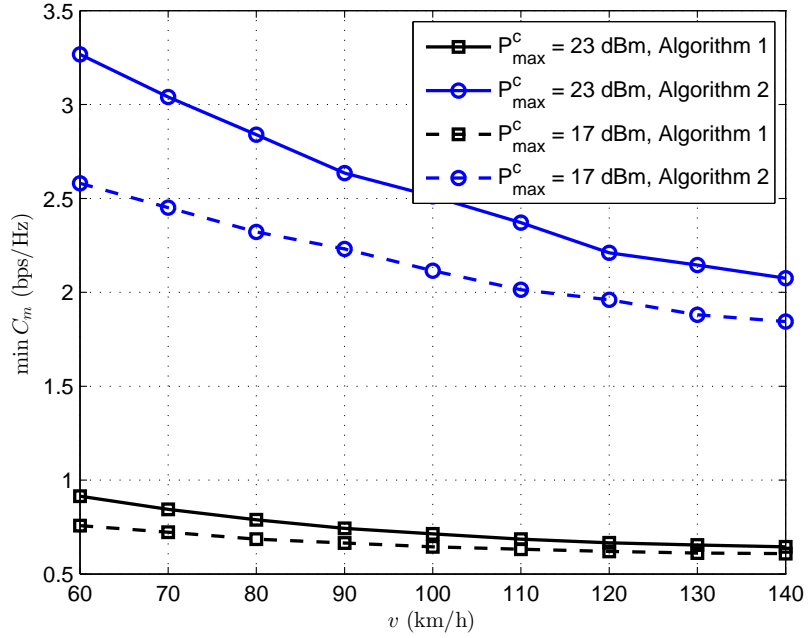
Figure 2.4: CDF of instantaneous system performance with Rayleigh fading, assuming $P_{\max}^d = P_{\max}^c = 23$ dBm, and targeted outage probability $p_0 = 0.01$.

capacity is the system metric. This validates the superior performance of the proposed Algorithm 1 in such cases. The reason for the performance gain of Algorithm 1 is twofold. The first is that Algorithm 1 takes a rigorous treatment of the small-scale fading effect when computing the capacity of V2I links, i.e., calculating the ergodic capacity in contrast to using only large-scale fading parameters to approximate the capacity as in [27]. The second reason is that the approach taken in [27] is not able to achieve exactly the targeted SINR threshold of V2V links, as illustrated in Fig. 2.4(b), where an arbitrarily chosen DUE's instantaneous SINR of SOLEN is found to slightly exceed $5$ dB (the desired threshold) at the targeted outage probability of $0.01$. Meanwhile, our proposed Algorithms 1 and 2 achieve exactly $5$ dB at the outage probability of $0.01$. This translates to stricter reliability requirements of V2V links in SOLEN, thus reducing the feasible region of power control parameters and degrading the capacity of V2I links. These two aspects also form the major differences between our proposed algorithms and the existing one in [27]. However, we also notice that the performance gain of Algorithm 1 is minimal, which might be due to the insensitivity of capacity to the small-scale fading effect and the fact that the SINR overshooting of SOLEN is essentially small.

Fig. 2.5 shows the sum and minimum ergodic capacities of all CUEs with an increasing vehicle speed on the road, respectively. From the figures, both sum and minimum CUE capacities decrease as the vehicles move faster. This is because higher speed induces sparser traffic according to the simulation setup, which would on average increase inter-vehicle distance and give rise to less reliable V2V links with lower received power. As such, less interference from CUEs can be tolerated given the maximum transmit power constraints of DUEs, which leads to less power being allocated to CUEs and decreases both their sum and minimum ergodic capacities. It also reveals that Algorithm 1 achieves higher sum ergodic capacity than Algorithm 2 while the reverse is true when comparing the minimum ergodic capacity. This makes sense since Algorithm 1 aims to maximize the sum ergodic capacity while Algorithm 2 takes the minimum ergodic capacity as its design objective. It is also in-

(a) Sum ergodic capacity of CUEs.
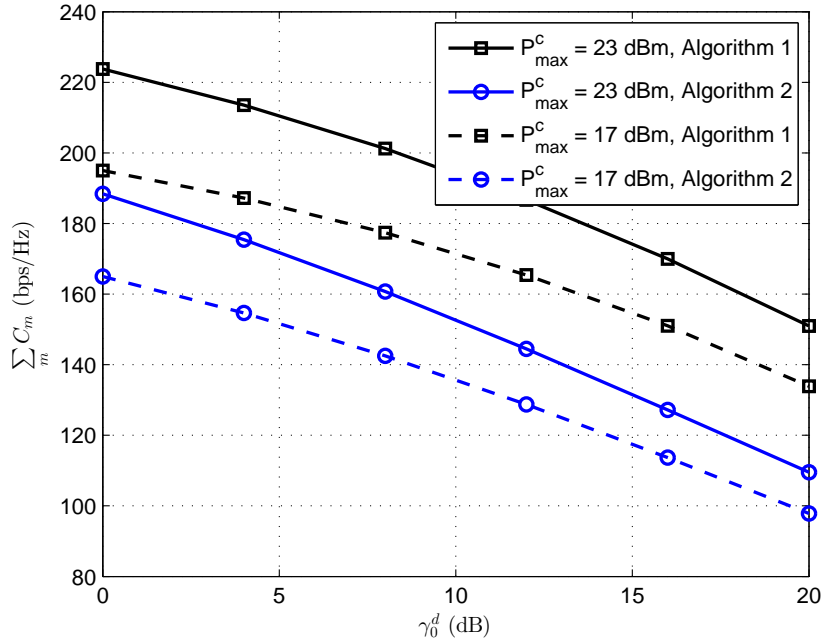


(b) Minimum ergodic capacity of CUEs.

Figure 2.5: Capacity performance of CUEs with varying vehicle speed $v$ on the highway, assuming $P_{\max}^d = P_{\max}^c$.
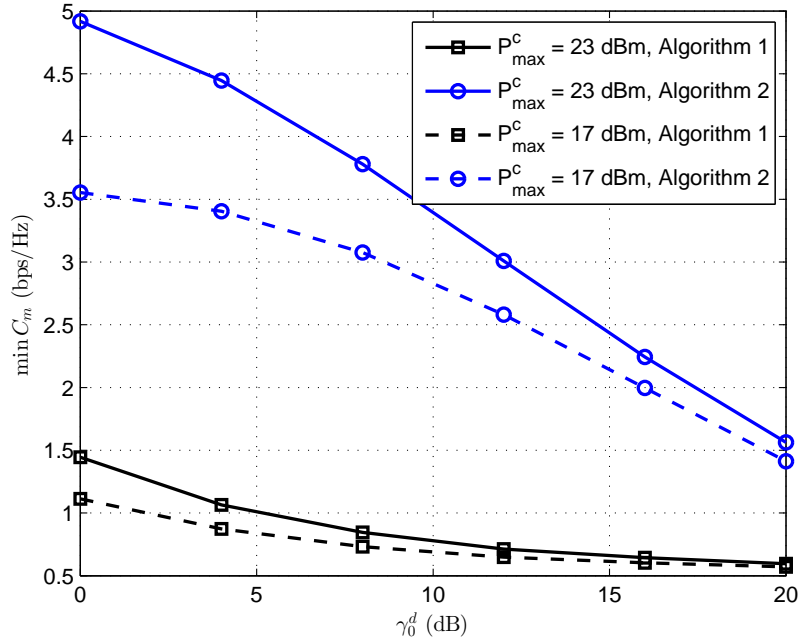
teresting to note in Fig. 2.5(a) that an increase of maximum transmit power has a relatively constant impact on the sum CUE capacity performance of both Algorithms 1 and 2 with respect to the vehicle speed increase. However, this does not hold when we investigate the minimum CUE capacity as shown in Fig. 2.5(b). At a low vehicle speed, a 6 dBm increase of the maximum transmit power brings significant gains for both Algorithms 1 and 2, e.g., some $40\%$ increase at $60$ km/h. In contrast, at a very high speed, e.g., $140$ km/h, the power increase has limited impact, which is especially true when we focus on Algorithm 1 in Fig. 2.5(b).

Fig. 2.6 demonstrates the sum and minimum ergodic capacities of CUEs with respect to increasing SINR threshold for DUEs, respectively. We observe that in both cases, the investigated ergodic capacity will decrease when the minimum QoS requirement for DUEs grows large. Such performance degradation results from the reduced interference tolerability of DUEs due to an increase in their required SINR threshold, which will impose stricter constraints on the allowable transmit power of the pairing CUEs. Reduced transmit power of CUEs directly translates into a decrease of the sum and minimum ergodic capacities they are capable of achieving given all QoS constraints satisfied. It is also observed that a 6 dBm increase of maximum transmit power has roughly uniform impact on the sum CUE capacity with respect to growing $\gamma_0^d$ while for the minimum CUE capacity, the impact gets smaller with increasing $\gamma_0^d$.

Fig. 2.7 shows the impact of the number of active V2V links on the quality of V2I connections. From the figures, as there are more and more V2V links sharing V2I's spectrum, both the sum and minimum CUE capacities decrease due to the growing amount of interference generated from V2V links. From Fig. 2.7(a), Algorithm 2 is more sensitive to the change of V2V numbers in terms of sum CUE capacity as evidenced from the steep slope of its sum capacity curve. As for the minimum CUE capacity in Fig. 2.7(b), Algorithm 1 achieves dramatically degrading performance at first, e.g., around $50\%$ decrease when $K/M$ is doubled from $0.1$ to $0.2$. Then the performance gradually flattens. This
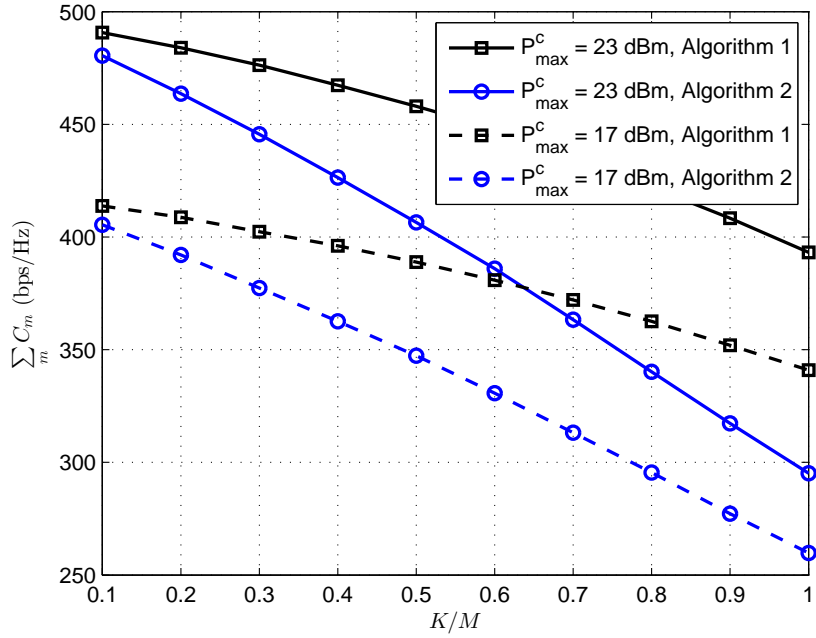
(a) Sum ergodic capacity of CUEs.
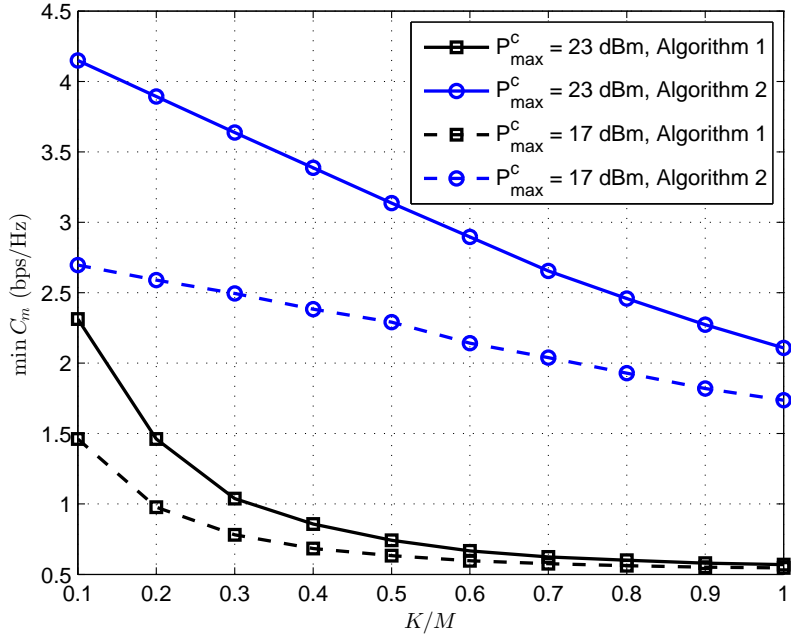


(b) Minimum ergodic capacity of CUEs.

Figure 2.6: Capacity performance of CUEs with varying DUE SINR threshold $\gamma_0^d$, assuming $P_{\max}^d = P_{\max}^c$.

(a) Sum ergodic capacity of CUEs.



(b) Minimum ergodic capacity of CUEs.

Figure 2.7: Capacity performance of CUEs with varying number of DUEs, assuming $P_{\max}^{d} = P_{\max}^{c}$ and $M = 40$.

is in contrast to Algorithm 2, where the minimum CUE capacity performance degrades gracefully with respect to growing interference generated from increasing numbers of V2V links. Again, it is worth pointing out that a $6$ dBm increase of maximum transmit power uniformly increases the sum CUE capacity with respect to growing $K/M$ while the impact gets weaker for the minimum CUE capacity with increasing number of active V2V links.

## 2.5 Summary

In this chapter, we have investigated the spectrum sharing and power allocation design for D2D-enabled vehicular networks. Due to fast channel variations arising from high vehicle mobility, instantaneous CSI is hard to track in practice, rendering traditional resource allocation schemes for D2D-based cellular networks requiring full CSI inapplicable. To address this issue, we have taken into account the differentiated QoS requirements of vehicular communications and formulated optimization problems aiming to design a resource allocation scheme based on slowly varying large-scale fading information only. Robust algorithms have been proposed to maximize the sum and minimum ergodic capacity of V2I links, respectively while ensuring reliability for all V2V links.

# CHAPTER 3

# SPECTRUM AND POWER ALLOCATION WITH DELAYED CSI FEEDBACK

In this chapter, we continue the study of resource allocation for vehicular communications, yet from another perspective. That is, we explore the communication performance when channel state information (CSI) of vehicular links is periodically reported to the base station (BS). We take into account the inevitable CSI latency during feedback in high-mobility vehicular environments. The proposed resource allocation problem incorporates heterogeneous quality-of-service (QoS) requirements for vehicle-to-infrastructure (V2I) and vehicle-to-vehicle (V2V) links corresponding to their supported services, i.e., large capacity for V2I links and high reliability for V2V links. Sum V2I throughput is maximized with a minimum QoS guarantee for both V2I and V2V links, where the V2V reliability is ensured by maintaining the outage probability of received signal-to-interference-plus-noise ratio (SINR) below a small threshold.

The rest of the chapter is organized as follows. Section 3.1 introduces the system model. Section 3.2 develops robust resource allocation schemes for vehicular communications with delayed CSI feedback. Simulation results are presented in Section 3.3 and concluding remarks are finally made in Section 3.4.

## 3.1 System Model

Consider a device-to-device (D2D)-enabled vehicular communication network as shown in Fig. 3.1, where $M$ vehicles require high-capacity V2I communications, denoted as I-UEs, and $K$ pairs of vehicles perform local V2V data exchange in the form of D2D communications, denoted as V-UEs. Denote the I-UE set as $\mathcal{M} = \{1, \cdots, M\}$ and the V-UE set as $\mathcal{K} = \{1, \cdots, K\}$. To improve spectrum utilization efficiency, orthogonally allocated uplink spectrum of I-UEs is reused by the V-UEs. The channel power gain, $g_{m,B}$, between

38
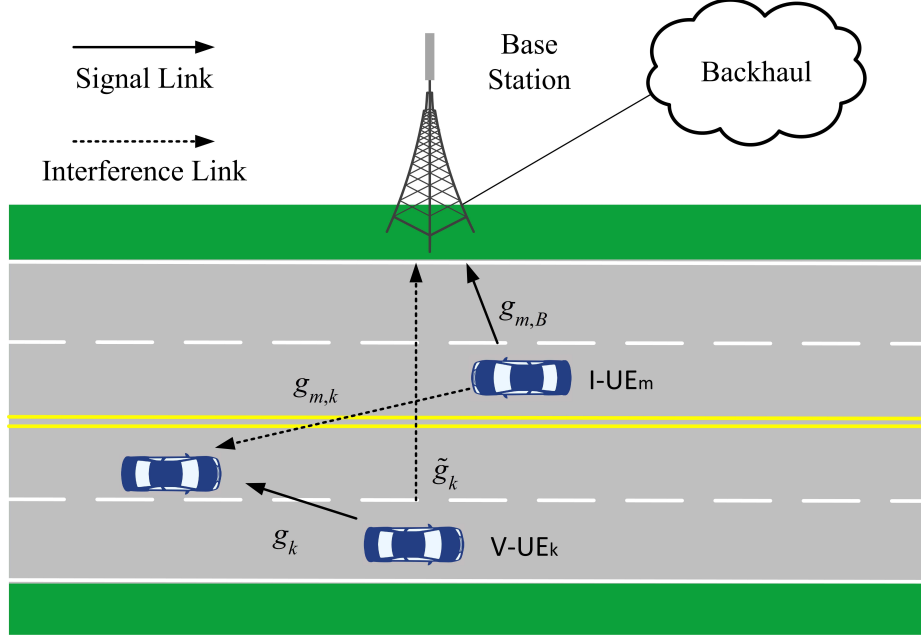
Figure 3.1: D2D-enabled vehicular communications.

the $m$th I-UE and the BS follows

$$g_{m,B} = |h_{m,B}|^2 \alpha_{m,B}, \tag{3.1}$$

where $h_{m,B}$ is the small-scale fast fading component, assumed to be independent and identically distributed (i.i.d.) distributed as $\mathcal{CN}(0,1)$, and $\alpha_{m,B}$ captures all large-scale fading effects including path loss and shadowing. The channel, $g_k$, between the $k$th V2V pair, the interfering channel, $\tilde{g}_k$, from the $k$th V-UE to the BS, and the interfering channel, $g_{m,k}$, from the $m$th I-UE to the $k$th V-UE are similarly defined.

We assume CSI of links connected to the BS, i.e., $g_{m,B}$ and $\tilde{g}_k$, is accurately known since it can be estimated at the BS while CSI of vehicular links, i.e., $g_k$ and $g_{m,k}$, is reported to the BS with a feedback period $T$ and therefore with latency. We use a first-order Gauss-Markov process [49] to model the channel variation (fast fading) over the period $T$

$$h = \epsilon \hat{h} + e, \tag{3.2}$$

where $\hat{h}$ and $h$ are the channels in the previous and current time, respectively, $e$ is the channel discrepancy term distributed according to $\mathcal{CN}(0, 1 - \epsilon^2)$ and independent of $\hat{h}$, and the coefficient $\epsilon$ quantifies channel correlation between the two consecutive time slots. For the Jakes' model [49], $\epsilon$ is given by $\epsilon = J_0(2\pi f_d T)$, where $J_0(\cdot)$ is the zero-order Bessel function of the first kind and $f_d = v f_c / c$ is the maximum Doppler frequency with $c = 3 \times 10^8$ m/s, $v$ being the vehicle speed, and $f_c$ being the carrier frequency.

The SINRs of the $m$th I-UE and $k$th V-UE are given by

$$\gamma_m^c = \frac{P_m^c \alpha_{m,B} |h_{m,B}|^2}{\sigma^2 + \sum\limits_{k=1}^{K} \rho_{m,k} P_k^d \tilde{\alpha}_k |\tilde{h}_k|^2} \tag{3.3}$$

and

$$\gamma_k^d = \frac{P_k^d \alpha_k \left( \epsilon_k^2 |\hat{h}_k|^2 + |e_k|^2 \right)}{\sigma^2 + \sum\limits_{m=1}^{M} \rho_{m,k} P_m^c \alpha_{m,k} \left( \epsilon_{m,k}^2 |\hat{h}_{m,k}|^2 + |e_{m,k}|^2 \right)}, \tag{3.4}$$

respectively, where $P_m^c$ and $P_k^d$ denote transmit powers of the $m$th I-UE and the $k$th V-UE, respectively, $\sigma^2$ is the noise power, and $\rho_{m,k} = 1$ indicates the $k$th V-UE reuses the spectrum of the $m$th I-UE and $\rho_{m,k} = 0$ otherwise.

To meet diverse requirements for different vehicular links, i.e., large capacity for V2I connections and high reliability for V2V connections, we maximize the sum capacity of $M$ I-UEs while guaranteeing the minimum reliability for each V-UE. In addition, we set a minimum capacity requirement for each I-UE as well to provide a minimum guaranteed

QoS for them. The optimization problem is formulated as

$$\max_{\substack{\{\rho_{m,k}\} \\ \{P_k^d\}, \{P_m^c\}}} \quad \sum_{m \in \mathcal{M}} \log_2\left(1 + \gamma_m^c\right) \tag{3.5}$$

$$\text{s. t.} \quad \log_2(1 + \gamma_m^c) \geq r_0^c, \forall m \in \mathcal{M} \tag{3.5a}$$

$$\Pr\{\gamma_k^d \leq \gamma_0^d\} \leq p_0, \forall k \in \mathcal{K} \tag{3.5b}$$

$$0 \leq P_m^c \leq P_{\max}^c, \forall m \in \mathcal{M} \tag{3.5c}$$

$$0 \leq P_k^d \leq P_{\max}^d, \forall k \in \mathcal{K} \tag{3.5d}$$

$$\sum_{m \in \mathcal{M}} \rho_{m,k} \leq 1, \rho_{m,k} \in \{0,1\}, \forall k \in \mathcal{K} \tag{3.5e}$$

$$\sum_{k \in \mathcal{K}} \rho_{m,k} \leq 1, \rho_{m,k} \in \{0,1\}, \forall m \in \mathcal{M}, \tag{3.5f}$$

where $r_0^c$ is the minimum capacity requirement of I-UEs and $\gamma_0^d$ is the minimum SINR needed by the V-UEs to establish a reliable link. $\Pr\{\cdot\}$ evaluates the probability of the input and $p_0$ is the tolerable outage probability. $P_{\max}^c$ and $P_{\max}^d$ are the maximum transmit powers of the I-UE and V-UE, respectively. (3.5a) and (3.5b) represent the minimum capacity and reliability requirements for each I-UE and V-UE, respectively, where the probability is evaluated in terms of the discrepancy term $e$ caused by the delay in CSI feedback. (3.5c) and (3.5d) ensure that the transmit powers of I-UEs and V-UEs cannot exceed the maximum limit. (3.5e) and (3.5f) mathematically model our assumption that one I-UE's spectrum can only be shared with a single V-UE and one V-UE is only allowed to access a single I-UE's spectrum. This assumption reduces the complexity brought by the complicated interference scenarios in D2D-enabled vehicular networks and serves as a good starting point to study the resource allocation problem in vehicular networks.

## 3.2 Robust Resource Allocation Design

3.2.1 Power Allocation for Single I-UE and V-UE Pairs

Decoupling the problem and focusing on each I-UE and V-UE pair, we aim to maximize the I-UE's capacity

$$C_{m,k} = \log_2 \left( 1 + \frac{P_m^c \alpha_{m,B} |h_{m,B}|^2}{\sigma^2 + P_k^d \tilde{\alpha}_k |\tilde{h}_k|^2} \right) \tag{3.6}$$

while satisfying all constraints, formulated as

$$\max_{P_k^d, P_m^c} \quad C_{m,k} \tag{3.7}$$

$$\text{s. t. } (3.5\text{b}), (3.5\text{c}), (3.5\text{d})$$

**Lemma.** *The feasible region of* (3.7) *is derived as*

$$\left\{ (P_k^d, P_m^c) : \exp \left( \frac{C\gamma_0^d}{B} \right) \left( 1 + \frac{D}{B}\gamma_0^d \right) \leq \frac{\exp \left( \frac{A}{B} \right)}{1 - p_0}, \right.$$
$$\left. C\gamma_0^d \geq A, 0 \leq P_m^c \leq P_{max}^c, 0 \leq P_k^d \leq P_{max}^d \right\}, \tag{3.8}$$

*or*

$$\left\{ (P_k^d, P_m^c) : \left( 1 + \frac{B}{\gamma_0^d D} \right) \exp \left( \frac{A - C\gamma_0^d}{\gamma_0^d D} \right) \geq \frac{1}{p_0}, \right.$$
$$\left. C\gamma_0^d < A, 0 \leq P_m^c \leq P_{max}^c, 0 \leq P_k^d \leq P_{max}^d \right\}, \tag{3.9}$$

*where* $A = P_k^d \alpha_k \epsilon_k^2 |\hat{h}_k|^2, B = P_k^d \alpha_k (1 - \epsilon_k^2), C = \sigma^2 + P_m^c \alpha_{m,k} \epsilon_{m,k}^2 |\hat{h}_{m,k}|^2$, *and* $D = P_m^c \alpha_{m,k}(1 - \epsilon_{m,k}^2)$.

*Proof.* The received SINR at the $k$th V-UE, $\gamma_k^d$, from (3.4) can be written as $\gamma_k^d = \frac{A+BX}{C+DY}$, where $X$ and $Y$ are two independent exponential random variables with unit mean. Two

42

cases are identified to evaluate V2V reliability $\Pr\{\gamma_k^d \le \gamma_0^d\}$:

- Case I: When $C\gamma_0^d \ge A$,

$$\Pr\{\gamma_k^d \le \gamma_0^d\} = \int_0^\infty \exp(-y)\mathrm{d}y \int_0^{\frac{(C+Dy)\gamma_0^d - A}{B}} \exp(-x)\mathrm{d}x$$

$$= 1 - \frac{\exp\left(-\frac{C\gamma_0^d - A}{B}\right)}{1 + \frac{D}{B}\gamma_0^d} \le p_0. \tag{3.10}$$

- Case II: When $C\gamma_0^d < A$,

$$\Pr\{\gamma_k^d \le \gamma_0^d\} = \int_0^\infty \exp(-x)\mathrm{d}x \int_{\frac{A+Bx-C\gamma_0^d}{D\gamma_0^d}}^\infty \exp(-y)\mathrm{d}y$$

$$= \frac{\exp(\frac{C}{D})}{\left(1 + \frac{B}{\gamma_0^d D}\right)\exp(\frac{A}{\gamma_0^d D})} \le p_0. \tag{3.11}$$

Rearranging terms of (3.10) and (3.11) completes the proof. $\qquad\square$

Based on the *Lemma*, we derive the optimal power allocation solution to (3.7) in the following *Theorem*.

**Theorem.** *The optimal power allocation solution to* (3.7) *is*

$$P_k^{d*} = \begin{cases} \min\{P_{max}^d, P_{c_1,max}^d\}, & \text{if } P_{max}^d \le P_0^d, \\[2mm] \min\{P_{max}^d, P_{c_2,max}^d\}, & \text{if } P_{max}^d > P_0^d \text{ and } P_{max}^c > P_0^c, \\[2mm] P_{c_1,max}^d, & \text{otherwise} \end{cases}$$

*and*

$$P_m^{c*} = \begin{cases} \min\{P_{max}^c, P_{d_1,max}^c\}, & \text{if } P_{max}^d \le P_0^d, \\[2mm] \min\{P_{max}^c, P_{d_2,max}^c\}, & \text{if } P_{max}^d > P_0^d \text{ and } P_{max}^c > P_0^c, \\[2mm] P_{max}^c, & \text{otherwise,} \end{cases}$$

*where*

$$P_0^c = \frac{\sigma^2}{\frac{1-\epsilon_{m,k}^2}{1-\epsilon_k^2}\left(\frac{1}{p_0}-1\right)\alpha_{m,k}\epsilon_k^2|\hat{h}_k|^2 - \alpha_{m,k}\epsilon_{m,k}^2|\hat{h}_{m,k}|^2},$$

*and*

$$P_0^d = \frac{P_0^c\gamma_0^d\alpha_{m,k}(1-\epsilon_{m,k}^2)(1-p_0)}{\alpha_k(1-\epsilon_k^2)p_0}.$$

$P_{c_1,max}^d$ *and* $P_{d_1,max}^c$ *are derived from the implicit functions*

$$F_1(P_{c_1,max}^d, P_{max}^c) = 0 \quad and \quad F_1(P_{max}^d, P_{d_1,max}^c) = 0,$$

$P_{c_2,max}^d$ *and* $P_{d_2,max}^c$ *are derived from the implicit functions*

$$F_2(P_{c_2,max}^d, P_{max}^c) = 0 \quad and \quad F_2(P_{max}^d, P_{d_2,max}^c) = 0,$$

*through bisection search by noting the monotonic relation between* $P_m^c$ *and* $P_k^d$ *in the implicit functions*

$$F_1(P_k^d, P_m^c) = \exp\left(\frac{C\gamma_0^d}{B}\right)\left(1 + \frac{D}{B}\gamma_0^d\right) - \frac{\exp\left(\frac{A}{B}\right)}{1-p_0} = 0$$

*when* $P_k^d \in (0, P_0^d)$ *and*

$$F_2(P_k^d, P_m^c) = \left(1 + \frac{B}{\gamma_0^d D}\right)\exp\left(\frac{A - C\gamma_0^d}{\gamma_0^d D}\right) - \frac{1}{p_0} = 0,$$

*when* $P_k^d \in (P_0^d, +\infty)$.

*Proof.* We provide a brief sketch for the proof. From the *Lemma*, the feasible region of (3.7) is divided into two parts, depending on if $C\gamma_0^d \geq A$ or not, with an example given in Fig. 3.2. Further analysis shows that the two regions's upper boundaries (as determined
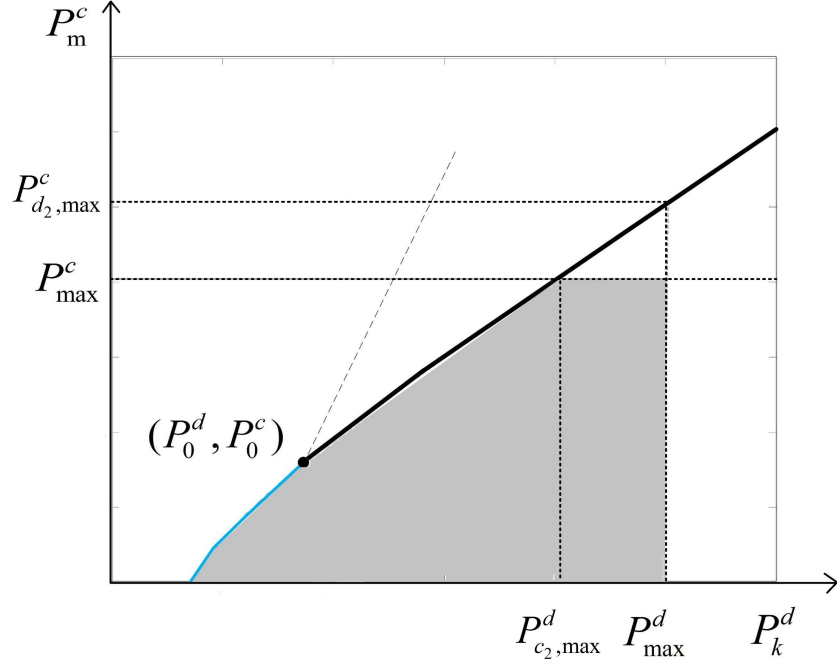
Figure 3.2: A sample feasible region depiction.

by implicit functions $F_1(P_k^d, P_m^c) = 0$ and $F_2(P_k^d, P_m^c) = 0$, respectively) intersect at $(P_0^d, P_0^c)$, which lies on the separating line $C\gamma_0^d = A$. In addition, $F_1(P_k^d, P_m^c) = 0$ and $F_2(P_k^d, P_m^c) = 0$ maintains a monotonically increasing relation between $P_m^c$ and $P_k^d$ in the range $(0, P_0^d)$ and $(P_0^d, +\infty)$, respectively. We note that the I-UE's capacity, or equivalently $\gamma_m^c$, increases with $P_m^c$ and decreases with $P_k^d$. Hence, the optimal solution must reside at the upper boundary of the feasible region, which is a continuous line jointly determined by $F_1(P_k^d, P_m^c) = 0$ and $F_2(P_k^d, P_m^c) = 0$. Further analysis reveals that $\gamma_m^c$ increases with growing $P_k^d$ along the boundary line. As a result, the optimal power allocation solution is determined by the relative magnitudes of $P_{max}^c$ and $P_{max}^d$ as well as their intersections with the boundary line, which is as summarized in the theorem. $\square$

### 3.2.2   Pair Matching for All Vehicles

Substituting the optimal power allocation from the *Theorem* in (3.6) yields the maximum capacity of the $m$th I-UE when it shares its spectrum with the $k$th V-UE, denoted as $C_{m,k}^*$. If

Table 3.1: Optimal Resource Allocation Algorithm for (3.5) in D2D-Enabled Vehicular Communications

---

**Algorithm 3** Optimal Resource Allocation Algorithm for (3.5)

---

1: **for** $m = 1 : M$ **do**
2:   **for** $k = 1 : K$ **do**
3:     Obtain the optimal power allocation $(P_k^{d*}, P_m^{c*})$ from the *Theorem* for the single I-UE and V-UE pair.
4:     Substitute $(P_k^{d*}, P_m^{c*})$ into (3.6) to obtain $C_{m,k}^*$.
5:     **if** $C_{m,k}^* < r_0^c$ **then**
6:       $C_{m,k}^* = -\infty$.
7:     **end if**
8:   **end for**
9: **end for**
10: Use the Hungarian method [33] to find the optimal reuse pattern $\{\rho_{m,k}^*\}$ based on $\{C_{m,k}^*\}$.
11: Return the optimal spectrum reuse pattern $\{\rho_{m,k}^*\}$ and the corresponding power allocation $\{(P_k^{d*}, P_m^{c*})\}$.

---

it is less than $r_0^c$, then this combination is unable to meet the minimum capacity requirement for the I-UE. Therefore, such a I-UE and V-UE pair is not feasible and we set $C_{m,k}^* = -\infty$. After evaluating all possible combinations of the reuse pairs, the resource allocation problem in (3.5) reduces to

$$\max_{\{\rho_{m,k}\}} \sum_{m \in \mathcal{M}} \sum_{k \in \mathcal{K}} \rho_{m,k} C_{m,k}^* \tag{3.12}$$

$$\text{s. t.} \quad (3.5\text{e}), (3.5\text{f}) \tag{3.13}$$

which turns out to be a maximum weight bipartite matching problem and can be efficiently solved by the Hungarian method in polynomial time [33].

From the above discussion, we propose Algorithm 1 to solve the problem in (3.5) as listed in Table 3.1. Algorithm 1 yields the globally optimal solution to (3.5) because it jointly finds the optimal power control for each I-UE and V-UE reuse pair and the best spectrum sharing among all possible reuse pairs.

Table 3.2: Simulation Parameters [10, 47]

| Parameter | Value | Parameter | Value |
|---|---|---|---|
| Carrier frequency | 2 GHz | BS receiver noise figure | 5 dB |
| Bandwidth | 10 MHz | Distance between BS and highway | 35 m |
| Cell radius | 500 m | Vehicle receiver noise figure | 9 dB |
| BS antenna height | 25 m | Absolute vehicle speed $v$ | 100 km/h |
| BS antenna gain | 8 dBi | Minimum capacity of I-UE $r_0^c$ | 0.5 bps/Hz |
| Vehicle antenna height | 1.5 m | SINR threshold of V-UE $\gamma_0^d$ | 5 dB |
| Vehicle antenna gain | 3 dBi | Reliability for V-UE $p_0$ | $10^{-3}$ |
| Maximum V-UE transmit power $P_{\max}^d$ | 23 dBm | Maximum I-UE transmit power $P_{\max}^c$ | 23 dBm |
| Number of lanes | 3x2 | Number of V-UEs $K$ | 20 |
| Lane width | 4 m | Number of I-UEs $M$ | 20 |
| Noise power $\sigma^2$ | -114 dB-m | Bisection search accuracy $\epsilon$ | $10^{-6}$ |
| Vehicle drop model | | spatial Poisson process | |
| Vehicle density | | Average inter-vehicle distance is $2.5v$, $v$ in m/s | |

Table 3.3: Channel Models for V2I and V2V Links [10]

| Parameter | V2I Link | V2V Link |
|---|---|---|
| Pathloss model | $128.1 + 37.6\log_{10} d$, $d$ in km | LOS in WINNER + B1 |
| Shadowing distribution | Log-normal | Log-normal |
| Shadowing standard deviation $\xi$ | 8 dB | 3 dB |
| Fast fading | Rayleigh fading | Rayleigh fading |

## 3.3 Simulation Results

In this section, we present simulation results to validate the proposed algorithm. We follow the simulation setup for the freeway case in 3GPP TR 36.885 [10] and model a multi-lane freeway that passes through a single cell as shown in Fig. 3.1. The vehicles are dropped according to spatial Poisson process, whose density is determined by the vehicle speed. The $M$ I-UEs and $K$ V-UEs are randomly chosen among generated vehicles, where V-UE pairs are formed between adjacent vehicles and the I-UEs have equal shares of the total
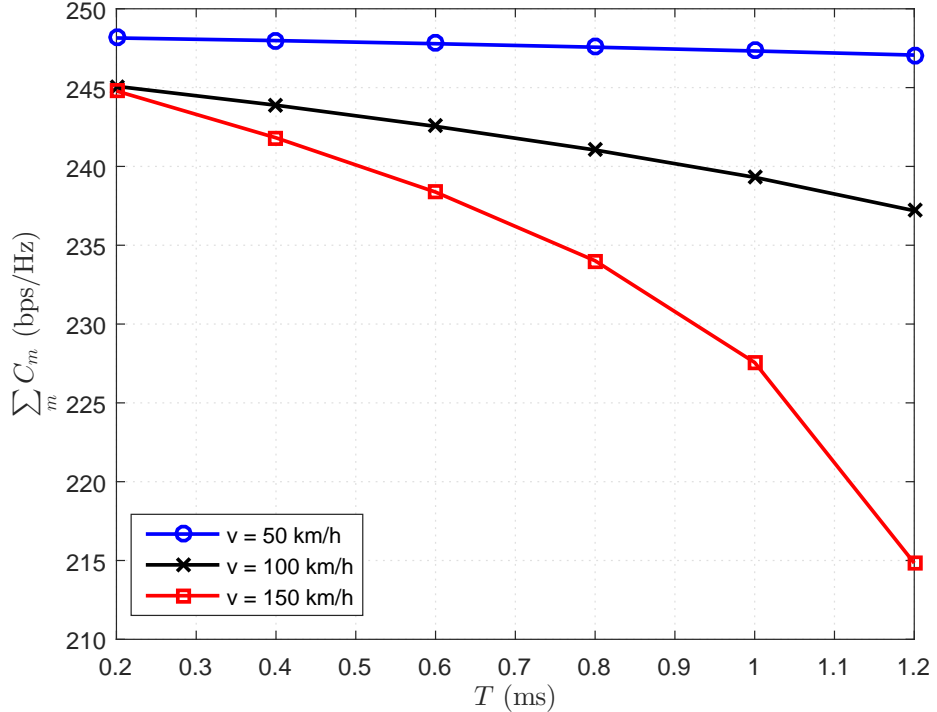
Figure 3.3: Sum capacity of I-UEs with varying feedback period $T$.

bandwidth. The major simulation parameters are listed in Table 3.2 and the channel models are described in Table 3.3. Note that all parameters are set according to Tables 3.2 and 3.3 by default, whereas the settings in each figure take precedence.

Fig. 3.3 demonstrates the sum V2I throughput of our proposed algorithm with an increasing CSI feedback period that indicates the channel latency. From the figure, the sum capacity of I-UEs decreases as the reporting period $T$ grows. This is due to growing $T$ increases uncertainty of V2V channels at the BS, motivating the BS to act conservatively when controlling I-UEs' transmit powers to meet the reliability constraint of V2V links, which suffer from interference generated by I-UEs. As the vehicle speed increases from $50$ to $150$ km/h, the sum capacity drops since higher speed induces a larger Doppler shift, which also increases channel uncertainty at the BS. Another reason for such degradation is due to sparser traffic according to the simulation setup, which on average increases inter-vehicle distance and gives rise to less reliable V2V links with lower received power. As such, less interference from I-UEs can be tolerated given the maximum transmit power
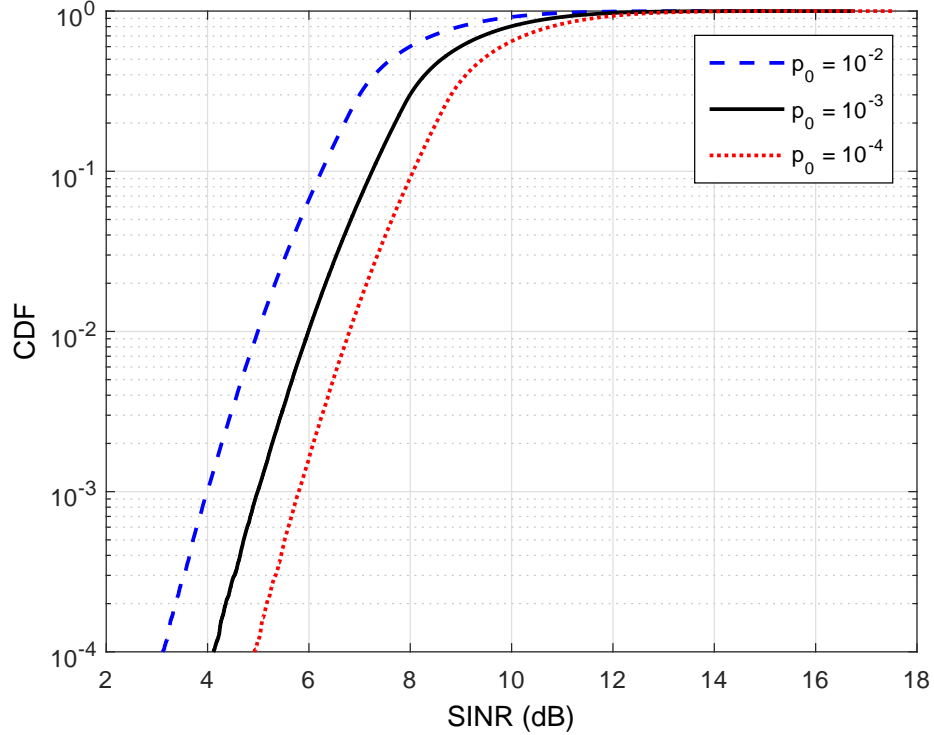
Figure 3.4: CDF of an arbitrary V-UE's SINR under Rayleigh fading with $T = 1$ ms and different targeted outage probabilities $p_0$.

constraints of V-UEs, leading to less power being allocated to I-UEs and decreasing their sum capacity. It is also interesting to note from Fig. 3.3 the I-UE's sum capacity is more sensitive to feedback frequency with a larger vehicle speed.

Fig. 3.4 evaluates the cumulative distribution function (CDF) of an arbitrary V-UE's received SINR under Rayleigh fading with different targeted outage probabilities. The desired SINR threshold for each V-UE is $5$ dB. From the figure, the reliability constraint in terms of the outage probability of V-UE's SINR is accurately satisfied, which confirms the effectiveness of our proposed algorithm.

## 3.4 Summary

In this chapter, we have investigated the spectrum sharing and power allocation design for D2D-enabled vehicular networks. Channel uncertainty caused by CSI feedback delay in a high mobility vehicular environment has been considered. The optimal resource allocation

strategy has been developed to maximize the sum capacity of all I-UEs while the reliability of all V2V links is strictly satisfied.

# CHAPTER 4

# GRAPH-BASED RESOURCE ALLOCATION WITH MULTIPLE V2V SHARING


In this chapter, we further our study of the resource allocation problem for device-to-device (D2D)-based vehicular networks. We generalize the problems in previous chapters to a more generic setting, where each vehicle-to-infrastructure (V2I) link shares spectrum with multiple vehicle-to-vehicle (V2V) links and the frequency spectrum is not assumed to be preassigned to V2I links. To support service heterogeneity of vehicular networks, we maximize the V2I link capacity for high bandwidth applications, such as video streaming over the Internet, and introduce the reliability constraint for V2V links (evaluated in terms of outage probabilities depending on large-scale CSI and the distribution of small-scale CSI), which is critical for safety message dissemination. We take advantage of both optimization and graph theoretic tools to develop a suite of algorithms that solve the problem with different performance guarantee and computational complexity tradeoffs. In the proposed baseline algorithm, we divide the V2V links into disjoint spectrum-sharing clusters using graph partitioning algorithms to mitigate their mutual interference. We then model and solve the spectrum allocation problem as a weighted 3-dimensional matching problem in graph theory, where weights of edges in the graph are obtained by optimizing powers of both V2I and V2V transmitters for each feasible spectrum sharing candidate. Based on the baseline algorithm, we further develop greedy and randomized graph-based resource allocation algorithms, leading to a substantial performance gain.

In terms of the chapter organization, Section 4.1 introduces the system model. Sections 4.2 and 4.3 investigate the resource allocation problems with different CSI resolutions. Section 4.4 delivers computer simulation results before the presentation of concluding remarks in Section 4.5.
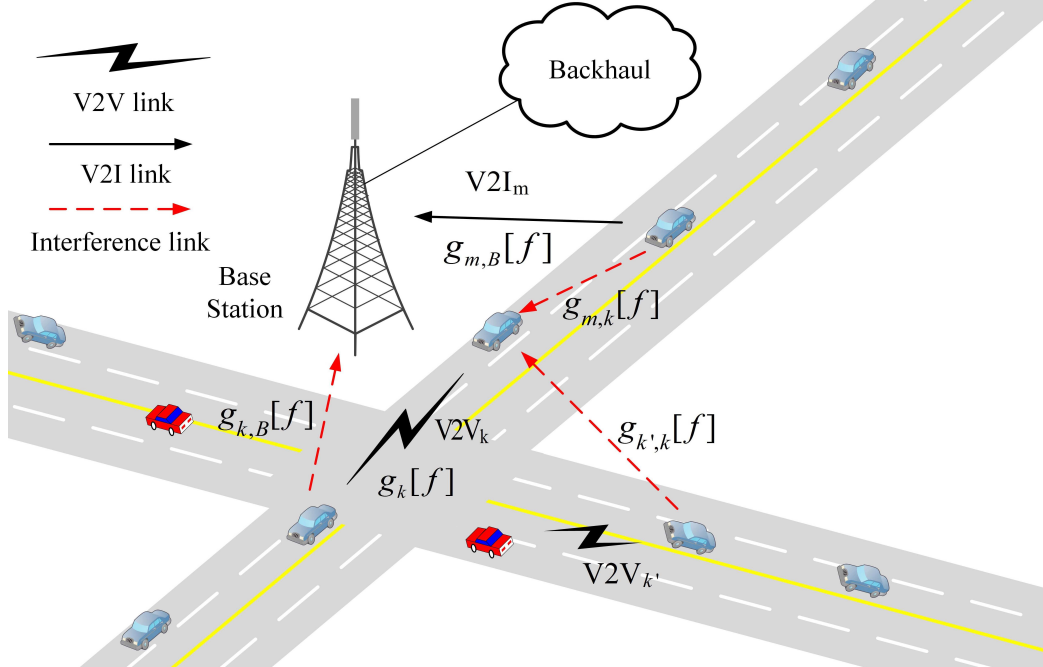
Figure 4.1: D2D-based vehicular communications.

## 4.1 System Model

Consider a D2D-based vehicular communications network as shown in Fig. 4.1. There are $M$ V2I and $K$ V2V communication links. The $M$ V2I links are initiated by $M$ single-antenna vehicles, demanding large-capacity uplink connection with the base station (BS) to support bandwidth intensive applications, such as cloud access, media streaming, and social networking. The $K$ V2V links are formed among the vehicles, designed with high reliability such that safety-critical information, such as the basic safety messages (BSM) defined in [10], can be shared among neighboring vehicles reliably, in the form of localized D2D communications.

It is noted that the $M$ V2I links and $K$ V2V links are illustrated separately in Fig. 4.1 for better presentation. Denote the set of V2I links as $\mathcal{M} = \{1, \cdots, M\}$ and the set of V2V links as $\mathcal{K} = \{1, \cdots, K\}$. The total available bandwidth is divided into $F$ resource blocks (RBs), denoted by $\mathcal{F} = \{1, \cdots, F\}$. Without loss of generality, we assume $M = F$ in this chapter and each of the $M$ V2I links uses a single RB, i.e., no spectrum sharing among

V2I links. To improve spectrum utilization, orthogonally allocated uplink spectrum of V2I links is reused by V2V links since uplink resource usage is less intensive and interference at the BS is more manageable. We note that in practice the number of V2V links tends to be larger than that of V2I links, i.e., $K \gg M$, making spectrum reuse among V2V links necessary.

As in Fig. 4.1, the channel power gain, $g_{m,B}[f]$, from the transmitter of the $m$th V2I link to the BS over the $f$th RB is

$$g_{m,B}[f] = \alpha_{m,B}|h_{m,B}[f]|^2, \tag{4.1}$$

where $h_{m,B}[f]$ is the small-scale fading component, assumed to be distributed according to $\mathcal{CN}(0,1)$ and independent across different RBs and links, and $\alpha_{m,B}$ captures large-scale fading effects, i.e., including path loss and shadowing, assumed to be independent of the RB index $f$. Similarly, we can define the $k$th V2V channel over the $f$th RB, $g_k[f]$, the interfering channel from the $k'$th V2V transmitter to the $k$th V2V receiver over the $f$th RB, $g_{k',k}[f]$, the interfering channel from the $m$th V2I transmitter to the $k$th V2V receiver over the $f$th RB, $g_{m,k}[f]$, and the interfering channel from the $k$th V2V transmitter to the BS over the $f$th RB, $g_{k,B}[f]$. See Table 4.1 for a summary.

The full CSI of links engaging the BS, including the V2I channels, $g_{m,B}[f]$, and the interfering channels from the V2V transmitters, $g_{k,B}[f]$, can be estimated at the BS, and is thus assumed known at the central controller. However, the CSI of mobile links, including the V2V channels, $g_k[f]$, the peer V2V interfering channels, $g_{k',k}[f]$, and the interfering channels from the V2I transmitters, $g_{m,k}[f]$, has to be estimated at the mobile receiver and then reported to the BS periodically. Frequent feedback of the fast fading information of rapidly varying mobile channels incurs substantial signaling overhead and thus makes tracking instantaneous CSI of mobile channels infeasible in practice. Therefore in this chapter, we assume that the BS only has access to the large-scale fading information of

Table 4.1: A Summary of Channel Symbol Notation

| Symbol | Definition |
|---|---|
| $g_{m,B}$ | the channel from the $m$th V2I transmitter to the BS |
| $g_k$ | the channel of the $k$th V2V link |
| $g_{k,B}$ | the interfering channel from the $k$th V2V transmitter to the BS |
| $g_{m,k}$ | the channel from the $m$th V2I transmitter to the $k$th V2V receiver |
| $g_{k',k}$ | the interfering channel from the $k'$th V2V transmitter to the $k$th V2V receiver |

such channels, which varies on a slow scale. In the meantime, each realization of the fast fading is unavailable at the BS while its statistical characterization is assumed to be known.

To this end, the received signal-to-interference-plus-noise ratios (SINRs) of the $m$th V2I link at the BS and the $k$th V2V link at the V2V receiver over the $f$th RB can be expressed as

$$\gamma_{m,f}^c = \frac{P_{m,f}^c g_{m,B}[f]}{\sigma^2 + \sum_k \rho_{k,f}^d P_{k,f}^d g_{k,B}[f]} \qquad (4.2)$$

and

$$\gamma_{k,f}^d = \frac{P_{k,f}^d g_k[f]}{\sigma^2 + \sum_m \rho_{m,f}^c P_{m,f}^c g_{m,k}[f] + \sum_{k' \neq k} \rho_{k',f}^d P_{k',f}^d g_{k',k}[f]}, \qquad (4.3)$$

respectively, where $P_{m,f}^c$ and $P_{k,f}^d$ denote transmit powers of the $m$th V2I transmitter and the $k$th V2V transmitter over the $f$th RB, respectively, $\sigma^2$ is the noise power, and $\rho_{m,f}^c \in \{0,1\}$ is the spectrum allocation indicator with $\rho_{m,f}^c = 1$ implying the $m$th V2I links is transmitting over the $f$th RB and $\rho_{m,f}^c = 0$ otherwise. The spectrum allocation indicator for the $k$th V2V link, $\rho_{k,f}^d$, is similarly defined.

To meet the diverse quality-of-service (QoS) requirements for different vehicular links, i.e., large capacity for V2I connections and high reliability for V2V connections, we maximize the sum capacity of the $M$ V2I links while guaranteeing the minimum reliability for

each V2V link. The spectrum and power allocation problems is formulated as:

$$\max_{\substack{\{\rho_{m,f}^c, \rho_{k,f}^d\} \\ \{P_{m,f}^c, P_{k,f}^d\}}} \sum_m \sum_f \rho_{m,f}^c \log_2(1 + \gamma_{m,f}^c) \tag{4.4}$$

$$\text{s.t.} \quad \rho_{k,f}^d \text{Pr}\left\{\gamma_{k,f}^d \leq \gamma_0^d\right\} \leq p_0, \forall k, f \tag{4.4a}$$

$$\sum_m \rho_{m,f}^c = 1, \forall f \tag{4.4b}$$

$$\sum_f \rho_{m,f}^c = 1, \forall m \tag{4.4c}$$

$$\sum_f \rho_{k,f}^d = 1, \forall k \tag{4.4d}$$

$$\sum_f \rho_{m,f}^c P_{m,f}^c \leq P_{\max}^c, \forall m \tag{4.4e}$$

$$\sum_f \rho_{k,f}^d P_{k,f}^d \leq P_{\max}^d, \forall k \tag{4.4f}$$

$$P_{m,f}^c \geq 0, P_{k,f}^d \geq 0, \forall m, k, f \tag{4.4g}$$

$$\rho_{m,f}^c, \rho_{k,f}^d \in \{0, 1\}, \forall m, k, f, \tag{4.4h}$$

where $\gamma_0^d$ in (4.4a) is the minimum SINR needed to establish a reliable V2V link and $p_0$ in (4.4a) is the tolerable outage probability. $P_{\max}^c$ in (4.4e) and $P_{\max}^d$ in (4.4f) are the maximum transmit powers of the V2I and V2V transmitters, respectively. Constraint (4.4a) represents the minimum reliability requirement for $K$ V2V links, where the probability is evaluated in terms of the random fast fading of mobile channels. Constraint (4.4b) restricts orthogonal spectrum to be allocated among $M$ V2I links. Constraints (4.4c) and (4.4d) model our assumption that each of the V2I and V2V links accesses a single RB. Constraints (4.4e) and (4.4f) ensure the transmit powers of V2I and V2V links cannot go beyond their maximum limits.

Extension to multi-RB access for both V2I and V2V links is possible through creating

multiple virtual V2I and V2V links and then properly defining their channel strengths as described in [50, 28]. Specifically, if one V2I link requests $N_R$ RBs, we create $N_R$ virtual V2I links at the beginning of the resource management and then equally split the maximum transmit power among these $N_R$ V2I links. If one V2V link requests multiple RBs, we can similarly create the same number of virtual V2V links and then set the strengths of the channels among them to be extremely high such that they cannot share the same RB in the following resource allocation stage. Likely, we split their maximum power limit among the virtual V2V links. Finally the RBs allocated to all virtual links originating from the same V2I or V2V link will be combined to allow multi-RB access.

## 4.2   Spectrum Allocation and Power Control

The optimization problem in (4.4) is combinatorial in nature and is further complicated by the nonlinear constraints and objective function. To address the problem, we propose in this section solution algorithms originating from a combination of graph theoretic and optimization tools. We first introduce a baseline low-complexity resource allocation algorithm, based on which some refined algorithms will then be proposed with significant performance improvement. Please note that the proposed algorithms are implemented in a centralized manner, where the central controller collects the CSI of all links with different levels of resolution from feedback or direct channel estimation, as described in Section 4.1, and then executes the algorithms step by step according to the algorithm description.

### 4.2.1   Baseline Graph-Based Resource Allocation

For the baseline resource allocation scheme, we first exploit graph partitioning algorithms to divide the V2V links into different clusters based on their mutual interference. This identifies proper V2V sets for spectrum sharing with minimum interference. Next, all V2V links in each cluster are allowed to share the same spectrum with one of the $M$ V2I links while V2V links in different clusters cannot share spectrum. We then optimize V2I and
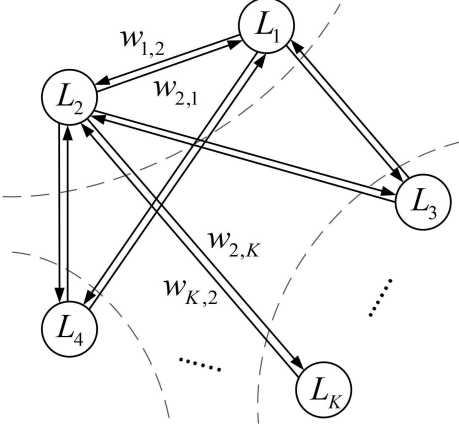
Figure 4.2: Graph representation for interfering links.

V2V transmit powers for all possible sharing patterns. Finally, we construct a 3-partite graph, with the $M$ V2I links, $F$ RBs, and $N$ V2V clusters as its vertices and with edge weights equal to the V2I capacity from applying optimized V2I and V2V transmit powers. The resource allocation problem in (4.4) can then be reduced to a weighted 3-dimensional matching problem.

*V2V Partitioning*

The interference management for V2V links can be captured using a graph in Fig. 4.2, where each V2V link $L_k$ is modeled as a vertex and two vertices are joined by an edge when they are mutually interfering. The edge weight is set to capture the interference level with $w_{k',k} = \alpha_{k',k}$, where $\alpha_{k',k}$ is the large-scale fading CSI of the interference channel from the $k'$th V2V transmitter to the $k$th V2V receiver. The goal is to partition the $K$ vertices into $N$ sets, $C_1, \cdots, C_N$, where $N \ll K$, minimizing the intra-cluster interference across all clusters, i.e., $\sum_n \left( \sum_{k',k \in C_n} w_{k',k} \right)$. Intuitively, this implies that we attempt to partition strongly interfering V2V links into different sets so that links within the same set can share the same RB without incurring too much mutual interference.

The above partitioning problem is equivalent to the MAX $N$-CUT problem in graph theory [31, 51] and a brief explanation is given here. Let $G$ be a graph with vertex set

57

Table 4.2: Heuristic Algorithm for MAX $N$-CUT [31, 51]

---

**Algorithm 4** Heuristic Algorithm for V2V Partitioning

---
1: Arbitrarily assign one V2V link to each of the $N$ clusters.
2: **for** $k \in \mathcal{K}$ **and** not already in any cluster **do**
3:     **for** $n = 1 : N$ **do**
4:         Compute the increased intra-cluster interference using $\sum_{k' \in C_n} (w_{k,k'} + w_{k',k})$.
5:     **end for**
6:     Assign the $k$th V2V link to the $n^*$th cluster with $n^* = \arg\min \sum_{k' \in C_n} (w_{k,k'} + w_{k',k})$.
7: **end for**
8: Return the V2V clustering result.

---

$V(G)$ and edge set $E(G)$. Let $w : E(G) \to \mathbb{R}$. The MAX $N$-CUT problem for a weighted graph is to find a partition of the graph $G$ into $N$ disjoint clusters $C_n, n = 1, \cdots, N$, such that $C_1 \cup \cdots \cup C_N = V(G)$ and $\sum_{a \in C_i, b \in C_j, i<j} w_{a,b}$ is maximized, where $w_{a,b}$ is the weight of the edge $(a, b)$. Since $\sum_n \left( \sum_{k',k \in C_n} w_{k',k} \right) + \sum_{a \in C_i, b \in C_j, i<j} w_{a,b} = \sum_{e \in E(G)} w(e)$, maximizing $\sum_{a \in C_i, b \in C_j, i<j} w_{a,b}$ is thus equivalent to minimizing $\sum_n \left( \sum_{k',k \in C_n} w_{k',k} \right)$.

A simple heuristic algorithm has been proposed in [51] and exploited for interference management in [31] for multicell OFDMA systems, achieving an absolute ratio of $(1 - 1/N)$ for a general $N$-CUT problem. This algorithm is listed in Table 4.2 and will be used in this chapter.

*Power Allocation Design*

As mentioned before, V2V links in one cluster can share the spectrum with one V2I link while those in different clusters are not allowed to share. For an arbitrary spectrum sharing pattern, e.g., when the $m$th V2I link is transmitting over the $f$th RB, which is shared by all V2V links in the $n$th cluster, $C_n$, we attempt to find its optimal power control for both V2I and V2V links. That is, we maximize the V2I capacity, defined as $R_{m,n}[f]$, with the reliability of all V2V links in the $n$th cluster guaranteed when they share the $f$th RB. The

power optimization problem is formulated as

$$\max_{P^c_{m,f}, \{P^d_{k,f}\}} \log_2 \left( 1 + \frac{P^c_{m,f} g_{m,B}[f]}{\sigma^2 + \sum\limits_{k \in C_n} P^d_{k,f} g_{k,B}[f]} \right) \triangleq R_{m,n}[f] \tag{4.5}$$

$$\text{s.t.} \quad \Pr \left\{ \frac{P^d_{k,f} g_k[f]}{\sigma^2 + P^c_{m,f} g_{m,k}[f] + \sum\limits_{k' \neq k} P^d_{k',f} g_{k',k}[f]} \leq \gamma^d_0 \right\}$$

$$\leq p_0, \forall k \in C_n \tag{4.5a}$$

$$0 \leq P^c_{m,f} \leq P^c_{\max} \tag{4.5b}$$

$$0 \leq P^d_{k,f} \leq P^d_{\max}, \forall k \in C_n. \tag{4.5c}$$

To evaluate the outage constraint of (4.5a), we will turn it to an analytical form by using the following result from [52].

**Lemma 3.** *Suppose $z_1, \cdots, z_n$ are independent exponentially distributed random variables with means $\mathbb{E}[z_i] = 1/\lambda_i$. Then we have [52]*

$$Pr \left\{ z_1 \leq \sum_{i=2}^{n} z_i + c \right\} = 1 - e^{-\lambda_1 c} \prod_{i=2}^{n} \frac{1}{1 + \frac{\lambda_1}{\lambda_i}}, \tag{4.6}$$

*where $c$ is a positive constant.*

In light of Lemma 3, we replace the outage constraint for each V2V links in (4.5a) with

$$1 - \frac{\exp\left(-\frac{\gamma^d_0 \sigma^2}{P^d_{k,f} \alpha_k}\right)}{1 + \frac{P^c_{m,f} \alpha_{m,k} \gamma^d_0}{P^d_{k,f} \alpha_k}} \prod_{k' \neq k} \frac{1}{1 + \frac{P^d_{k',f} \alpha_{k',k} \gamma^d_0}{P^d_{k,f} \alpha_k}} \leq p_0, \forall k \in C_n. \tag{4.7}$$

This is still a fairly complex constraint and is hard to deal with. To avoid the difficulty of manipulating such complicated inequalities, we further use the following result in [53] to

bound the derived outage constraints

$$
1 - \frac{\exp\left(-\frac{\gamma_0^d \sigma^2}{P_{k,f}^d \alpha_k}\right)}{1 + \frac{P_{m,f}^c \alpha_{m,k} \gamma_0^d}{P_{k,f}^d \alpha_k}} \prod_{k' \neq k} \frac{1}{1 + \frac{P_{k',f}^d \alpha_{k',k} \gamma_0^d}{P_{k,f}^d \alpha_k}}
$$

$$
\leq 1 - \exp\left(-\frac{\gamma_0^d \left(\sigma^2 + P_{m,f}^c \alpha_{m,k} + \sum_{k' \neq k} P_{k',f}^d \alpha_{k',k}\right)}{P_{k,f}^d \alpha_k}\right)
$$

$$
\leq p_0, \quad \forall k \in C_n, \tag{4.8}
$$

where tightness of the upper bound on outage probability has been demonstrated in [53].

To this end, the power control problem in (4.5) for all V2V links in the $n$th cluster, $C_n$, and the associated $m$th V2I link over the $f$th RB can be cast as

$$
\max_{P_{m,f}^c, \{P_{k,f}^d\}} \log_2\left(1 + \frac{P_{m,f}^c g_{m,B}[f]}{\sigma^2 + \sum_{k \in C_n} P_{k,f}^d g_{k,B}[f]}\right) \tag{4.9}
$$

$$
\text{s.t.} \quad \frac{P_{k,f}^d \alpha_k}{\sigma^2 + P_{m,f}^c \alpha_{m,k} + \sum_{k' \neq k} P_{k',f}^d \alpha_{k',k}} \geq \frac{\gamma_0^d}{\ln \frac{1}{1-p_0}},
$$

$$
\forall k \in C_n \tag{4.9a}
$$

$$
0 \leq P_{m,f}^c \leq P_{\max}^c \tag{4.9b}
$$

$$
0 \leq P_{k,f}^d \leq P_{\max}^d, \forall k \in C_n. \tag{4.9c}
$$

**Remark 1.** *For generalized fast fading distributions with unit mean power, i.e., $\mathbb{E}[|h|^2] = 1$, we exploit the results from [54] to find an upper bound of the outage probability of V2V links, i.e., the left hand side of (4.5a), by*

$$
O_k \leq F_{|h_k|^2}\left(\gamma_0^d \frac{\sigma^2 + P_{m,f}^c \alpha_{m,k} + \sum_{k' \neq k} P_{k',f}^d \alpha_{k',k}}{P_{k,f}^d \alpha_k}\right), \tag{4.10}
$$

60

$\forall k \in C_n$, where $F_{|h_k|^2}(\cdot)$ is the fading cumulative distribution function (CDF) of the $k$th V2V link, which is assumed to be concave on $\mathbb{R}^+$. The outage constraint in (4.5a) can be further derived as

$$\frac{P_{k,f}^d \alpha_k}{\sigma^2 + P_{m,f}^c \alpha_{m,k} + \sum_{k' \neq k} P_{k',f}^d \alpha_{k',k}} \geq \frac{\gamma_0^d}{F_{|h_k|^2}^{-1}(p_0)}, \forall k \in C_n, \tag{4.11}$$

where $F_{|h_k|^2}^{-1}(\cdot)$ denotes the inverse of the CDF. For the popular double-Rayleigh fading to model non line-of-sight (NLoS) V2V channels, the CDF is given by [55]

$$F_{|h_k|^2}(x) = 1 - \sqrt{x}K_1(\sqrt{x}), \tag{4.12}$$

where $K_1(\cdot)$ is the first order modified Bessel function of the second kind.

We note that the optimality of (4.9) will be achieved when the outage constraints in (4.9a) are satisfied with equality. This can be proved by contradiction. Suppose the optimal solution to (4.9) contains at least one V2V link, $k \in C_n$, with

$$\frac{P_{k,f}^d \alpha_k}{\sigma^2 + P_{m,f}^c \alpha_{m,k} + \sum_{k' \neq k} P_{k',f}^d \alpha_{k',k}} > \frac{\gamma_0^d}{\ln \frac{1}{1-p_0}}. \tag{4.13}$$

Due to the fact that the left hand side of (4.9a) is monotonically increasing in $P_{k,f}^d$ and decreasing in $P_{k',f}^d$, $k' \neq k$, we can always lower the $k$th V2V's transmit power, $P_{k,f}^d$, such that constraints for all V2V links are still satisfied. Also notice that the objective function in (4.9) is monotonically increasing with decreasing V2V transmit powers. As such, it can be improved with lowering $P_{k,f}^d$, thus contradicting the optimality assumption.

Letting $N_{c_n}$ denote the number of V2V links in the cluster $C_n$, we further notice that the relations in (4.9a) are linear in $N_{c_n} + 1$ related transmit powers: one V2I transmit power, $P_{m,f}^c$; and $N_{c_n}$ V2V transmit powers, $\{P_{k,f}^d\}$. In addition, the number of equality constraints in (4.9a) at the optimal solution is $N_{c_n}$. Therefore, we can easily derive the

V2V transmit powers in the $n$th cluster, i.e., $\{P^d_{k,f}\}, \forall k \in C_n$, in terms of the V2I transmit power, $P^c_{m,f}$, as

$$\mathbf{P}^d_{n,f} = \mathbf{\Phi}^{-1} \bar{\gamma}_0 \left( P^c_{m,f} \boldsymbol{\alpha}_m + \sigma^2 \right), \qquad (4.14)$$

where $\mathbf{P}^d_{n,f} \in \mathbb{R}^{N_{cn} \times 1}$ stores $N_{cn}$ V2V transmit powers in the $n$th cluster, $\bar{\gamma}_0 = \frac{\gamma^d_0}{-\ln(1-p_0)}$, $\boldsymbol{\alpha}_m = (\alpha_{m,1}, \cdots, \alpha_{m,N_{cn}})^T \in \mathbb{C}^{N_{cn} \times 1}$, and $\mathbf{\Phi} \in \mathbb{C}^{N_{cn} \times N_{cn}}$ is given by

$$\mathbf{\Phi}_{i,j} = \begin{cases} \alpha_i, & \text{if } i = j, \\ -\bar{\gamma}_0 \alpha_{j,i}, & \text{otherwise.} \end{cases} \qquad (4.15)$$

Here, in the above we have relabeled the $N_{cn}$ V2V links in the $n$th cluster as $\{1, 2, \cdots, N_{cn}\}$ and slightly changed the notation by using $i$ in place of the original V2V index $k$.

Similar to the argument in [28], we can then substitute (4.14) in the objective function of (4.9), which can be shown to monotonically increase with $P^c_{m,f}$. Hence, after considering the maximum power constraints, the optimal solution to the problem in (4.9) is given by[1]

$$P^{c*}_{m,f} = \min \left\{ P^c_{\max}, \left\{ \frac{P^d_{\max} - \bar{\gamma}_0 \sigma^2 \boldsymbol{\phi}^H_i \mathbf{1}}{\bar{\gamma}_0 \boldsymbol{\phi}^H_i \boldsymbol{\alpha}_m} \right\}^{N_{cn}}_{i=1} \right\}, \qquad (4.16)$$

and

$$\mathbf{P}^{d*}_{n,f} = \mathbf{\Phi}^{-1} \bar{\gamma}_0 \left( P^{c*}_{m,f} \boldsymbol{\alpha}_m + \sigma^2 \right), \qquad (4.17)$$

where $\mathbf{1}$ is an all-one vector and $\boldsymbol{\phi}^H_i$ is the $i$th row of $\mathbf{\Phi}^{-1}$.

---

[1]Should either the optimal V2I transmit power, i.e., $P^{c*}_{m,f}$, or any of the optimal V2V transmit powers in the $n$th cluster, i.e., $P^{d*}_{k,f}, k \in C_n$, be negative, we declare the problem in (4.9) to be infeasible and set $R_{m,n}[f] = -\infty$.
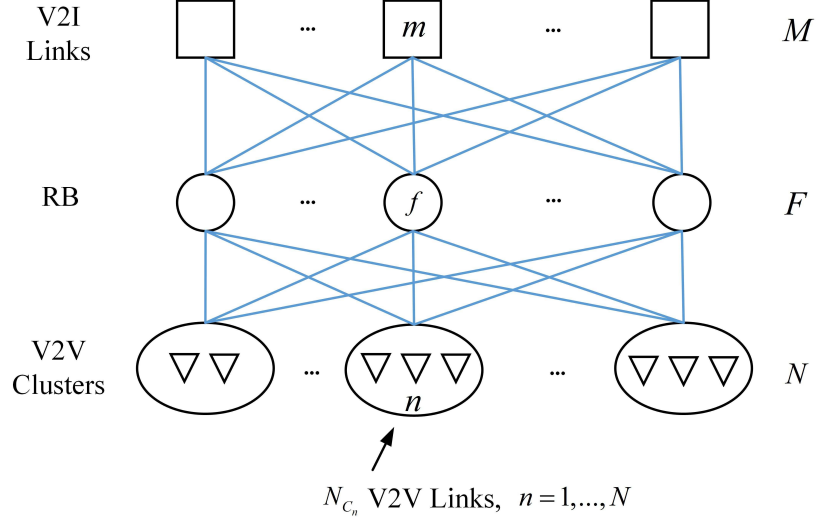
Figure 4.3: Graph representation for spectrum sharing among V2I and V2V links.

*Resource Matching*

To this end, essential elements of the resource allocation problem in (4.4) can be modeled as a 3-partite graph in Fig. 4.3. For each of the possible V2I-RB-V2V resource sharing patterns ($MFN$ in total), we formulate the optimization problem as in (4.5) and then find the resulting V2I capacity $R_{m,n}[f], \forall m, n, f$. The weight for the edge linking from the $m$th V2I vertex in the upper layer, through the $f$th RB vertex in the middle layer, and to the $n$th cluster vertex in the lower layer, is set to be $R_{m,n}[f]$. Then the spectrum allocation problem reduces to

$$\max_{\{\rho_{m,f}^{c}, \rho_{n,f}^{cl}\}} \sum_{m} \sum_{f} \sum_{n} \rho_{m,f}^{c} \rho_{n,f}^{cl} R_{m,n}[f] \tag{4.18}$$

$$\text{s.t.} \quad \sum_{m} \rho_{m,f}^{c} = 1, \sum_{n} \rho_{n,f}^{cl} = 1, \forall f \tag{4.18a}$$

$$\sum_{f} \rho_{m,f}^{c} = 1, \forall m, \sum_{f} \rho_{n,f}^{cl} = 1, \forall n \tag{4.18b}$$

$$\rho_{m,f}^{c}, \rho_{n,f}^{cl} \in \{0, 1\}, \forall m, n, f \tag{4.18c}$$

This problem can be transformed into a weighted 3-dimensional matching problem with

weights of $w(m, f, n) = R_{m,n}[f]$, for $1 \leq m \leq M, 1 \leq f \leq F$, and $1 \leq n \leq N$, to which we now turn our attention.

Formally, a hypergraph $H = (V, E)$ consists of a set $V$ of vertices and a set $E$ of edges where each edge is a nonempty subset of $V$. A matching in $H$ is a subset $M_0 \subseteq E$ of edges such that for any distinct edges $e_1, e_2 \in M_0$, $e_1 \cap e_2 = \emptyset$. A $k$-uniform hypergraph is a hypergraph in which all edges have size $k$. Further, a $k$-uniform hypergraph is said to be $k$-partite if the set of vertices can be partitioned into $k$ disjoint sets such that every edge contains one vertex from each set. A $k$-dimensional matching is a matching in a $k$-partite hypergraph. The $k$-dimensional matching problem is to find a matching in a $k$-partite hypergraph with the maximum number of edges. The weighted $k$-dimensional matching problem is that given a $k$-partite hypergraph $H = (V, E)$ and a function $w : E \rightarrow \mathbb{R}$, find a matching $M_0$ in $H$ such that $w(M_0) = \sum_{e \in M_0} w(e)$ is maximized.

In our case, the V2I-RB-V2V resource allocation problem in (4.18) is equivalent to the weighted 3-dimensional matching problem, which can be seen as follows. We first construct a 3-partite hypergraph $H = (V, E)$, by letting $V = \{[m, 0, 0] : 1 \leq m \leq M\} \cup \{[0, f, 0] : 1 \leq f \leq F\} \cup \{[0, 0, n] : 1 \leq n \leq N\}$, and $E = \{(m, f, n) : 1 \leq m \leq M, 1 \leq f \leq F, 1 \leq n \leq N\}$, where $(m, f, n) = \{[m, 0, 0], [0, f, 0], [0, 0, n]\}$. We define the weight function $w : E \rightarrow \mathbb{R}$ by letting $w(m, f, n) = R_{m,n}[f]$, for all $1 \leq m \leq M, 1 \leq f \leq F, 1 \leq n \leq N$. Now, we can see that solving our V2I-RB-V2V resource allocation problem is equivalent to solving the weighted 3-dimensional matching problem on $H = (V, E)$ with weight function $w$.

Note that for $k \geq 3$, the $k$-dimensional matching problem is NP-hard. In fact, the 3-dimensional matching problem is one of Karp's famous 21 NP-complete problems. Thus, we are not expecting a polynomial time algorithm to solve our problem. Instead, we will use efficient algorithms to approximately solve the 3-dimensional matching problem, and provide guarantees that our approximate solutions will be close to the optimum.

We adopt and modify the polynomial time algorithm proposed in [56], which gives a

solution to the weighted 3-dimensional matching problem with approximation factor 2 (but without the additive constant $\epsilon$ as in [42]). The algorithm in [56] combines the use of the iterative rounding method and the fractional local ratio method, by using the basic solutions of the standard linear programming relaxation of the weighted 3-dimensional matching problems. Iterative rounding [57] is a way for designing approximation algorithms to obtain solutions to integer programs. It begins with obtaining a basic solution by solving a linear programming relaxation. Then it tries to obtain an integral solution by rounding up variables of large values and iteratively solving the residual problems.

Let $H = (V, E)$ be a 3-partite hypergraph, and let $w : E \to \mathbb{R}$. For $v \in V$, let $\delta(v)$ be the set of edges containing $v$. The weighted 3-dimensional matching problem can be formulated as the following integer program:

$$\max \sum_{e \in E} w(e)x(e)$$

$$\text{s.t.} \sum_{e \in \delta(v)} x(e) \leq 1, \forall v \in V$$

$$x(e) \in \{0, 1\}, \forall e \in E.$$

The linear programming relaxation of this integer program is given by

$$\max \sum_{e \in E} w(e)x(e) \qquad (4.19)$$

$$\text{s.t.} \sum_{e \in \delta(v)} x(e) \leq 1, \forall v \in V$$

$$x(e) \geq 0, \forall e \in E.$$

Algorithm 2 in Table 4.3 is obtained from the weighted 3-dimensional matching algorithm from [56] by adding Step 10. For any $e \in E$, let $N[e]$ be the set of edges of $H$ having nonempty intersection with $e$. Note that $e \in N[e]$. In Algorithm 5, the solution $x$ of linear program (4.19) must be basic; or else in Step 4, one cannot guarantee the existence

65

Table 4.3: Weighted 3-Dimensional Matching Algorithm [56]

---

**Algorithm 5** Weighted 3-Dimensional Matching Algorithm

---

1: Input: $H = (V, E), w : E \to \mathbb{R}$ and $x$, where $x$ is a basic solution of linear program (4.19) obtained by some linear programming algorithm.
2: Let $F \subseteq E$ with initialization $F = \emptyset$.
3: **repeat**
4:   Search for an edge $e \in E - F$ such that $x(N[e] \cap (E - F)) \leq 2$.
5:   Let $F = F \cup \{e\}$.
6:   Let $i = |F| + 1$, and let $i$ be the index of $e$.
7: **until** $E - F = \emptyset$
8: Implement Local-Ratio algorithm in Table 4.4 with input $F$ and $w$, where $w$ is the weight function on the edges of $H$.
9: Let $M_0$ be the output of Local-Ratio algorithm.
10: Use the greedy algorithm to find a maximal set $E'$ of edges, such that $M_0 \cup E'$ is a matching, and $w(e) \geq 0$ for all $e \in E'$. Then let $M_0 \leftarrow M_0 \cup E'$, and output $M_0$.

---

Table 4.4: Local Ratio Algorithm [56]

---

**Algorithm 6** Local Ratio Algorithm [56]

---

1: Input: Hypergraph $H = (V, E)$, $F \subseteq E$, $w : E \to \mathbb{R}$, and an ordering of the edges in $E$.
2: Let $F' = \{e \in F : w(e) > 0\}$.
3: **if** $F' = \emptyset$ **then**
4:   Return $\emptyset$.
5: **end if**
6: Let $e'$ be the smallest edge in $F'$ based on the ordering of $E$. Decompose the weight function $w = w_1 + w_2$, where

$$w_1(e) = \begin{cases} w(e'), & \text{if } e \in N[e']. \\ 0, & \text{otherwise.} \end{cases}$$

7: $M' \leftarrow$Local-Ratio$(F', w_2)$. (Note: this is a recursion.)
8: **if** $M' \cup \{e'\}$ is a matching in $H$ **then**
9:   Return $M' \cup \{e'\}$.
10: **else**
11:   Return $M'$.
12: **end if**

---

of an edge $e \in E - F$ such that $x(N[e] \cap (E - F)) \leq 2$. To obtain a basic solution of

the linear program (4.19), we could use some existing linear programming algorithm, such

as the simplex algorithm or the dual-simplex algorithm. Indeed, any linear programming algorithm, which produces a basic solution, can be used here. We modified the algorithm in [56] by adding Step 10, because the original algorithm does not necessarily produce a maximal matching in $H$, since it only guarantees a matching with weights at least one half of the optimum. So, here, we use greedy algorithm to test whether or not $M_0$ is a maximal matching. If not, then we will find $E'$, with $w(e) \geq 0\ \forall e \in E'$, such that $M_0 \cup E'$ is a matching. In some cases, this added step could greatly improve the performance of the whole algorithm.

Now, we analyze the time complexity of the above weighted 3-dimensional matching algorithm. A basic solution of the linear programming relaxation of the weighted 3-dimensional matching problem can be found in polynomial time. Let $H = (V, E)$ be a 3-partite hypergraph with $|V| = n$ and $|E| = m$, let $w : E \to \mathbb{R}$, and let $x$ be a basic solution of the linear programming relaxation of the corresponding weighted 3-dimensional matching problem. We show that Algorithm 2, producing a matching whose weights is at least one half of the optimum, has time complexity $O(mn^2 \log_2 n)$.

First, we see that Steps 3 to 7 of Algorithm 2 constitute a loop, which is executed until we have $F = E$. This loop gives an ordering of edges in $E$ to be used in implementing Algorithm 3 (Local Ratio Algorithm). The total number of iterations of this loop is $m$. For each iteration, we need to search in $E - F$ for an edge $e$ with $x(N[e] \cap (E - F)) \leq 2$. For efficiency, we construct a binary tree data structure to store the data $x(N[e] \cap (E - F))$ for all $e \in E - F$ such that the value of any vertex in the tree is always no more than the value of its "children". By updating this tree in each iteration, we can find $\min\{x(N[e] \cap (E - F)) : e \in E - F\}$ in $O(1)$ time, which is guaranteed to be no more than 2. However, once we add $e$ into $F$, we need to delete this data in our binary tree and modify the values of $x(N[e'] \cap (E - F))$ for those edges $e' \in (E - F) \cap N[e]$. The total number of modifications is $O(n^2)$, and each modification can be implemented in $O(\log_2 n)$ time. Hence, each iteration of the loop will take $O(n^2 \log_2 n)$ Since we have $m$ iterations, the total time of Steps 3 to 7

is $O(mn^2 \log_2 n)$.

Step 8 can be implemented in $O(mn^2)$. This is because in Step 8, we call Algorithm 3 (Local Ratio Algorithm) at most $m$ times. In each call of Local Ratio Algorithm, we need to construct $w_1$ and $w_2$, which needs $O(n^2)$ time. Therefore, Step 8 can be implemented in $O(mn^2)$ time.

In Step 10, we use the greedy algorithm to find a set $E'$ of edges in $E - M_0$, such that $M_0 \cup E'$ is a matching with $w(e) > 0, \forall e \in E'$. So, we need to check all the edges in $E - M_0$, and see whether or not we can add more edges into $E'$. The total number of such checking is $O(m)$, and for each checking, we can complete it in $O(1)$ time. So, Step 10 can be implemented in $O(m)$ time.

Thus, given $H = (V, E)$, $w : E \to R$, and the basic solution $x$, the weighted 3-dimensional matching algorithm has approximation factor 2 and time complexity $O(mn^2 \log_2 n)$.

The proposed baseline algorithm to solve the problem in (4.4) is summarized in Table 4.5. With $N = M = F$, The V2V clustering has a complexity of $\mathcal{O}(KM)$, the complexity to construct the weighted 3-partite graph is $\mathcal{O}(M^3)$, and finally, the complexity of the weighted 3-dimensional matching Algorithm is $\mathcal{O}(M^5 \log M)$. Therefore, the total complexity of Algorithm 7 is $\mathcal{O}(KM + M^3 + M^5 \log M)$.

### 4.2.2 Greedy Resource Allocation

Built on the baseline resource allocation in Algorithm 7, we further propose a greedy algorithm, which substantially improves the system performance. Before delving into details, we briefly introduce the main problem setup and the motivation for such a greedy approach. We claim that with the power optimization control and 3-dimensional resource matching introduced in Sections 4.2.1 and 4.2.1, respectively, the original problem in (4.4) can be described as follows: Given a real value function $g(\cdot)$ defined on $X = \{(x_1, x_2, \cdots, x_K) : x_k \in \{1, \cdots, N\}, k \in \{1, \cdots, K\}\}$, find $x \in X$ such that $g(x)$ is maximized.

As introduced earlier, we have $K$ V2V links and $N$ clusters. Let the vector $x =$

Table 4.5: Baseline Graph-based Resource Allocation

---

**Algorithm 7** Baseline Graph-based Resource Allocation

---

1: Use Algorithm 4 to divide $K$ V2V links into $N$ clusters, denoted by $C_1, \cdots, C_N$.
2: **for** $m = 1 : M$ **do**
3:   **for** $n = 1 : N$ **do**
4:     **for** $f = 1 : F$ **do**
5:       Use (4.16) and (4.17) to find the optimal V2I and V2V transmit powers, respectively.
6:       Compute the V2I capacity, $R_{m,n}[f]$, with the optimized power control parameters.
7:     **end for**
8:   **end for**
9: **end for**
10: Construct a 3-partite graph, where the $M$ V2I links, $F$ RBs, and $N$ V2V clusters form the vertices in three layers and the weight for each V2I-RB-V2V edge is set to $R_{m,n}[f]$.

11: Use Algorithm 5 to find a matching solution $M_0$.
12: Return the 3-dimensional matching (spectrum sharing) result $M_0$ and the corresponding power allocation $\{(P_{m,f}^{c*}, P_{k,f}^{d*})\}$.

---

$(x_1, \cdots, x_K)$ denote the situation that the $k$th V2V link is put into the $x_k$th cluster, for $k \in \{1, 2, \cdots, K\}$. Let $g(x)$ denote the objective function value of (4.4), after executing Algorithm 7, corresponding to the allocation of V2V links into $N$ clusters based on $x$. More precisely, $g(x) = \sum_m r_m$, with $r_m = \sum_f \rho_{m,f}^c \log_2(1 + \gamma_{m,f}^c)$. Up to this end, it is easy to see that our problem in (4.4) is transformed to finding $x \in X$ such that $g(x)$ is maximized. Obviously, finding $x \in X$ to maximize $g(x)$ cannot be solved in polynomial time with respect to $K$ and $N$, as a general integer program problem is NP-hard.

The essential idea behind our greedy approach is to first use Algorithm 4 as an initialization, and then for each of the $K$ V2V links, sequentially decide the best cluster to join, where the sum V2I capacity is determined by executing Algorithm 7. This whole process is repeated for several times until convergence or until time bound is reached. Formally, the algorithm is listed in Table 4.6. The complexity is $\mathcal{O}(C(K^2M^2 + KM^4 + KM^6 \log M))$, where $C$ is the number of iterations for the greedy algorithm to converge.

Table 4.6: Greedy Resource Allocation

---

**Algorithm 8** Greedy Resource Allocation

---

1: Initialize $x = (x_1, x_2, \cdots, x_K)$ using Algorithm 4.

2: **repeat**

3:     **for** $k = 1 : K$ **do**

4:         Initialize an all-zero vector $w = (w_1, w_2, \cdots, w_N)$ of length $N$.

5:         **for** $n = 1 : N$ **do**

6:             **if** $k$th V2V is not the only link in its current cluster **then**

7:                 Set $x_k = n$.

8:                 Execute Steps 2-12 of Algorithm 7 to obtain the matching solution $M_0$ based on $x$ and the corresponding power allocation $\{(P_{m,f}^{c^*}, P_{k,f}^{d^*})\}$.

9:                 Compute the sum V2I capacity $g(x) = \sum_m r_m^*$ using the matching (spectrum sharing) solution $M_0$ and the optimized powers $\{(P_{m,f}^{c^*}, P_{k,f}^{d^*})\}$.

10:                 Set $w_n = g(x)$.

11:             **end if**

12:         **end for**

13:         Set $x_k = n^*$ with $n^* = \arg\max_n w_n$.

14:     **end for**

15: **until** Convergence

16: Return the 3-dimensional matching (spectrum sharing) result $M_0$ and the corresponding power allocation $\{(P_{m,f}^{c^*}, P_{k,f}^{d^*})\}$.

---

### 4.2.3   Randomized Resource Allocation

We observe that with the power optimization control and 3-dimensional resource matching introduced in Sections 4.2.1 and 4.2.1, respectively, the original problem in (4.4) is essentially a combinatorial problem as described in Section 4.2.2. The greedy algorithm proposed in Table 4.6 tends to get trapped at a local optimum, which might be far away from the global optimum due to the combinatorial nature of the problem. To address this issue, we propose a randomized procedure in this subsection, where a V2V link is allowed to join a suboptimal cluster with an appropriate probability associated with its achieved sum capacity. The proposed randomized algorithm is listed in Table 4.7, where we use the generic symbols defined in Section 4.2.2 for notational compactness.

For this randomized algorithm, let $x^{(n)} = (x_1, x_2, \cdots, x_{k-1}, n, x_{k+1}, \cdots, x_K)$ and

Table 4.7: Randomized Resource Allocation

---

**Algorithm 9** Randomized Resource Allocation

---

1: Initialize $x = (x_1, x_2, \cdots, x_K)$, amplification coefficient $a \geq 1$, the number of iterations $I$, temperature $T$, and maximum temperature $T_{max}$.

2: **for** $i = 1 : I$ **do**

3:   **if** $a \cdot T \leq T_{max}$ **then**

4:     $T \leftarrow a \cdot T$.

5:   **end if**

6:   **for** $k = 1 : K$ **do**

7:     Let $x^{(n)} = (x_1, x_2, \cdots, x_{k-1}, n, x_{k+1}, \cdots, x_K), n = 1, 2, \cdots, N$.

8:     Let $w = (w_1, w_2, \cdots, w_N)$ with $w_n = g(x^{(n)}), n = 1, 2, \cdots, N$.

9:     Let $w = \exp(T \cdot w)$.

10:     Let $w = w/(\sum_{n=1}^{N} w_n)$.

11:     Generate a random number $R \in (0, 1)$ according to standard uniform distribution, and let $r$ be the minimum number such that $\sum_{n=1}^{r} w_n > R$.

12:     Let $x_k = r$.

13:   **end for**

14: **end for**

15: Return the 3-dimensional matching (spectrum sharing) result $M_0$ and the corresponding power allocation $\{(P_{m,f}^{c*}, P_{k,f}^{d*})\}$.

---

$w_n = g(x^{(n)})$, for $n = 1, 2, \cdots, N$. We calculate $w = (w_1, w_2, \cdots, w_N)$. Instead of choosing $x_k$ such that $g(\cdot)$ is maximized as in the greedy approach listed in Algorithm 8, we will probabilistically update $x_k$ to an appropriate cluster using the procedure described below. We amplify each entry of $w$ by some factor $T$, termed as *temperature*, and then let $w = \exp(T \cdot w)$. Our goal here is to make large entries $w_n$ larger, such that when transformed into a probability distribution, those large entries of $w$ will have corresponding large probabilities. Next, we normalize $w$ to get a probability distribution $w$ with $\sum_{n=1}^{N} w_n = 1$. Based on this distribution, we will determine the value of $x_k$. Obviously, those choices of $x_k$ with larger corresponding objective function value $g(\cdot)$ will be more likely chosen. However, we also allow $x_k$ to take a value with smaller corresponding objective function since it may induce larger objective function value in future iterations. After each sweep of all V2V links, we will change our temperature parameter by setting $T = a \cdot T$ such that in the next iteration, it is more likely for us to pick the number with the largest objec-

tive function value for $x_k$. Such a procedure makes the iteration process more stable and could potentially avoid being trapped at a local optimum. Note that we also set a parameter $T_{max}$. When $a \cdot T > T_{max}$, we will not update $T$. This is because if $T$ is too large, then in practice, we may get $+\infty$ in calculation. Here, $a$ and $T_{max}$ are empirical parameters, which will be determined in the simulation experiments. Please note that the complexity of the proposed randomized algorithm is essentially close to the greedy resource allocation in Algorithm 8, which is $\mathcal{O}(C(K^2M^2 + KM^4 + KM^6 \log M))$ with $C$ depending on the number of iterations for the algorithm to converge.

The intuition of this randomized algorithm is obtained from simulated annealing [58], which is a probabilistic technique for approximating the global optimum of a given function. When the search space is discrete and large, simulated annealing is useful for approximating global optimization. The temperature parameter plays an important role in the simulated annealing algorithm. When the temperature parameter is large, the algorithm will more likely accept a bad move. Normally, the distribution used to determine whether or not we accept a bad move is known as Boltzmann distribution. At the beginning of simulated annealing, the temperature will be set to a very high level to ensure that the space in which we search for a solution is large. Moreover, the temperature will decrease as the search proceeds. When the temperature reaches a very low level, the algorithm becomes a greedy hill-climbing algorithm and the approximate solutions will converge to an optimal solution. If we decrease the temperature more slowly, then the algorithm can approximate a global optimum with higher probability.

Instead of using Boltzmann distribution to calculate the probability of accepting a state when applying simulated annealing, we use the temperature parameter and amplification coefficient in our randomized algorithm. If the temperature is high, then our algorithm is less likely to accept a bad move, which is opposite to the simulated annealing algorithm. The amplification coefficient controls the increasing speed of the temperature parameter. If the amplification coefficient is extremely close to $1$, then the algorithm will eventually

Table 4.8: Resource Allocation with Slow Fading CSI

---

**Algorithm 10** Resource Allocation with Slow Fading CSI

---

1: Use Algorithm 4 to divide $K$ V2V links into $N$ clusters, $C_1, \cdots, C_N$.
2: Use Algorithm 9 to update the clustering result, where the optimal power control parameter is obtained from solving (4.20) and Hungarian algorithm in [33] is used to find the matching between the $M$ V2I links and $N$ V2V clusters.
3: Return the matching (spectrum sharing) result and the corresponding power allocation $\{(P_m^{c*}, P_{k,m}^{d*})\}$.

---

converge to a global optimum like simulated annealing, but at the expense of dramatically increased implementation time. Therefore, in practice, we will set the amplification coefficient large to make the approximate solution converge quickly. Although in theory, the algorithm may lead to a local optimum, it works well in practice, as demonstrated by our simulation results.

## 4.3  Resource Allocation with Slow Fading CSI

In this section, we consider the resource allocation problem when the vehicular networks further reduce signaling overhead by adapting spectrum allocation and power control to slow fading CSI. In this case, in spite of the availability of fast fading CSI for links connecting the BS, such information is not used in the resource allocation process.

In the first step, Algorithm 4 will be used to find appropriate V2V clustering result, which will be used in later stages.

As the slow fading components are assumed to be frequency flat, i.e., independent of the RB index $f$, the original problem in (4.4) will be transformed to a problem for finding a matching between the $M$ V2I links and the $N$ V2V clusters, which is then a maximum matching problem for weighted bipartite graphs and can be solved efficiently in polynomial time by the Hungarian algorithm [33]. More precisely, the feasible combination will only be

indexed by $(m, n)$ instead of $(m, f, n)$ and the associated power control problem becomes

$$\max_{P_m^c, \{P_{k,m}^d\}} \log_2 \left( 1 + \frac{P_m^c \alpha_{m,B}}{\sigma^2 + \sum_{k \in C_n} P_{k,m}^d \alpha_{k,B}} \right) \triangleq R_{m,n} \qquad (4.20)$$

$$\text{s.t.} \quad \Pr \left\{ \frac{P_{k,m}^d g_k[f]}{\sigma^2 + P_m^c g_{m,k}[f] + \sum_{k' \neq k} P_{k',m}^d g_{k',k}[f]} \leq \gamma_0^d \right\}$$

$$\leq p_0, \forall k \in C_n$$

$$0 \leq P_m^c \leq P_{\max}^c$$

$$0 \leq P_{k,m}^d \leq P_{\max}^d, \forall k \in C_n$$

The same procedure in 4.2.1 can be executed to find a solution to the above formulated power control problem. Finally, we will exploit the randomized procedure in Algorithm 9 to optimize the clustering process and improve the system performance. The algorithm for resource allocation with slow fading CSI is listed in Table 4.8, whose essential complexity is $\mathcal{O}(C(K^2 M^2 + KM^3 + KM^4))$ with $C$ depending on the number of iterations for the algorithm to converge.

## 4.4 Simulation Results

In this section, simulation results are presented to validate the proposed spectrum and power allocation algorithms for D2D-based vehicular networks. We follow the simulation setup for the freeway case detailed in 3GPP TR 36.885 [10] and model a multi-lane freeway that passes through a single cell where the BS is located at its center as illustrated in Fig. 4.1. The vehicles are dropped on the roads according to spatial Poisson process and the vehicle density is determined by the vehicle speed. The $M$ V2I links are randomly chosen among generated vehicles and the $K$ V2V links are formed between each of the V2I transmitter with its closest surrounding neighbors. The major simulation parameters are listed in Table 4.9 and the channel models for V2I and V2V links are described in Table 4.10. Note

Table 4.9: Simulation Parameters [10, 47]

| Parameter | Value |
|---|---|
| Carrier frequency | 2 GHz |
| Bandwidth | 10 MHz |
| Cell radius | 500 m |
| BS antenna height | 25 m |
| BS antenna gain | 8 dBi |
| BS receiver noise figure | 5 dB |
| Distance from BS to highway | 35 m |
| Vehicle antenna height | 1.5 m |
| Vehicle antenna gain | 3 dBi |
| Vehicle receiver noise figure | 9 dB |
| Absolute vehicle speed $v$ | 70 km/h |
| Vehicle drop model | spatial Poisson process |
| Number of lanes | 3 in each direction (6 in total) |
| Lane width | 4 m |
| Average inter-vehicle distance | $2.5v$, $v$ in m/s. |
| SINR threshold for V2V $\gamma_0^d$ | 5 dB |
| Reliability for V2V $p_0$ | 0.01 |
| Number of V2I links $M$ | 10 |
| Number of V2V links $K$ | 30 |
| Maximum V2I transmit power $P_{\max}^c$ | 17, 23 dBm |
| Maximum V2V transmit power $P_{\max}^d$ | 17, 23 dBm |
| Noise power $\sigma^2$ | -114 dBm |

Table 4.10: Channel Models for V2I and V2V Links [10]

| Parameter | V2I Link | V2V Link |
|---|---|---|
| Pathloss model | $128.1 + 37.6\log_{10} d$, $d$ in km | LOS in WINNER + B1 [48] |
| Shadowing distribution | Log-normal | Log-normal |
| Shadowing standard deviation $\xi$ | 8 dB | 3 dB |
| Fast fading | Rayleigh fading | Rayleigh fading |

that all parameters are set to the values specified in Tables 4.9 and 4.10 by default, whereas the settings in each figure take precedence wherever applicable. In the simulation, the number of V2V clusters, $N$, is set to be equal to the number of V2I links, $M$.

Fig. 4.4 compares the CDF of the instantaneous sum V2I capacity achieved by the proposed algorithms against the benchmark CROWN scheme developed in [28] and its ex-

tended version, termed CROWN-F, where we have exploited the method in [28, Lemma 1] to generate an equivalent SINR threshold in terms of the slow fading CSI. In the CROWN-F scheme, we randomly allocate orthogonal RBs to V2I links and then make use of the available fast-fading CSI of links terminating at the BS, including $g_{m,B}$ and $g_{k,B}$, to perform spectrum and power allocation. We observe that all of the proposed algorithms, i.e., Algorithms 4, 5, 6, and 7 outperform the benchmark CROWN and CROWN-F schemes. In particular, the proposed greedy approach (Algorithm 5) and randomized resource allocation (Algorithm 6) achieve substantially improved performance compared with the baseline scheme (Algorithm 4) at the cost of increased complexity of further adjusting the V2V clustering. It is noted that the CROWN-F scheme and Algorithms 4, 5, and 6 use the slow fading CSI of mobile links, i.e., links among vehicles while adapting to the fast fading CSI of links involving the BS. In contrast, Algorithm 7 and the benchmark CROWN scheme only adapt to the slow fading CSI of all links in the system despite the availability of fast fading CSI of BS-involved links, thus incurring reduced network signaling overhead. For the same level of signaling overhead, Algorithm 7 significantly outperforms the benchmark CROWN scheme due to its fine tuning of V2V clustering through the proposed randomized procedure. Surprisingly, Algorithm 7 can even approach the performance of the baseline Algorithm 4, which adapts to fast fading CSI but has not employed the proposed greedy or randomized procedures to further adjust V2V clustering.

The reliability of V2V links is demonstrated in Fig. 4.5, where the CDF of the instantaneous SINR of an arbitrary V2V link has been plotted. From the figure, all proposed algorithms and the benchmark CROWN and CROWN-F schemes achieve the SINR threshold, $\gamma_0^d = 5$ dB, at the targeted outage probability of $p_0 = 0.01$, justifying the effectiveness of the reliability guarantee of the proposed resource allocation schemes. In addition, the observation that the SINR threshold is achieved fairly accurately verifies the tightness of the outage upper bound in (4.8), used to facilitate the derivation of power control designs.

Fig. 4.6 shows the performance of the proposed greedy and randomized algorithms
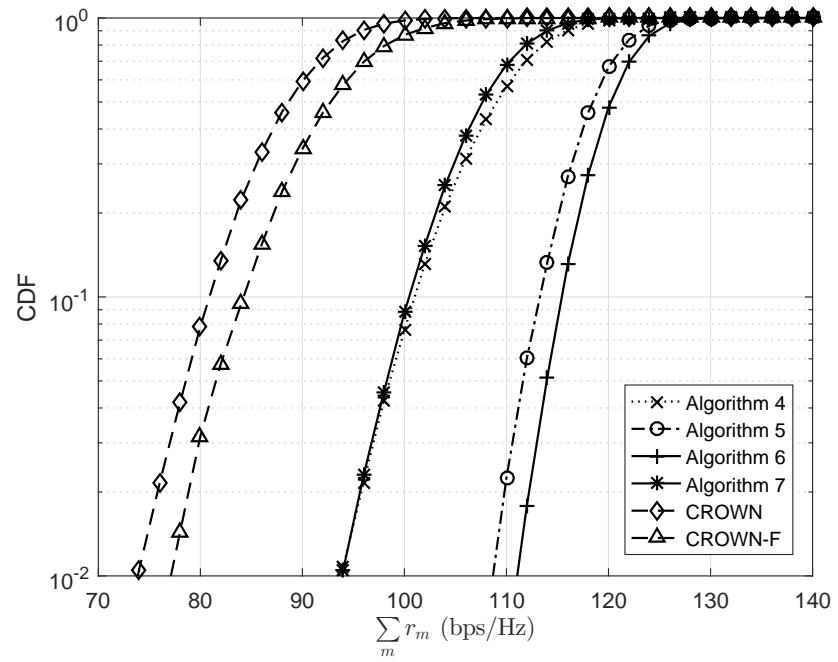
Figure 4.4: CDF of instantaneous sum V2I capacity with Rayleigh fading and $P_{\max}^d = P_{\max}^c = 23$ dBm.
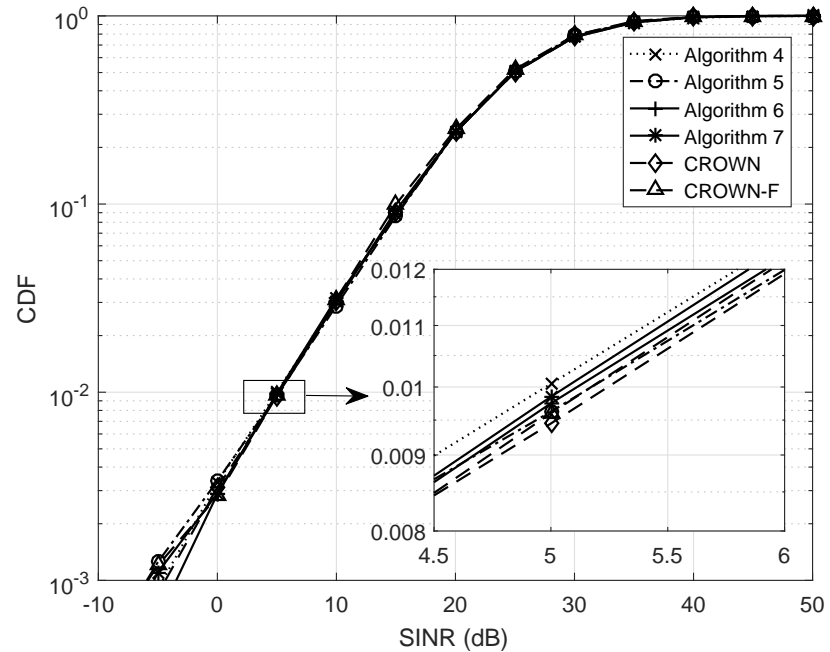


Figure 4.5: CDF of instantaneous SINR of V2V links with Rayleigh fading, $P_{\max}^d = P_{\max}^c = 23$ dBm, SINR threshold $\gamma_0^d = 5$ dB, and targeted outage probability $p_0 = 0.01$.
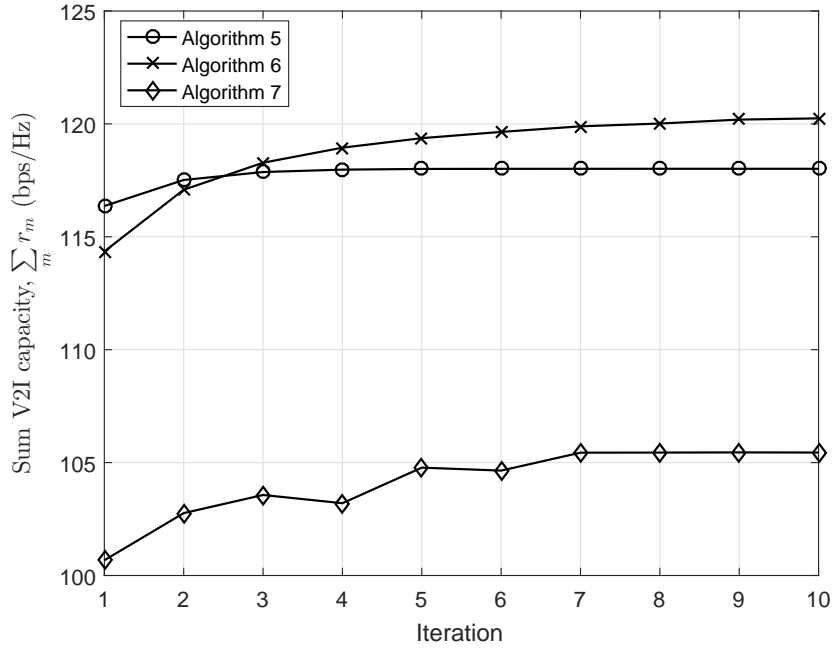
Figure 4.6: Sum V2I capacity with increasing iterations of randomized clustering, assuming $P_{\max}^d = P_{\max}^c = 23$ dBm.

with an increasing number of iterations to update V2V clustering. From the figure, the greedy approach (Algorithm 5) quickly converges to a local optimum and will not improve as the iteration number increases while the randomized Algorithm 6 keeps increasing and finally converges to a better solution. The advantage of the randomized procedure is better exemplified by Algorithm 7, where the performance can slightly decrease at the first few iterations and finally converge to a good solution. This demonstrates the effectiveness of the probabilistic approach of approximating the global optimum of a combinatorial problem. Please note that in the simulation, we have deliberately set the amplification coefficient in the randomized procedure to be large for quick convergence, whose performance turns out to be desirable. In practice, trial and error need to be performed to fine tune the parameters.

Fig. 4.7 shows the sum V2I capacity of the two proposed randomized algorithms with an increasing vehicle speed. We observe that the sum V2I capacity of both Algorithms 6 and 7 decreases as the vehicle speed increases. This is due to that the growing vehicle speed induces sparser traffic on the highway according to our simulation model as described in
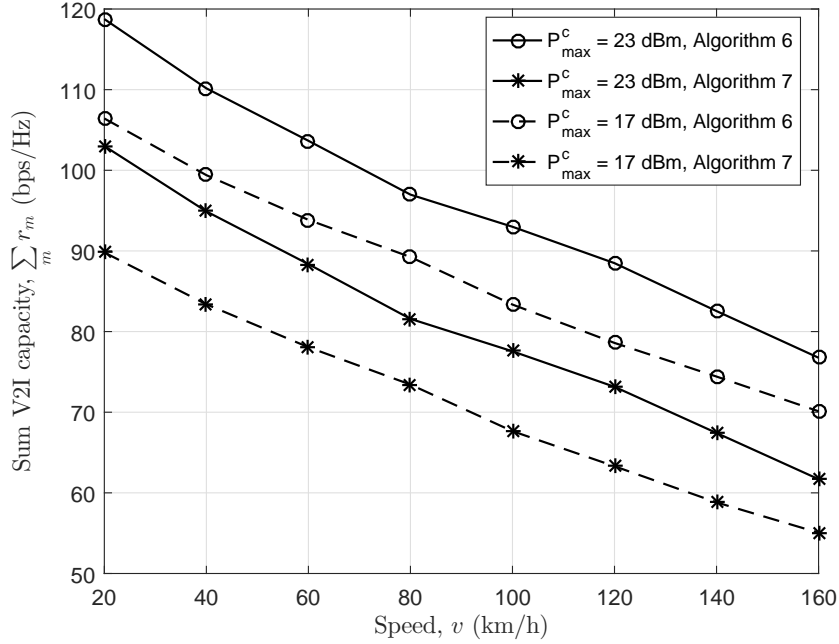
Figure 4.7: Sum V2I capacity with varying vehicle speed $v$, assuming $P_{\max}^d = P_{\max}^c$.

[10]. Here, in order to guarantee the reliability of V2V links, increased V2V transmit power is needed to compensate for higher path loss of the V2V signal channels and, meanwhile, less interference from V2I transmitters can be tolerated at the V2V receivers. As a result, the maximum allowed transmit power of V2I links will be restricted and more interference from V2V links is generated towards the V2I links, whose capacity will thus decrease. From Fig. 4.7, it is interesting to note that the sum V2I capacity decrease of both Algorithms 6 and 7 is approximately linear in growing vehicle speed, i.e., the vehicle speed roughly has a uniform impact on the sum V2I capacity. In addition, an increase of maximum transmit power of vehicular links, from 17 to 23 dBm, improves the sum V2I capacity and such capacity improvement is also roughly uniform with respect to the vehicle speed.

Fig. 4.8 demonstrates the impact of the number of active V2V links on the quality of V2I connections. We observe from the figure that the sum V2I capacity of both Algorithms 6 and 7 decreases as the number of V2V links grows larger. The reasons for such capacity decrease are two fold. On the one hand, with more active V2V links, each V2I link needs
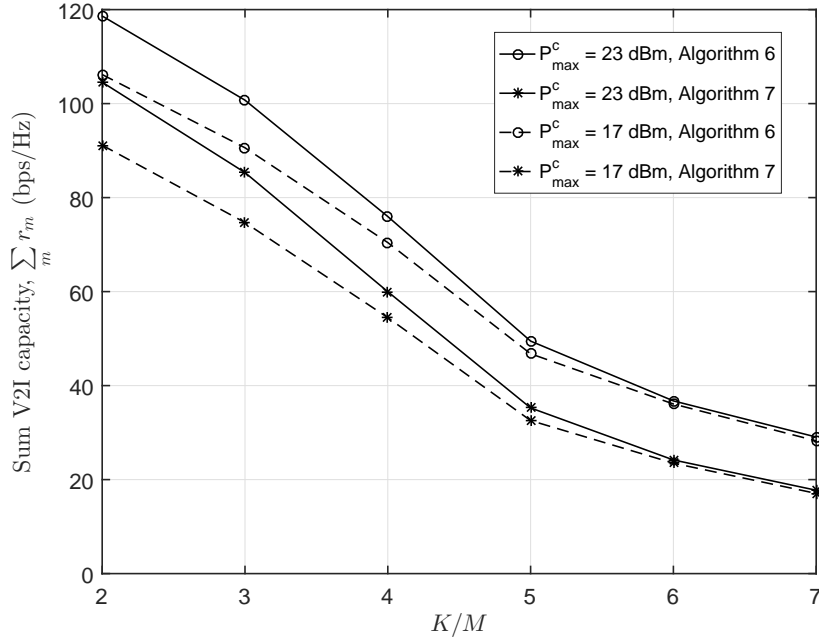
Figure 4.8: Sum V2I capacity with varying number of V2V links, assuming $P_{\max}^d = P_{\max}^c$ and $M = 10$.

to share the spectrum with more V2V links simultaneously. To guarantee the reliability of all of these V2V links, the interference from V2I transmitters needs to be controlled and thus the allowed transmit power of V2I links will be restricted, leading to decreased V2I signal power. On the other hand, more interference from the increased number of sharing V2V links will be generated towards the V2I links, which further reduces the received SINR of V2I links. We also note that the system performance of Algorithms 6 and 7 is very sensitive to the V2V link increase when only a few V2V links exist to share spectrum with V2I links, as evidenced from the steep slope of the capacity curve. Such performance degradation becomes less significant when the number of V2V links grows beyond 5 times that of V2I links, which can be attributed to the fact that the V2V interference towards V2I link is very severe in these cases and the sum V2I capacity suffers significantly, leaving very little room for further performance degradation. Besides, the sum V2I capacity increases as the transmit power budget grows from 17 to 23 dBm. However, such capacity gain becomes marginal when the number of active V2V links grows large.

## 4.5  Summary

In this chapter, we studied the resource allocation problem in D2D-based vehicular networks, in which each V2I link shares spectrum with multiple V2V links and the BS only has access to the slow fading CSI of all vehicular links except those terminating at the BS. We exploited graph partitioning algorithms to divide V2V links into disjoint spectrum-sharing clusters to minimize mutual interference before formulating the spectrum allocation problem as a weighted 3-dimensional matching problem, tackled through adapting a high performance approximation algorithm. We also proposed greedy and randomized resource allocation schemes based on our baseline algorithm, leading to substantially improved performance. To further reduce network signaling overhead, we developed a low-complexity randomized algorithm, which adapts to the slow fading CSI of all vehicular links.

# CHAPTER 5

# RESOURCE ALLOCATION WITH MULTI-AGENT REINFORCEMENT

# LEARNING

The majority of existing resource allocation methods for vehicular communications rely on some level of channel information, large- or small-scale, in a discrete and independent manner. That is, they ignore the dynamics underlying channel evolution and thus find difficulties in providing direct answers to problems of sequential nature, such as the requirement of "successfully transmitting $B$ bytes within time $T$", commonly seen in vehicular networks.

Reinforcement learning (RL) has been shown effective in addressing a wide variety of sequential decision making problems [59]. In particular, recent success of deep RL in human-level video game play [60] and Alpha Go [61] has sparked a flurry of interest in the topic and remarkable progress has been made ever since, especially in the domain of multi-agent RL. For example, a deep RL based approach has been developed in [62] to address job scheduling in computing clusters such that the average job slowdown is minimized. We believe RL is also well-suited to resource allocation problems in vehicular networks in that it can train for objectives that are hard to model or optimize in a principled manner, such as the "transmitting $B$ bytes within $T$" example. Another potential advantage of using RL for resource allocation is that distributed algorithms can be made possible, as demonstrated in [63], which treats each vehicle-to-vehicle (V2V) link as an agent that learns to refine its resource sharing strategy through interacting with the unknown vehicular environment. Detailed discussions of the challenges and opportunities of applying RL, or more generally machine learning, in vehicular networks have been presented in [64] and interested readers are referred there for an overview.

In this chapter, we consider the spectrum sharing problem in high mobility vehicular
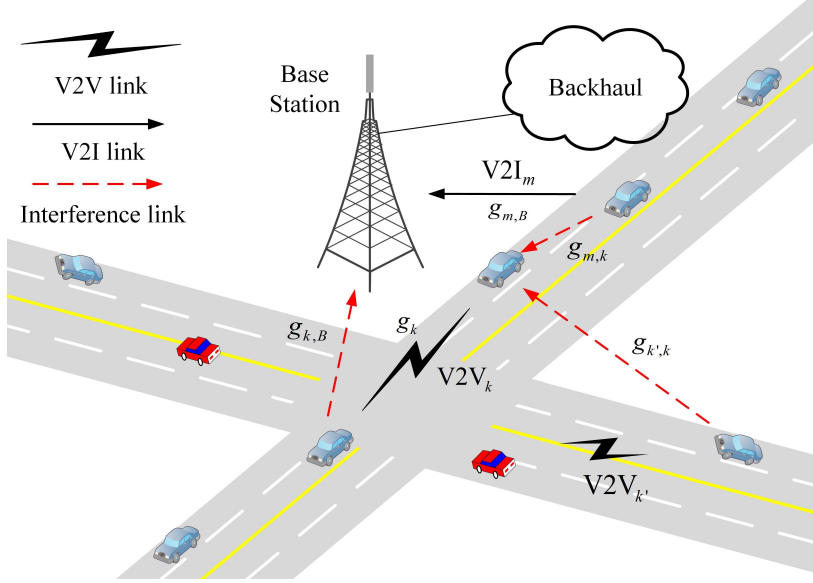
Figure 5.1: An illustrative structure of vehicular networks.

networks, where multiple V2V links attempt to share the frequency spectrum preoccupied by vehicle-to-infrastructure (V2I) links. Different from pure graph-enabled centralized [65] or RL-based decentralized [63] resource allocation methods, we develop a semi-distributed spectrum sharing scheme such that decision-making is based on a mix of fast-varying local observations and slowly-changing global large-scale fading information, seeking to harness the benefits of both. In addition, the spectrum access of multiple V2V links is naturally modeled as a multi-agent problem and we ask if recent progress of multi-agent RL [66, 67] can be exploited to enable each V2V link to learn from its own experiences while working cooperatively to optimize system-level performance.

The rest of the chapter is organized as follows. The system model is presented in Section 5.1. We introduce the basics of RL and the multi-agent RL based resource sharing design in Section 5.2. Section 5.3 provides our experiment results and concluding remarks are finally made in Section 5.4.

## 5.1 System Model

Consider a vehicular communications network with $M$ V2I and $K$ V2V links, shown in Fig. 5.1. The V2I links connect $M$ vehicles to the base station (BS) to support bandwidth intensive applications, such as social networking and media streaming. The $K$ V2V links are formed among vehicles, designed with high reliability such that safety critical information can be shared among neighboring vehicles reliably, in the form of localized D2D communications. We assume all transceivers use a single antenna. The set of V2I links and V2V links are denoted by $\mathcal{M} = \{1, \cdots, M\}$ and $\mathcal{K} = \{1, \cdots, K\}$, respectively.

In this chapter, we assume that the $M$ V2I links (uplink considered) have been preassigned $M$ orthogonal spectrum bands, one for each. To improve spectral efficiency, these bands are reused by the $K$ V2V links. In practice, the number of V2V links tends to be much larger than that of V2I links, i.e., $K \gg M$, making spectrum reuse among V2V links necessary. As a result, the major challenge is to design an efficient spectrum sharing scheme for these V2V links such that both types of vehicular links achieve their respective goals with minimal signaling overhead.

The channel power gain, $g_k[m]$, of the $k$th V2V link over the $m$th band (occupied by the $m$th V2I link) follows

$$g_k[m] = \alpha_k h_k[m], \tag{5.1}$$

where $h_k[m]$ is the frequency dependent fast (small-scale) fading power component and assumed to be exponentially distributed with unit mean, and $\alpha_k$ captures the large-scale fading effect, including path loss and shadowing, assumed to be frequency independent. The interfering channel from the $k'$th V2V transmitter to the $k$th V2V receiver over the $m$th band, $g_{k',k}[m]$, the interfering channel from the $k$th V2V transmitter to the BS over the $m$th band, $g_{k,B}[m]$, the channel from the $m$th V2I transmitter to the BS, $\hat{g}_{m,B}$, and the interfering channel from the $m$th V2I transmitter to the $k$th V2V receiver, $\hat{g}_{m,k}$, are

similarly defined.

The received signal-to-interference-plus-noise ratios (SINRs) of the $m$th V2I link and the $k$th V2V link (over the $m$th band) are expressed as

$$\gamma_m^c = \frac{P_m^c \hat{g}_{m,B}}{\sigma^2 + \sum_k \rho_k[m] P_k^d[m] g_{k,B}[m]},$$

(5.2)

and

$$\gamma_k^d[m] = \frac{P_k^d[m] g_k[m]}{\sigma^2 + I_k[m]},$$

(5.3)

respectively, where $P_m^c$ and $P_k^d[m]$ denote transmit powers of the $m$th V2I transmitter and the $k$th V2V transmitter over the $m$th band, respectively, $\sigma^2$ is the noise power, and

$$I_k[m] = P_m^c \hat{g}_{m,k} + \sum_{k' \neq k} \rho_{k'}[m] P_{k'}^d[m] g_{k',k}[m],$$

(5.4)

denotes the interference power. $\rho_k[m]$ is the binary spectrum allocation indicator with $\rho_k[m] = 1$ implying the $k$th V2V link uses the $m$th band and $\rho_k[m] = 0$ otherwise. We assume each V2V link only accesses one band, i.e., $\sum_m \rho_k[m] \leq 1$.

Capacities of the V2I and V2V links are obtained as

$$C_m^c = W \log(1 + \gamma_m^c),$$

(5.5)

and

$$C_k^d[m] = W \log(1 + \gamma_k^d[m]),$$

(5.6)

where $W$ is the bandwidth of each spectrum band.

Per requirements of different vehicular links, the objective is to design power con-

trol and spectrum allocation schemes that simultaneously maximize the sum V2I capacity, $\sum_{m} C_m^c$, and the V2V payload transmission probability,

$$\Pr\left\{\sum_{t=1}^{T}\sum_{m=1}^{M}\rho_k[m]C_k^d[m,t] \geq B/\Delta_T\right\}, k \in \mathcal{K}, \tag{5.7}$$

where $B$ is the payload size, $\Delta_T$ is channel coherence time, $T$ is the payload generation period, and the index $t$ is added in $C_k^d[m,t]$ to indicate V2V capacity at different time slots.

## 5.2 Multi-Agent RL Based Resource Allocation

After briefly introducing the basics of RL as well as its multi-agent variant, we formulate the spectrum sharing design in vehicular networks as a multi-agent RL problem. For detailed treatment of RL, we refer interested readers to [59].

### 5.2.1 Reinforcement Learning

RL addresses the problem of sequential decision making, where an agent learns to map situations to actions so as to maximize certain numerical rewards through interacting with the environment. Mathematically, the RL problem can be modeled as a Markov decision process (MDP). As shown in Fig. 5.2, at each discrete time step $t$, the agent observes some representation of the environment state $S_t$ from the state space $\mathcal{S}$, and then selects an action $A_t$ from the action set $\mathcal{A}$. Following the action, the agent receives a numerical reward $R_{t+1}$ and the environment transitions to a new state $S_{t+1}$, with transition probability $p(s',r|s,a) \triangleq \Pr\{S_{t+1} = s', R_{t+1} = r | S_t = s, A_t = a\}$.

In RL, decision making manifests itself in a policy $\pi(a|s)$, which is a mapping from states in $\mathcal{S}$ to probabilities of selecting each action in $\mathcal{A}$. The goal of learning is to find an optimal policy $\pi_*$ that maximizes the expected return $G_t$ from any initial state $s$, where $G_t$ is defined as the cumulative discounted rewards with a discount rate $\gamma$, i.e., $G_t = \sum_{k=0}^{\infty}\gamma^k R_{t+k+1}$ with $0 \leq \gamma \leq 1$.
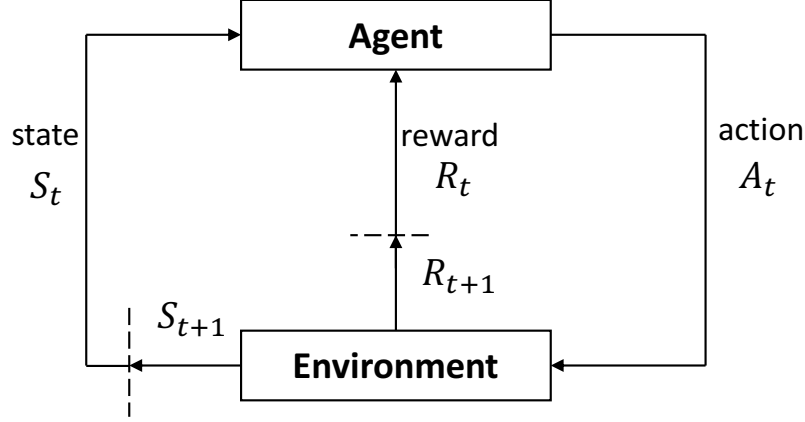
Figure 5.2: The agent-environment interaction in a reinforcement learning problem.

*Q-Learning*

Q-Learning [68] is a popular model-free method (meaning explicit knowledge of MDP dynamics $p(s', r|s, a)$ is not required) to solve RL problems. It is based on the concept of action-value function, $q_\pi(s, a)$ for policy $\pi$, which is defined as the expected return starting from the state $s$, taking the action $a$, and thereafter following the policy $\pi$, formally expressed as

$$q_\pi(s, a) = \mathbb{E}_\pi \left[ G_t | S_t = s, A_t = a \right]. \tag{5.8}$$

The action-value function of the optimal policy, $q_*(s, a)$, satisfies recursive relationships, known as the Bellman optimality equation:

$$q_*(s, a) = \sum_{s', r} p(s', r|s, a) \left[ r + \gamma \max_{a'} q_*(s', a') \right], \tag{5.9}$$

for any state $s$, action $a$, successor state $s'$ and action $a'$. In principle, one can solve the systems of nonlinear equations for $q_*(s, a)$ if the dynamics $p(s', a'|s, a)$ are known. Once

$q_*$ is obtained, it is easy to determine the optimal policy:

$$\pi_*(a|s) = \begin{cases} 1, & \text{if } a = \arg\max_{a \in \mathcal{A}} q_*(s, a), \\ 0, & \text{otherwise.} \end{cases} \tag{5.10}$$

Q-learning avoids the difficulties of acquiring exact dynamics $p(s', a'|s, a)$ and directly solving the nonlinear optimality equations in (5.9) and resorts to an iterative update method, given by

$$Q(S_t, A_t) \leftarrow Q(S_t, A_t) + \alpha \left[ R_{t+1} + \gamma \max_a Q(S_{t+1}, a) - Q(S_t, A_t) \right], \tag{5.11}$$

where $\alpha$ is the step-size parameter and the choice of $A_t$ in state $S_t$ follows some soft policies, e.g., the $\epsilon$-greedy policy, meaning that the action with maximal estimated value is chosen with probability $1 - \epsilon$ while a random action is instead selected with probability $\epsilon$. It has been shown in [59] that with a variant of the stochastic approximation conditions on $\alpha$ and the assumption that all state-action pairs continue to be updated, $Q$ converges with probability $1$ to the optimal action-value function $q_*$.

*Deep Q-Network with Experience Replay*

In many problems of practical interest, the state and action space can be too large to store all action-value functions in a tabular form. As a result, it is common to use function approximation to estimate these value functions. Another advantage of doing so is the generalization ability from limited seen state-action pairs to produce approximation in a much larger space. In deep Q-learning [60], a deep neural network parameterized by $\theta$, called deep Q-network (DQN), is used to represent the action-value function. The state-action space is explored with some soft policies, e.g., $\epsilon$-greedy, and the transition tuple $(S_t, A_t, R_{t+1}, S_{t+1})$ is stored in a replay memory at each time step. The replay memory accumulates experiences over many episodes of the MDP. At each step, a mini-batch of
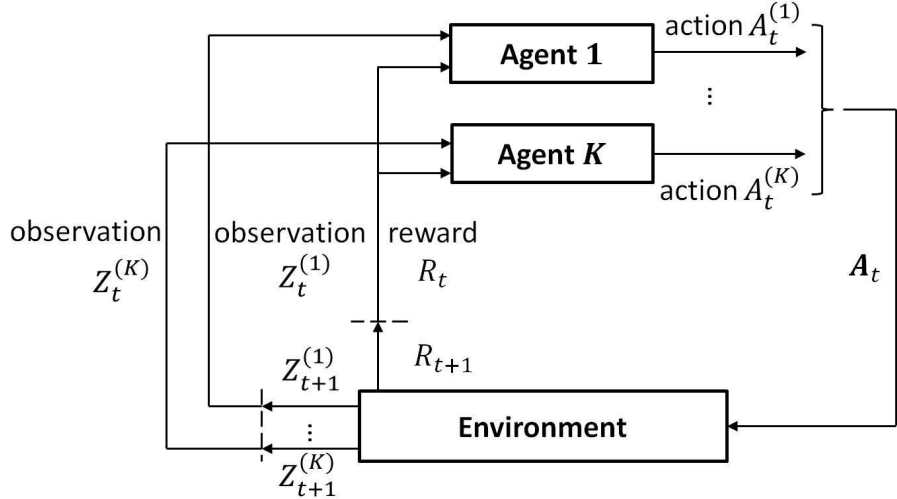
Figure 5.3: The agent-environment interaction in a multi-agent reinforcement learning problem.

experiences $\mathcal{D}$ are uniformly sampled from the memory for updating $\theta$ with variants of stochastic gradient-descent methods, hence the name experience replay, to minimize the sum-squared error:

$$\sum_{\mathcal{D}} \left[ R_{t+1} + \gamma \max_{a'} Q(S_t, a'; \theta^-) - Q(S_t, A_t; \theta) \right]^2, \tag{5.12}$$

where $\theta^-$ are the parameters of a target Q-network, which are duplicated from the training Q-network parameters $\theta$ periodically and fixed for a couple of updates. Experience replay improves sample efficiency through repeatedly sampling stored experiences and breaks correlation in successive updates, thus also stabilizing learning.

### 5.2.2  Multi-Agent Reinforcement Learning

Different from single-agent RL, the multi-agent RL problem setup consists of multiple agents, denoted by $i \in \mathcal{I} = \{1, \cdots, I\}$, concurrently exploring the unknown environment [66, 67]. The underlying MDP is described in the following. As shown in Fig. 5.3, at each time step $t$, given the current environment state $S_t$, each agent $i$ receives an observation $Z_t^{(i)}$ of the environment, determined by the observation function $O$ as $Z_t^{(i)} = O(S_t, i)$, and

then takes an action $A_t^{(i)}$, forming a joint action $\mathbf{A}_t$. Thereafter, the agent receives a reward $R_t$ and the environment evolves to the next state $S_{t+1}$ with probability $p(s', r | s, \mathbf{a})$. Please note that all agents share the same reward in this article such that cooperative behavior is encouraged among them.

Independent Q-learning [69] is among the most popular methods to solve multi-agent RL problems, where each agent learns a decentralized policy based on its own action and observation, treating other agents as part of the environment. However, naively combining DQN with independent Q-learning is problematic since each agent would face a nonstationary environment while other agents are also learning to adjust their behaviors. The issue grows even more severe with experience replay, which is the key to the success of DQN, in that sampled experiences no longer reflect current dynamics and thus destabilize learning.

5.2.3   Resource Sharing with Multi-Agent RL

In the investigated resource sharing scenario illustrated in Fig. 5.1, multiple V2V links attempt to access limited spectrum occupied by V2I links, which would naturally be modeled as a multi-agent RL problem. Each V2V link acts as an agent and interacts with the unknown communication environment to gain experiences, which are then used to direct its own policy design. Multiple V2V agents collectively explore the environment and refine spectrum allocation and power control strategies based on their own observations of the environment state. While the resource sharing problem may appear a competitive game, we turn it into a fully cooperative one through using the same reward for all agents, in the interest of global network performance.

The proposed multi-agent RL formulation bases resource sharing design on a mix of fast-varying local observations of each individual V2V link and the slowly-changing global large-scale fading information. The global information is collected at the BS and then broadcasted to all vehicles in its coverage [70], as evidenced in the following observation

space design. It is noted that we focus on settings with centralized learning and semi-distributed execution. This means in the learning phase, the global performance-oriented reward (to be defined in the following) is readily accessible to each individual V2V agent, which then adjusts its actions towards an optimal policy. This is a feasible practice since our group of V2V agents are trained on an environment simulator. In the execution phase, each V2V agent receives a mix of local fast-varying observations of the environment and the periodically broadcasted global channel information, and then selects an action according to its trained DQN on a time scale on par with the local observations. Key elements of the multi-agent RL based resource sharing design are described below in detail.

*State and Observation Space*

In the multi-agent RL formulation of the resource sharing problem, each V2V link acts as an agent while everything beyond itself is treated as part of the environment. The true environment state, $S_t$, which could include global channel conditions and all agents' behaviors, is unknown to each individual V2V agent. Each agent can only acquire knowledge of the underlying environment through the lens of an observation function. In part, the observation space includes the global large-scale fading information, i.e., $\boldsymbol{\alpha} = \{\alpha_k, \alpha_{k',k}, \alpha_{k,B}, \hat{\alpha}_{m,B}, \hat{\alpha}_{m,k}\}$, for all $k \in \mathcal{K}$ and $m \in \mathcal{M}$, which varies slowly and can be periodically collected at the BS and broadcast to all vehicles. Additionally, the observation space of an individual V2V agent $k$ contains fast-changing local information, including its own small-scale channel fading, $h_k[m]$, for all $m \in \mathcal{M}$, interference channels from other V2V transmitters, $h_{k',k}[m]$, for all $k' \neq k$ and $m \in \mathcal{M}$, the interference channel from its own transmitter to the BS, $h_{k,B}[m]$, for all $m \in \mathcal{M}$, and the interference channel from V2I transmitters, $\hat{h}_{m,k}$, for all $m \in \mathcal{M}$. The relationship between overall channel gain, $g$, and small-scale channel fading, $h$, is given in (5.2). The received interference power over all bands, $I_k[m]$, for all $m \in \mathcal{M}$, expressed in (5.4), can be measured and introduced in the local observation. In addition, the local observation space also includes the remaining V2V payload, $B_k$, and the remaining

time budget, $T_k$. Hence, the observation function for an agent $k$ is

$$O(S_t, k) = \{\boldsymbol{\alpha}, B_k, T_k, \{H_k[m]\}_{m \in \mathcal{M}}\}, \tag{5.13}$$

with $H_k[m] = \{h_k[m], h_{k',k}[m], h_{k,B}[m], \hat{h}_{m,k}, I_k[m]\}$.

To address the issue of combining independent Q-learning with DQN as discussed in Section 5.2.2, we adopt the fingerprint-based method developed in [67]. The idea is that while the action-value function of an agent is nonstationary with other agents changing their behaviors over time, it can be made stationary conditioned on other agents' policies. This means we can augment each agent's observation space with an estimate of other a-gents' policies to avoid nonstationarity, which is the essential idea of hyper Q-learning [71]. However, it is undesirable for the action-value function to include as input all param-eters of other agents' neural networks, $\boldsymbol{\theta}_{-i}$, since the policy of each agent consists of a high dimensional DQN. Instead, it is proposed in [67] to simply include a low-dimensional fingerprint that tracks the trajectory of the policy change of other agents. This method po-tentially works since nonstationarity of the action-value function results from changes of other agents' policies over time, as opposed to the policies themselves. Further analysis reveals that each agent's policy change is highly correlated with the training iteration num-ber $e$ as well as its rate of exploration, e.g., the probability of random action selection, $\epsilon$, in the $\epsilon$-greedy policy widely used in Q-learning. As a result, we include both of them in the observation for an agent $k_0$, expressed as

$$Z_t^{(k_0)} = \{O(S_t, k_0), e, \epsilon\}. \tag{5.14}$$

*Action Space*

The resource sharing design of vehicular links comes down to the spectrum band selection and transmission power control. While the spectrum naturally breaks into $M$ disjoint bands,

each preoccupied by one V2I link, the V2V transmission power typically takes continuous value in most power control literature. In this chapter, however, we limit the power control options to four levels, i.e., $[23, 10, 5, 0]$ dBm, for the sake of both ease of learning and practical circuit restrictions. As a result, the dimension of the action space is $4 \times M$, with each action corresponding to one particular combination of band and power selection.

*Reward Design*

What makes RL particularly appealing for solving problems with hard-to-optimize objectives using precise mathematical methods is the flexibility in its reward design. In the studied V2X spectrum sharing problem, our objectives are twofold: maximizing the sum V2I capacity while increasing V2V payload transmission success probability.

In response to the first goal, we simply include the instantaneous sum V2I capacity, $\sum_{m \in \mathcal{M}} C_m^c(t)$, in the reward at each step. To achieve the second goal, we give a reward of 1 to each V2V agent if the payload transmission is finished at the current step, and 0 for all other cases. We observe that if setting the discount rate $\gamma$ to 1, the designed reward encourages each agent to finish payload transmission to achieve higher reward values but will not distinguish if the finishing moment comes early or late. A salient feature of this design is that the system can now learn to balance the progress of the two spectrum sharing objectives. For example, the V2V agent may choose to lower its power for the benefit of V2I capacity improvement if it is optimistic about its own future transmission instead of always selfishly increasing power to finish early.

Specifically, we set the reward at each time step $t$ as

$$R_t = \lambda_c \sum_m C_m^c(t) + \lambda_d \sum_k L_k(t), \tag{5.15}$$

where $L_k(t)$ is the V2V reward component designed as described above. $\lambda_c$ and $\lambda_d$ are positive weights to balance V2I and V2V objectives.

**Algorithm 11** Resource Sharing with Multi-Agent RL

---

1: Start environment simulator, generating vehicles and links
2: Initialize Q-networks for all agents randomly
3: **for** each episode **do**
4:     Update vehicle locations and large-scale fading $\alpha$
5:     Reset $B_k = B$ and $T_k = T$, for all $k \in \mathcal{K}$
6:     **for** each step $t$ **do**
7:         **for** each V2V agent $k$ **do**
8:             Observe $Z_t^{(k)}$
9:             Choose action $A_t^{(k)}$ from $Z_t^{(k)}$ according to $\epsilon$-greedy policy
10:        **end for**
11:        Update channel small-scale fading
12:        All agents take actions and receive reward $R_{t+1}$
13:        **for** each V2V agent $k$ **do**
14:            Observe $Z_{t+1}^{(k)}$
15:            Store $\left( Z_t^{(k)}, A_t^{(k)}, R_{t+1}, Z_{t+1}^{(k)} \right)$ in replay memory $\mathcal{D}_k$
16:        **end for**
17:    **end for**
18:    **for** each V2V agent $k$ **do**
19:        Uniformly sample mini-batches from $\mathcal{D}_k$
20:        Optimize error between Q-network and learning targets (5.12) using variant of stochastic gradient descent
21:    **end for**
22: **end for**

---

*Training Algorithm*

We focus on an episodic setting with each episode spanning the safety message generation period $T$. Each episode starts with a randomly initialized environment state (determined by the initial transmission powers of all vehicular links, channel states, etc.) and a full V2V load of size $B$ for transmission, and lasts until the end of $T$. The change of channel small-scale fading triggers a transition of the environment state and causes each individual V2V agent to adjust its actions.

Each V2V agent $k$ has a Q-network that takes as input the current observation $Z_t^{(k)}$ and outputs the value functions corresponding to all actions. We train the Q-networks through running multiple episodes and, at each training step, all V2V agents select their actions

Table 5.1: Simulation Parameters [10, 47]

| Parameter | Value |
|---|---|
| Number of V2I links $M$ | 4 |
| Number of V2V links $K$ | 4 |
| Carrier frequency | 2 GHz |
| Bandwidth | 4 MHz |
| BS antenna height | 25 m |
| BS antenna gain | 8 dBi |
| BS receiver noise figure | 5 dB |
| Vehicle antenna height | 1.5 m |
| Vehicle antenna gain | 3 dBi |
| Vehicle receiver noise figure | 9 dB |
| Absolute vehicle speed $v$ | 36 km/h |
| Vehicle drop and mobility model | Urban case of A.1.2 in [10]* |
| V2I transmit power $P^c$ | 23 dBm |
| V2V transmit power $P^d$ | [23,10,5,0] dBm |
| Noise power $\sigma^2$ | -114 dBm |
| V2V payload generation period | 100 ms |
| V2V payload size | $[1, 2, \cdots] \times$ 1060 bytes |

* We shrink the height and width of the simulation area by a factor of 2.

based on the observations and their current Q-networks as well as the exploration rate $\epsilon$. Following the environment transition due to actions taken by all V2V agents, each agent $k$ collects and stores the transition tuple, $\left(Z_t^{(k)}, A_t^{(k)}, R_{t+1}, Z_{t+1}^{(k)}\right)$, in a replay memory. At each episode, we uniformly sample batches of stored transitions $\mathcal{D}$ from the replay memory and update the Q-network of each V2V agent through minimizing the sum-squared error in (5.12). The training procedure is summarized in Algorithm 11.

## 5.3 Simulation Results

In this section, simulation results are presented to validate the proposed multi-agent RL based resource sharing scheme. We follow the simulation setup for the urban case in 3GPP TR 36.885 [10] detailing models used for vehicle drop and mobility, vehicular channels, and V2V data traffic. The V2I links are started by $M$ generated vehicles and the $K$ V2V links are formed between each vehicle with its closest surrounding neighbor. Major simu-

Table 5.2: Channel Models for V2I and V2V Links [10]

| Parameter | V2I Link | V2V Link |
|---|---|---|
| Path loss model | $128.1 + 37.6\log_{10} d$, $d$ in km | LOS in WINNER + B1 Manhattan [48] |
| Shadowing distribution | Log-normal | Log-normal |
| Shadowing standard deviation $\xi$ | 8 dB | 3 dB |
| Decorrelation distance | 50 m | 10 m |
| Path loss and shadowing update | A.1.4 in [10] every 100 ms | A.1.4 in [10] every 100 ms |
| Fast fading | Rayleigh fading | Rayleigh fading |
| Fast fading update | Every 1 ms | Every 1 ms |

lation parameters are listed in Table 5.1 and the channel models for V2I and V2V links are described in Table 5.2.

The DQN for each V2V agent consists of 3 fully connected hidden layers, whose numbers are $500, 250$, and $120$, respectively. The rectified linear unit (ReLU), $f(x) = \max(0, x)$, is used as the activation function and RMSProp optimizer [72] is used to update network parameters with a learning rate of $0.001$. We train each agent's Q-network for a total of $4000$ episodes and the exploration rate $\epsilon$ is linearly annealed from $1$ to $0.02$ over the beginning $3000$ episodes and remains constant afterwards.

We compare Algorithm 11, termed MARL, with the single-agent RL based algorithm in [63], termed SARL, and a random baseline method in terms of V2V payload transmission success probability and sum V2I capacity, respectively. The random baseline chooses the spectrum band and transmission power level in a random fashion at each time step. It is noted that in our currently presented simulation results, we fix the large-scale fading of the channels and only alter small-scale fading at each time step to obtain some preliminary evaluation results. In the training stage, we fix the payload size to be of $2 \times 1060$ bytes, but vary the sizes in the testing stage to verify method robustness.

Fig. 5.4 shows the V2I performance with respect to increasing V2V payload sizes for different resource sharing designs. From the figure, the performance drops for all schemes with growing V2V payload sizes and the proposed Algorithm 11 achieves better perfor-
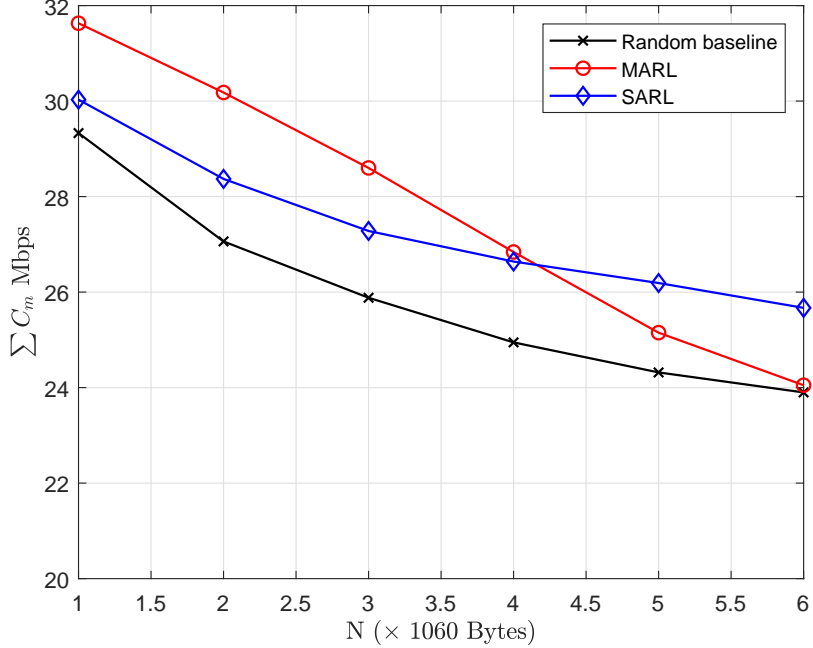
Figure 5.4: Sum capacity performance of V2I links with varying V2V payload sizes.

mance than the other two benchmarks with low V2V payloads. Increased V2V payload leads to longer V2V transmission duration and possibly higher V2V transmit power in order to improve V2V payload transmission success probability. This will inevitably cause stronger interference to V2I links for a longer period and thus jeopardize their capacity performance.

Fig. 5.5 demonstrates the performance of the V2V payload transmission success probability against growing payload sizes using different spectrum sharing schemes. From the figure, as the V2V payload size grows larger, the transmission success probabilities of all schemes drop as expected. However, the proposed multi-agent RL based method achieves significantly better performance than benchmarks due to effective reward designs, which maximize the V2V payload transmission success probability. Remarkably, for $B = 1060$ and $B = 2 \times 1060$ bytes, the proposed method attains $100\%$ V2V transmission probability and meanwhile improves V2I capacity, as shown in Fig. 5.4. However, it is also more sensitive (less robust) to V2V payload increase compared with SARL and the degradation becomes more pronounced when payload grows beyond $4 \times 1060$ bytes.
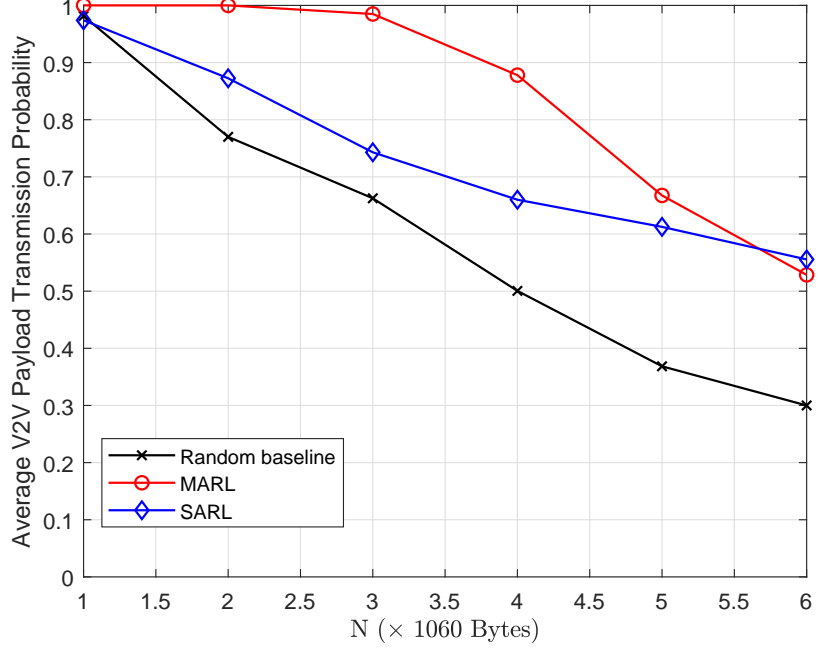
Figure 5.5: V2V payload transmission success probability with varying payload sizes.

## 5.4 Summary

We have presented a semi-distributed resource sharing scheme using multi-agent RL for vehicular networks, which adapts spectrum allocation and power control to a mix of fast-varying local observations and slowly-changing global channel information. A fingerprint-based method has been exploited to address nonstationary issues of independent Q-learning for multi-agent RL problems when combined with DQN with experience replay. Initial simulation results demonstrate improved performance of the proposed resource sharing scheme in terms of both V2I capacity and V2V payload transmission probability compared with a random baseline method.

# CHAPTER 6

## CONCLUSION

This thesis has focused on resource allocation for vehicular communications under the D2D-based network architecture. We have presented four distinctive yet coherent design schemes that maximize capacity of vehicle-to-infrastructure (V2I) links and guarantee the reliability of vehicle-to-vehicle (V2V) links based on careful treatment of unique characteristics of vehicular environments. First, we propose to employ the slowly-varying large-scale fading information of all channels to perform spectrum and power allocation for vehicular communications when the underlying channels experience Rayleigh fading. This relieves the harsh requirement to accurately track vehicular channels that undergo fast temporal variations. Novel algorithms that yield optimal resource allocation performance have been developed to maximize the sum and minimum capacity of all V2I links, respectively. Then, we revisit the channel state information (CSI) requirement of vehicular communications by reporting such CSI periodically to the base station. We take into account the inevitable delay in CSI feedback and propose optimal spectrum and power allocation design to maximize V2I capacity while guaranteeing V2V reliability. Afterwards, we further generalize the resource allocation problems to a generic setting, where multiple V2V links share the spectrum with one or more V2I links and the frequency spectrum is not assumed to be assigned to V2I links beforehand. Graph theoretic tools have been exploited to solve the formulated resource allocation problem and a suite of algorithms, including a baseline graph-based algorithm, a greedy scheme, and a novel algorithm involving randomized procedures, have been developed to address the performance-complexity tradeoffs. Finally, we approach the resource allocation problem from a learning perspective and model resource sharing as a multi-agent reinforcement learning (RL) problem. The V2V links, each acting as an agent, collectively explore the unknown communication environment and

gain experiences to guide their sharing strategy design. A mix of fast-varying local observations and slowly-changing global large-scale fading information is used for resource sharing related decision making, which causes resource management to change on a time scale comparable to small-scale fading of vehicular channels. The four proposed schemes, which include both centralized and semi-distributed designs with varying performance-complexity tradeoffs, constitute a comprehensive study of resource allocation for vehicular communications.

# REFERENCES

[1] L. Liang, H. Peng, G. Y. Li, and X. Shen, "Vehicular communications: A physical layer perspective," *IEEE Trans. Veh. Technol.*, vol. 66, no. 12, pp. 10 647–10 659, Dec. 2017.

[2] H. Peng, L. Liang, X. Shen, and G. Y. Li, "Vehicular communications: a network layer perspective," to appear in *IEEE Trans. Veh. Technol.*, Jun. 2018.

[3] G. Araniti, C. Campolo, M. Condoluci, A. Iera, and A. Molinaro, "LTE for vehicular networking: A survey," *IEEE Commun. Mag*, vol. 51, no. 5, pp. 148–157, May 2013.

[4] P. Papadimitratos, A. D. L. Fortelle, M. Paristech, K. Evenssen, R. Brignolo, and S. Cosenza, "Vehicular communication systems: Enabling technologies, applications, and future outlook on intelligent transportation," *IEEE Commun. Mag.*, vol. 47, no. 11, pp. 84–95, Nov. 2009.

[5] H. Seo, K. D. Lee, S. Yasukawa, Y. Peng, and P. Sartori, "LTE evolution for vehicle-to-everything services," *IEEE Commun. Mag.*, vol. 54, no. 6, pp. 22–28, Jun. 2016.

[6] S. Schwarz, T. Philosof, and M. Rupp, "Signal processing challenges in cellular-assisted vehicular communications: Efforts and developments within 3GPP LTE and beyond," *IEEE Signal Process. Mag.*, vol. 34, no. 2, pp. 47–59, Mar. 2017.

[7] X. Cheng, L. Yang, and X. Shen, "D2D for intelligent transportation systems : A feasibility study," *IEEE Trans. Intell. Transp. Syst.*, vol. 16, no. 4, pp. 1784–1793, Aug. 2015.

[8] J. B. Kenney, "Dedicated short-range communications (DSRC) standards in the United States," *Proc. IEEE*, vol. 99, no. 7, pp. 1162–1182, Jul. 2011.

[9] *Intelligent Transport Systems (ITS); Cooperative ITS (C-ITS); Release 1*. ETSI TR 101 607 V1.1.1, May 2013.

[10] *3rd Generation Partnership Project; Technical Specification Group Radio Access Network; Study on LTE-based V2X Services; (Release 14)*. 3GPP TR 36.885 V14.0.0, Jun. 2016.

[11] *3rd Generation Partnership Project; Technical Specification Group Radio Access Network; Study on enhancement of 3GPP Support for 5G V2X Services; (Release 15)*. 3GPP TR 22.886 V15.1.0, Mar. 2017.

[12] *Scenarios, requirements and KPIs for 5G mobile and wireless system.* METIS ICT-317669-METIS/D1.1, METIS deliverable D1.1, Apr. 2013. [Online]. Available: `https://www.metis2020.com/documents/deliverables/`.

[13] *IEEE Standard for Information Technology–Telecommunications and information exchange between systems–Local and metropolitan area networks–Specific requirements–Part 11: Wireless LAN Medium Access Control (MAC) and Physical Layer (PHY) specifications Amendment 6: Wireless Access in Vehicular Environments.* IEEE Std. 802.11p-2010, Jul. 2010.

[14] Z. H. Mir and F. Filali, "LTE and IEEE 802.11p for vehicular networking: A performance evaluation," *EURASIP J. Wireless Commun. Netw.*, vol. 11, no. 89, pp. 1–15, May 2014.

[15] D. Feng, L. Lu, Y. Yuan-Wu, G. Y. Li, S. Li, and G. Feng, "Device-to-device communications in cellular networks," *IEEE Commun. Mag.*, vol. 52, no. 4, pp. 49–55, Apr. 2014.

[16] K. Abboud, H. Omar, and W. Zhuang, "Interworking of DSRC and cellular network technologies for V2X communications: A Survey," *IEEE Trans. Veh. Technol.*, vol. 65, no. 12, pp. 9457–9470, Dec. 2016.

[17] A. Asadi, Q. Wang, and V. Mancuso, "A survey on device-to-device communication in cellular networks," *IEEE Commun. Surveys Tuts.*, vol. 16, no. 4, pp. 1801–1819, 4th Quart., 2014.

[18] K. Doppler, M. Rinne, C. Wijting, C. B. Ribeiro, and K. Hug, "Device-to-device communication as an underlay to LTE-advanced networks," *IEEE Commun. Mag.*, vol. 47, no. 12, pp. 42–49, Dec. 2009.

[19] H. Min, J. Lee, S. Park, and D. Hong, "Capacity enhancement using an interference limited area for device-to-device uplink underlaying cellular networks," *IEEE Trans. Wireless Commun.*, vol. 10, no. 12, pp. 3995–4000, Dec. 2011.

[20] W. Xu, L. Liang, H. Zhang, S. Jin, J. C. F. Li, and M. Lei, "Performance enhanced transmission in device-to-device communications: Beamforming or interference cancellation?," in *Proc. IEEE GLOBECOM*, Dec. 2012, pp. 4296–4301.

[21] C. H. Yu, K. Doppler, C. B. Ribeiro, and O. Tirkkonen, "Resource sharing optimization for device-to-device communication underlaying cellular networks," *IEEE Trans. Wireless Commun.*, vol. 10, no. 8, pp. 2752–2763, Aug. 2011.

[22] P. Jänis, V. Koivunen, Ć. Ribeiro, J. Korhonen, K. Doppler, and K. Hugl, "Interference-aware resource allocation for device-to-device radio underlaying cellular networks," in *Proc. IEEE VTC-Spring*, Apr. 2009, pp. 1–5.

[23] D. Feng, L. Lu, Y. Yuan-Wu, G. Y. Li, G. Feng, and S. Li, "Device-to-device communications underlaying cellular networks," *IEEE Trans. Commun.*, vol. 61, no. 8, pp. 3541–3551, Aug. 2013.

[24] Z. Zhao, X. Cheng, M. Wen, B. Jiao, and C.-X. Wang, "Channel estimation schemes for IEEE 802.11p standard," *IEEE Intell. Transp. Syst. Mag.*, vol. 5, no. 4, pp. 38–49, Winter, 2013.

[25] M. Botsov, M. Klügel, W. Kellerer, and P. Fertl, "Location dependent resource allocation for mobile device-to-device communications," in *Proc. IEEE WCNC*, Apr. 2014, pp. 1679–1684.

[26] Y. Ren, F. Liu, and Z. Liu, "Power control in D2D-based vehicular communication networks," *IEEE Trans. Veh. Technol.*, vol. 64, no. 12, pp. 5547–5562, Dec. 2015.

[27] W. Sun, E. G. Ström, F. Brännström, K. Sou, and Y. Sui, "Radio resource management for D2D-based V2V communication," *IEEE Trans. Veh. Technol.*, vol. 65, no. 8, pp. 6636–6650, Aug. 2016.

[28] W. Sun, D. Yuan, E. G. Ström, and F. Brännström, "Cluster-based radio resource management for D2D-supported safety-critical V2X communications," *IEEE Trans. Wireless Commun.*, vol. 15, no. 4, pp. 2756–2769, Apr. 2016.

[29] N. Cheng, H. Zhou, L. Lei, N. Zhang, Y. Zhou, X. Shen, and F. Bai, "Performance analysis of vehicular device-to-device underlay communication," *IEEE Trans. Veh. Technol.*, vol. 66, no. 6, pp. 5409–5421, Jun. 2016.

[30] R. Y. Chang, Z. Tao, J. Zhang, and C.-C. J. Kuo, "A graph approach to dynamic fractional frequency reuse (FFR) in multi-cell OFDMA networks," in *Proc. IEEE ICC*, Jun. 2009, pp. 1–6.

[31] —, "Multicell OFDMA downlink resource allocation using a graphic framework," *IEEE Trans. Veh. Technol.*, vol. 58, no. 7, pp. 3494–3507, Sep. 2009.

[32] L. Lu, D. He, X. Yu, and G. Y. Li, "Energy-efficient resource allocation for cognitive radio networks," in *Proc. IEEE GLOBECOM*, Dec. 2013, pp. 1026–1031.

[33] D. B. West et al., *Introduction to Graph Theory*. Prentice Hall Upper Saddle River, 2001, vol. 2.

[34] D. Gale and L. S. Shapley, "College admissions and the stability of marriage," *American Mathematical Monthly*, vol. 69, pp. 9–14, 1962.

[35] A. Leshem, E. Zehavi, and Y. Yaffe, "Multichannel opportunistic carrier sensing for stable channel access control in cognitive radio systems," *IEEE J. Sel. Areas Commun.*, vol. 30, no. 1, pp. 82–95, Jan. 2012.

[36] L. Lu, D. He, G. Y. Li, and X. Yu, "Graph-based robust resource allocation for cognitive radio networks," *IEEE Trans. Signal Process.*, vol. 63, no. 14, pp. 3825–3835, Jul. 2015.

[37] L. Lu, D. He, Q. Xie, G. Y. Li, and X. Yu, "Graph-based path selection and power allocation for DF relay-aided transmission," to appear in *IEEE Wireless Commun. Lett.*, 2017.

[38] Q. Wei, W. Sun, B. Bai, L. Wang, E. G. Ström, and M. Song, "Resource allocation for V2X communiations: A local search based 3D matching approach," in *Proc. IEEE ICC*, May 2017, pp. 1–6.

[39] Z. Füredi, J. Kahn, and P. D. Seymour, "On the fractional matching polytope of a hypergraph," *Combinatorica*, vol. 13, no. 2, pp. 167–180, Jun. 1993.

[40] E. M. Arkin and R. Hassin, "On local search for weighted k-set packing," *Mathematics of Operations Research*, vol. 23, no. 3, pp. 640–648, Aug. 1998.

[41] B. Chandra and M. M. Halldórsson, "Greedy local improvement and weighted set packing approximation," *J. Algorithms*, vol. 39, no. 2, pp. 223–240, May 2001.

[42] P. Berman, "A d/2 approximation for maximum weight independent set in d-claw free graphs," *Algorithm Theory-SWAT 2000*, pp. 31–40, Jul. 2000.

[43] D. Tse and P. Viswanath, *Fundamentals of wireless communication*. Cambridge, U.K.: Cambridge University Press, 2005.

[44] I. S. Gradshteyn and I. M. Ryzhik, *Table of Integrals, Series, and Products*, 7th ed. San Diego, CA: Academic Press, 2007.

[45] E. Björnson, E. A. Jorswieck, M. Debbah, and B. Ottersten, "Multiobjective signal processing optimization: The way to balance conflicting metrics in 5G systems," *IEEE Signal Process. Mag.*, vol. 31, no. 6, pp. 14–23, Nov. 2014.

[46] G. Yu, Y. Jiang, L. Xu, and G. Y. Li, "Multi-objective energy-efficient resource allocation for multi-RAT heterogeneous networks," *IEEE J. Sel. Areas Commun.*, vol. 33, no. 10, pp. 2118–2127, Oct. 2015.

[47] *WF on SLS Evaluation Assumptions for eV2X*. R1-165704, 3GPP TSG RAN WG1 Meeting #85, May 2016.

[48]  *WINNER II Channel Models*. IST-4-027756, WINNER II D1.1.2 V1.2, Sep. 2007. [Online]. Available: `http://projects.celtic-initiative.org/winner+/WINNER2-Deliverables/D1.1.2v1.1.pdf`.

[49]  T. Kim, D. J. Love, and B. Clerckx, "Does frequent low resolution feedback outperform infrequent high resolution feedback for multiple antenna beamforming systems?," *IEEE Trans. Signal Process.*, vol. 59, no. 4, pp. 1654–1669, Apr. 2011.

[50]  T. D. Hoang, L. B. Le, and T. Le-Ngoc, "Resource allocation for D2D communication underlaid cellular networks using graph-based approach," *IEEE Trans. Wireless Commun.*, vol. 15, no. 10, pp. 7099–7113, Oct. 2016.

[51]  S. Sahni and T. Gonzalez, "P-complete approximation problems," *J. Assoc. Comput. Mach.*, vol. 23, no. 3, pp. 555–565, Jul. 1976.

[52]  S. Kandukuri and S. Boyd, "Optimal power control in interference-limited fading wireless channels with outage-probability specifications," *IEEE Trans. Wireless Commun.*, vol. 1, no. 1, pp. 46–55, Jan. 2002.

[53]  J. Papandriopoulos, J. Evans, and S. Dey, "Optimal power control for Rayleigh-faded multiuser systems with outage constraints," *IEEE Trans. Wireless Commun.*, vol. 4, no. 6, pp. 2705–2715, Nov. 2005.

[54]  —, "Outage-based optimal power control for generalized multiuser fading channels," *IEEE Trans. Commun.*, vol. 54, no. 4, pp. 693–703, Apr. 2006.

[55]  I. Z. Kovács, P. C. F. Eggers, K. Olesen, and L. G. Petersen, "Investigations of outdoor-to-indoor mobile-to-mobile radio communication channels," in *Proc. IEEE VTC Fall*, Sep. 2002, pp. 430–434.

[56]  Y. H. Chan and L. C. Lau, "On linear and semidefinite programming relaxations for hypergraph matching," *Mathematical Programming*, vol. 135, no. 1-2, pp. 123–148, Oct. 2012.

[57]  K. Jain, "A factor 2 approximation algorithm for the generalized steiner network problem," *Combinatorica*, vol. 21, no. 1, pp. 39–60, Jan. 2001.

[58]  S. Kirkpatrick, C. D. Gelatt, M. P. Vecchi, et al., "Optimization by simulated annealing," *Science*, vol. 220, no. 4598, pp. 671–680, May 1983.

[59]  R. S. Sutton, A. G. Barto, et al., *Reinforcement learning: An introduction*. MIT press, 1998.

[60]  V. Mnih, K. Kavukcuoglu, D. Silver, A. A. Rusu, J. Veness, M. G. Bellemare, A. Graves, M. Riedmiller, A. K. Fidjeland, G. Ostrovski, et al., "Human-level control

through deep reinforcement learning," *Nature*, vol. 518, no. 7540, pp. 529–533, Feb. 2015.

[61] D. Silver, A. Huang, C. J. Maddison, A. Guez, L. Sifre, G. Van Den Driessche, J. Schrittwieser, I. Antonoglou, V. Panneershelvam, M. Lanctot, et al., "Mastering the game of go with deep neural networks and tree search," *Nature*, vol. 529, no. 7587, pp. 484–489, Jan. 2016.

[62] H. Mao, M. Alizadeh, I. Menache, and S. Kandula, "Resource management with deep reinforcement learning," in *Proc. ACM Workshop Hot Topics Netw. (HotNets)*, 2016, pp. 50–56.

[63] H. Ye and G. Y. Li, "Deep reinforcement learning for resource allocation in V2V communications," in *Proc. IEEE ICC*, May 2018, pp. 1–6.

[64] H. Ye, L. Liang, G. Y. Li, J. Kim, L. Lu, and M. Wu, "Machine learning for vehicular networks: recent advances and application examples," *IEEE Veh. Technol. Mag.*, vol. 13, no. 2, pp. 94–101, Jun. 2018.

[65] L. Liang, G. Y. Li, and W. Xu, "Resource allocation for D2D-enabled vehicular communications," *IEEE Trans. Commun.*, vol. 65, no. 7, pp. 3186–3197, Jul. 2017.

[66] S. Omidshafiei, J. Pazis, C. Amato, J. P. How, and J. Vian, "Deep decentralized multi-task multi-agent reinforcement learning under partial observability," in *Proc. Int. Conf. Mach. Learning (ICML)*, 2017, pp. 2681–2690.

[67] J. Foerster, N. Nardelli, G. Farquhar, T. Afouras, P. H. S. T. 1, P. Kohli, and S. Whiteson, "Stabilising experience replay for deep multi-agent reinforcement learning," in *Proc. Int. Conf. Mach. Learning (ICML)*, 2017, pp. 1146–1155.

[68] C. J. Watkins and P. Dayan, "Q-learning," *Machine learning*, vol. 8, no. 3-4, pp. 279–292, May 1992.

[69] M. Tan, "Multi-agent reinforcement learning: independent vs. cooperative agents," in *Proc. Int. Conf. Mach. Learning (ICML)*, 1993, pp. 330–337.

[70] L. Liang, S. Xie, G. Y. Li, Z. Ding, and X. Yu, "Graph-based resource sharing in vehicular communication," *IEEE Trans. Wireless Commun.*, vol. 17, no. 7, pp. 4579–4592, Jul. 2018.

[71] G. Tesauro, "Extending Q-learning to general adaptive multi-agent systems," in *Proc. Advances Neural Inf. Process. Syst. (NIPS)*, 2004, pp. 871–878.

[72] S. Ruder, "An overview of gradient descent optimization algorithms," *arXiv preprint arXiv:1609.04747*, 2016.

# VITA

Le Liang was born in June 1990 in Huaian, China. He received the B.E. degree in information engineering from Southeast University, Nanjing, China, in 2012, and the M.A.Sc degree in electrical engineering from the University of Victoria, Victoria, BC. Canada, in 2015. From June 2011 to June 2012, he was with the National Mobile Communications Research Laboratory at Southeast University as an undergraduate research assistant. From September 2012 to December 2015, he was a graduate research assistant in the Department of Electrical and Computer Engineering at the University of Victoria. From January 2016 to December 2018, he was a graduate research assistant at the Information Transmission and Processing Laboratory, Georgia Institute of Technology. He spent the summer of 2017 working as a research scientist intern at Intel Labs, Hillsboro, OR. He completed his Ph.D. in electrical engineering with the Georgia Institute of Technology in December 2018. His research interests include vehicular communications, multiple-input multiple-output systems, and machine learning for wireless communications.